Technical Memorandum ERL AOML-61

HEAT BUDGET AND CLIMATIC ATLAS OF THE EQUATORIAL ATLANTIC OCEAN DURING FGGE (1979)

Eric Marmolejo
John F. Festa
Robert L. Molinari

Atlantic Oceanographic and Meteorological Laboratory
Miami, Florida
August 1985

noaa NATIONAL OCEANIC AND ATMOSPHERIC ADMINISTRATION / Environmental Research Laboratories

NOAA Technical Memorandum ERL AOML-61

HEAT BUDGET AND CLIMATIC ATLAS OF THE EQUATORIAL ATLANTIC OCEAN DURING FGGE (1979)

Eric Marmolejo
John F. Festa
Robert L. Molinari

Atlantic Oceanographic and Meteorological Laboratory
Miami, Florida
August 1985

UNITED STATES
DEPARTMENT OF COMMERCE

Malcolm Baldrige,
Secretary

NATIONAL OCEANIC AND
ATMOSPHERIC ADMINISTRATION

Environmental Research
Laboratories

Vernon E. Derr,
Director

NOTICE

Contents

HEAT BUDGET AND CLIMATIC ATLAS OF THE EQUATORIAL ATLANTIC OCEAN DURING FGGE (1979)

Eric Marmolejo, John F. Festa, and Robert L. Molinari

ABSTRACT. Observations of surface oceanographic and meteorological fields collected during the first GARP Global Experiment (FGGE) in the equatorial Atlantic Ocean have been combined and averaged by month onto a 2° x 2° grid. Monthly distributions of sea-surface temperature, wind speed and direction, air temperature, specific humidity, and cloud cover have been generated for the period from December 1978 through November 1979. Net short-wave and long-wave radiation, and sensible and latent heat flux distributions have been generated from surface data using the bulk aerodynamic formulas. Standard errors of the mean values have been computed along with monthly contoured plots of each oceanographic and meteorological variable.

1. INTRODUCTION

Equatorial oceans apparently play a large role in the global energy balance. Recent studies have shown that the eastern equatorial Atlantic and Pacific Oceans experience a significant net annual heat gain through the sea surface (Hastenrath and Lamb, 1978, for instance). Through advection this heat may serve to balance net heat deficits at poleward latitudes (Hastenrath, 1980). The historical studies have used data averaged over many years to derive the surface oceanic, meteorological, and energy exchange fields.

Molinari et al. (1984) considered the evolution of the sea-surface temperature (SST) field, meteorological variables, and surface energy in the equatorial Atlantic Ocean during the First GARP Global Experiment (FGGE), which was conducted in 1979. They compared the FGGE year with a climatological year given in Hastenrath and Lamb (1977). This atlas is a byproduct of the Molinari et al. (1984) study in that all the mean monthly fields of SST, meteorological variables, and surface energy fluxes derived from the FGGE data are presented. Following Figs. 1-6, which show monthly distributions of surface observations, the fields are presented in a form similar to the one employed by Hastenrath and Lamb (1977, 1978) to permit a comparison of the two data sets. The following monthly smoothed and edited fields are presented: sea surface observations (Figs. 7-12); air temperatures (Figs. 13-18); wind speed and direction (Figs. 19-24); cloud cover (Figs. 25-30); and specific humidity (Figs. 31-36). Included are the following fields computed from the above monthly smoothed and edited fields: latent heat flux (Figs. 37-42); sensible heat flux (Figs. 43-48); long-wave radiation (Figs. 49-54); short-wave radiation (Figs. 55-60); and total heat gain (Figs. 61-66). Five annual average fields are computed: latent heat flux and sensible heat flux (Fig. 67); long-wave radiation and short-wave radiation (Fig. 68); and total heat gain (Fig. 69).

2. DATA SOURCES AND ANALYSIS

Data were collected from several institutions for the time period December 1978 through November 1979 (Table 1). Only data in the region 9°N-9°S and 60°W-10°E were considered in the analysis. The following steps were taken to edit, smooth, and fill in the SST and meteorological fields. Obvious outliers were removed by setting specified ranges for each of the parameters (Table 2). Daily averages of each parameter were computed on a 2° x 2° grid to reduce the influence of time-series stations (the grid size was a necessary compromise between data availability and desired spatial resolution). The daily averages were then averaged on the 2° x 2° grid to yield mean monthly distributions. Whenever sufficient data existed, a biased sample variance was computed for the grid point. A mean standard error for the entire domain was computed by averaging the resulting root mean square (rms) values.

The fields were further smoothed by first computing differences between mean daily, and mean monthly values at each grid point. When the difference exceeded two mean standard errors, the daily average was removed and new monthly averages and rms values were computed. Several regions outside the shipping lanes had few if any data points (Figs. 1-6). A nine-point Laplacian estimator was used to edit and fill in values at grid points within these regions. The functional form of the estimator, similar to a weighted average over a plane, is as follows:

$$\hat{A}_{KL} = \frac{\sum_{i=K-1}^{K+1} \sum_{j=L-1}^{L+1} w_{ij} A_{ij}}{\sum_{i=K-1}^{K+1} \sum_{j=L-1}^{L+1} w_{ij}}$$

such that when K = i and L = j, $\hat{A}_{KL} = \hat{A}_{ij} = 0$. The parameters are defined as follows:

A_{ij} = available monthly average at grid location i, j

$\hat{A}_{KL}$ = estimated value at location K, L

w_{ij} = weight values assigned as follows:

1	4	1
4	KL	4
1	4	1

To edit the data, the Laplacian operator was used as follows: if the number of observations making up the monthly average was less than 5, the data were removed if $|\hat{A}_{ij} - A_{ij}| > 2$ MSE.

To smooth the data, the following criteria were used:

(1) Data values based on 5 or more observations were left unchanged.

(2) Data values based on less than 5 days within a month were changed as follows:

$$A_{ij} = \hat{A}_{ij} \text{ if } |\hat{A}_{ij} - A_{ij}| > 2 \text{ MSE.}$$

$$A_{ij} = 1/2(\hat{A}_{ij} + A_{ij}) \text{ if } |\hat{A}_{ij} - A_{ij}| < 2 \text{ MSE.}$$

3. COMPUTATION OF HEAT BUDGET PARAMETERS

The latent heat flux (Q_e) and sensible heat flux (Q_s) were computed by using the bulk aerodynamic formulas following Hastenrath and Lamb (1978):

$$Q_s = \rho_a C_d \, C_p (T_s - T_a) w$$

$$Q_e = \rho_a C_d \, L (q_s - q_a) w$$

ρ_a = density of air, 1.175 kg/m^3

C_d = drag coefficient, 1.4×10^{-3}

C_p = specific heat of air, 1.012 (kj/kg)/°C

T_s, T_a = sea surface temperature and air temperature respectively (°C)

w = scalar wind speed (m/s)

L = latent heat of vaporization, $(2484 - 2.39 \times T_s)$ kj/kg

T_d = dew point temperature (K) = T_a - dew point depression

$$q_s = \frac{621.97 \times E_s}{p - .377 \times E_s} \text{ saturation specific humidity (g/kg) at } T_s$$

$$q_a = \frac{621.97 \times E_a}{p - .377 \times E_a} \text{ specific humidity (g/kg) at } T_d$$

$$E_s = 10^{(22.5578 - (2937.4)/T_s \; 4.92831 \times \log(T_s))}$$

$$E_a = 10^{(22.5578 - (2937.4)/T_s \; 4.92831 \times \log(T_d))}$$

p = atmospheric pressure (mb)

The shortwave radiation balance (SW) and the net longwave radiation balance (LW) are computed following Hastenrath and Lamb (1978) and Bunker (1976), respectively, as

$$LW = \epsilon T_s^4 \sigma \times (0.39 - .056\sqrt{q_a}) \times (1 - 0.53C^2) + 4\epsilon\sigma T_s^3 \times (T_s - T_a)$$

$$SW = Q_o \times (1 - aC - bC) \times (1 - \alpha)$$

ϵ = emissivity = 1

σ = Stefan Boltzmann's constant, 567 x 10 $(W/m^2)/K^4$

C = fraction of cloud cover in tenths

Q_o = shortwave radiation incident on Earth's surface on a cloudless day, from a table developed by Berliand (1960)

a=b = 0.38 from Bunker (1976)

α = albedo = .06

The net oceanic heat gain Q is computed as

$$Q = SW - LW - Q_s - Q_e \ (W/m^2).$$

The heat budget parameters were computed from the monthly mean Laplacian interpolated observed fields of T_s, T_a, w, etc.

4. ERROR ANALYSIS

Standard error of the mean (SEM) values have been computed for each variable at each grid point. Ensemble average values of SEM, computed from a biased sample variance, are given in Table 3 for observed values. The SEM is computed as follows:

$$S_x = \frac{\text{variance in } x}{\sqrt{n}}$$

where n = the number of values in the sample, and variance in x = the biased sample variance of the values. Typically larger errors are found outside the shipping lanes (where quadrangles typically have less than 10 data points). A propagation-of-error analysis was performed to determine errors in computed quantities. Considering a monthly average function $z = \overline{f(x,y,\ldots)}$ of two or more measured quantities x,y,..., the SEM of z can be written as

$$S_z = \sqrt{\frac{\partial \overline{f(x,y)}}{dx}^2 S_x^2 + \frac{\partial \overline{f(x,y)}}{\partial y}^2 S_y^2 + \ldots}$$

where S_y, S_x = SEM of measured quantity y and x, respectively, and

$\frac{\partial \overline{f(x,y)}}{\partial x}$ $\frac{d\overline{f(x,y)}}{dy}$ = partial derivatives of the monthly average function $z = \overline{f(x,y)}$ with respect to the measured quantity.

Table 4 lists the average SEM's of the computed quantities. As before, errors are considerably larger outside the shipping lanes.

5. REFERENCES

Berliand, T. C. (1960). Method of climatological estimation of global radiation. Meteor. Gidrol., 6, 9-12.

Bunker, A. F. (1976). Computations of surface energy flux and annual air-sea interaction cycles of the North Atlantic Ocean. Mon. Wea. Rev., 104, 112-114.

Hastenrath, S. (1980). Heat budget of tropical ocean and atmosphere. J. Phys. Oceanogr., 10, 159-170.

Hastenrath, S., and P. Lamb (1977). Climatic atlas of the tropical Atlantic and eastern Pacific Oceans. University of Wisconsin Press.

Hastenrath, S., and P. Lamb (1978). Heat budget atlas of the tropical Atlantic and eastern Pacific Oceans. University of Wisconsin Press.

Molinari, R. L., J. F. Festa, and E. Marmolejo (1985). Evolution of sea-surface temperature and surface meteorological fields in the tropical Atlantic Ocean during FGGE, 1979. I. Description of surface fields and computation of surface energy fluxes. Progress in Oceanography, Pergamon Press, 14, 401-420.

Table 1. Sources of Data

Institution	Type of Data
National Climate Center	Surface meteorological and oceanic observations from merchant vessels
National Oceanographic Data Center	XBT-MBT temperature observations
World Data Center A.	Sea surface and subsurface temperature observations and meteorological observations
National Oceanic and Atmospheric Administration/Atlantic Oceanographic and Meteorological Laboratory	XBT-CTD measurements from the RV Researcher
Institute of Marine Research of the Academy of Sciences of the GDR	CTD measurements from the RV Humboldt
Columbia University/Lamont Doherty Geological Observatory	CTD measurements from the RV Conrad and Oceanus
Fleet Numerical Oceanographic Center	Subsurface temperature observations
University of Kiel, Federal Republic of Germany	CTD measurements from the RV Meteor
Office de la Recherche Scientifique et Technique Outre-Mer, France	CTD measurements from the RV Capricorn

Table 2. Ranges of Parameters

Parameter	Acceptable Range
Sea surface temperature	
Coastal grid points	15°-31°C
Interior grid points	18°-31°C
Scalar wind speed	0-20 m/s
Air temperature	16°-38°C
Dew point depression	0°-15°C

Table 3. Ensemble average SEM's for measured quantities as a function of the number of data points (n) used in the monthly average.*

	n < 10	n > 15
Sea surface temperature	.31°C	.16°C
Air temperature	.42°C	.22°C
U-component of the wind	.66 m/s	.36 m/s
V-component of the wind	.73 m/s	.38 m/s
Cloud cover	.8	.4

*Quadrangles with more than 15 points within each month are typically within the shipping lanes; those with fewer than 10 points are outside the lanes.

Table 4. Ensemble average SEM's for computed quantities as a function of the number of data points (n) used in the computation.*

	n < 10	n > 10
Specific humidity	0.59 g/kg	0.38 g/kg
Saturation specific humidity	0.54 g/kg	0.38 g/kg
Latent heat flux	23.5 W/m^2	15.9 W/m^2
Sensible heat flux	8.0 W/m^2	5.5 W/m^2
Long-wave radiation	5.5 W/m^2	3.8 W/m^2
Short-wave radiation	23.2 W/m^2	18.3 W/m^2

*Quadrangles with more than 10 points within each month are typically within the shipping lanes; those with fewer than 10 points are outside the lanes.

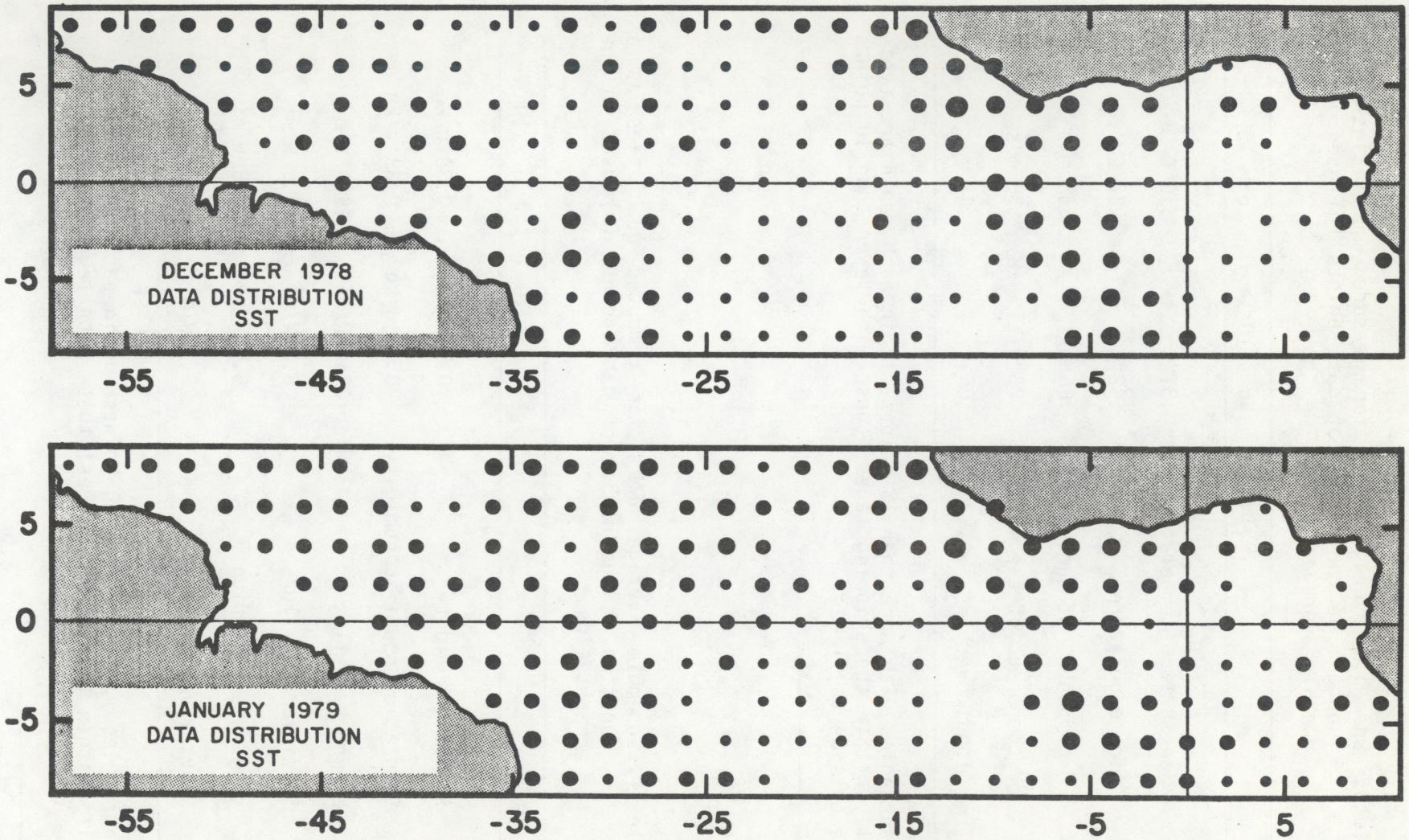

Figure 1. Monthly distribution of surface observations for December 1978 and January 1979, on a 2° x 2° grid. Dot size corresponds to number of observations in the month: Smallest dot stands for 1-4 observations; next larger, 5-14 observations; next larger, 15-24; largest, 25-31.

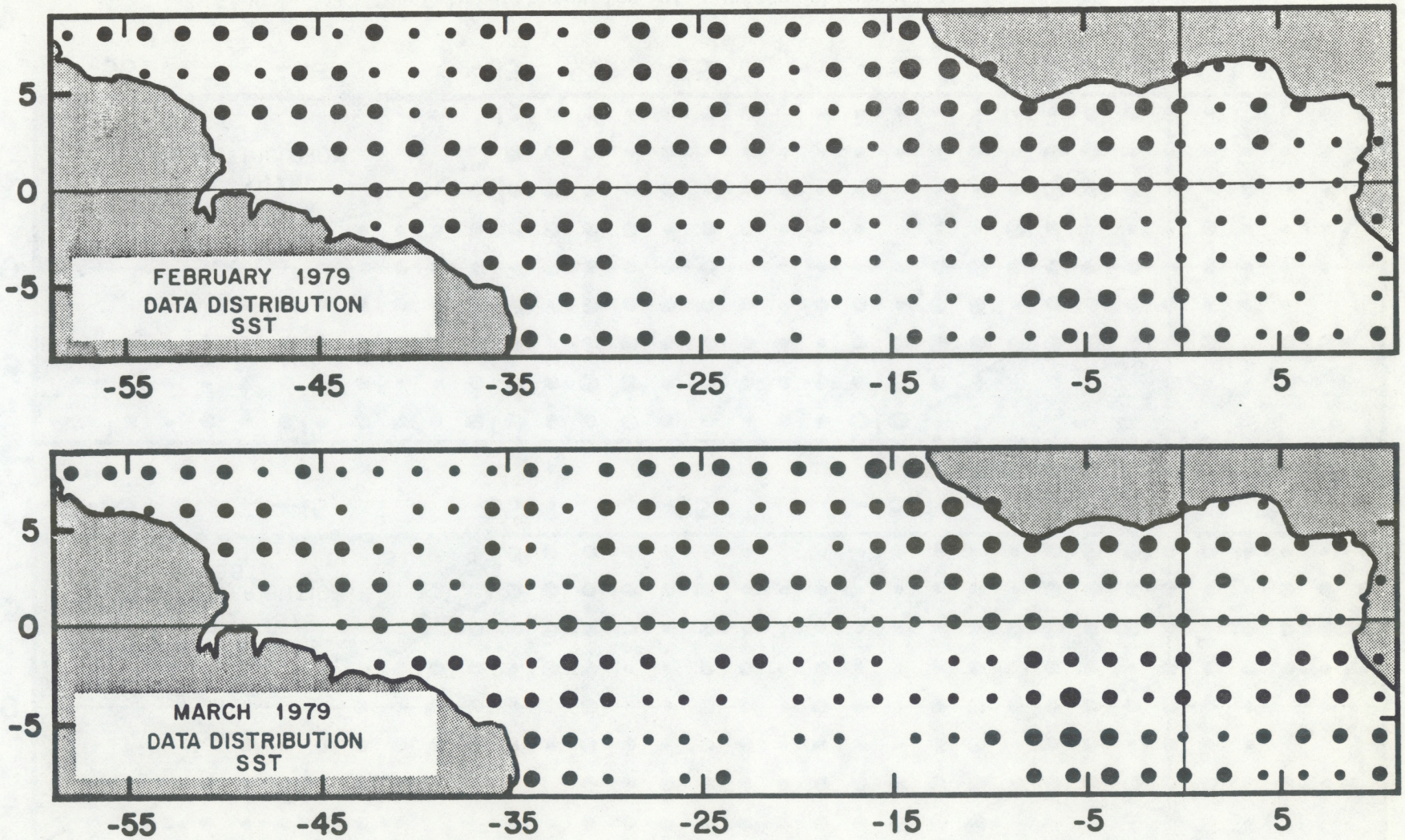

Figure 2. Monthly distribution of surface observations for February and March 1979 (as in Figure 1).

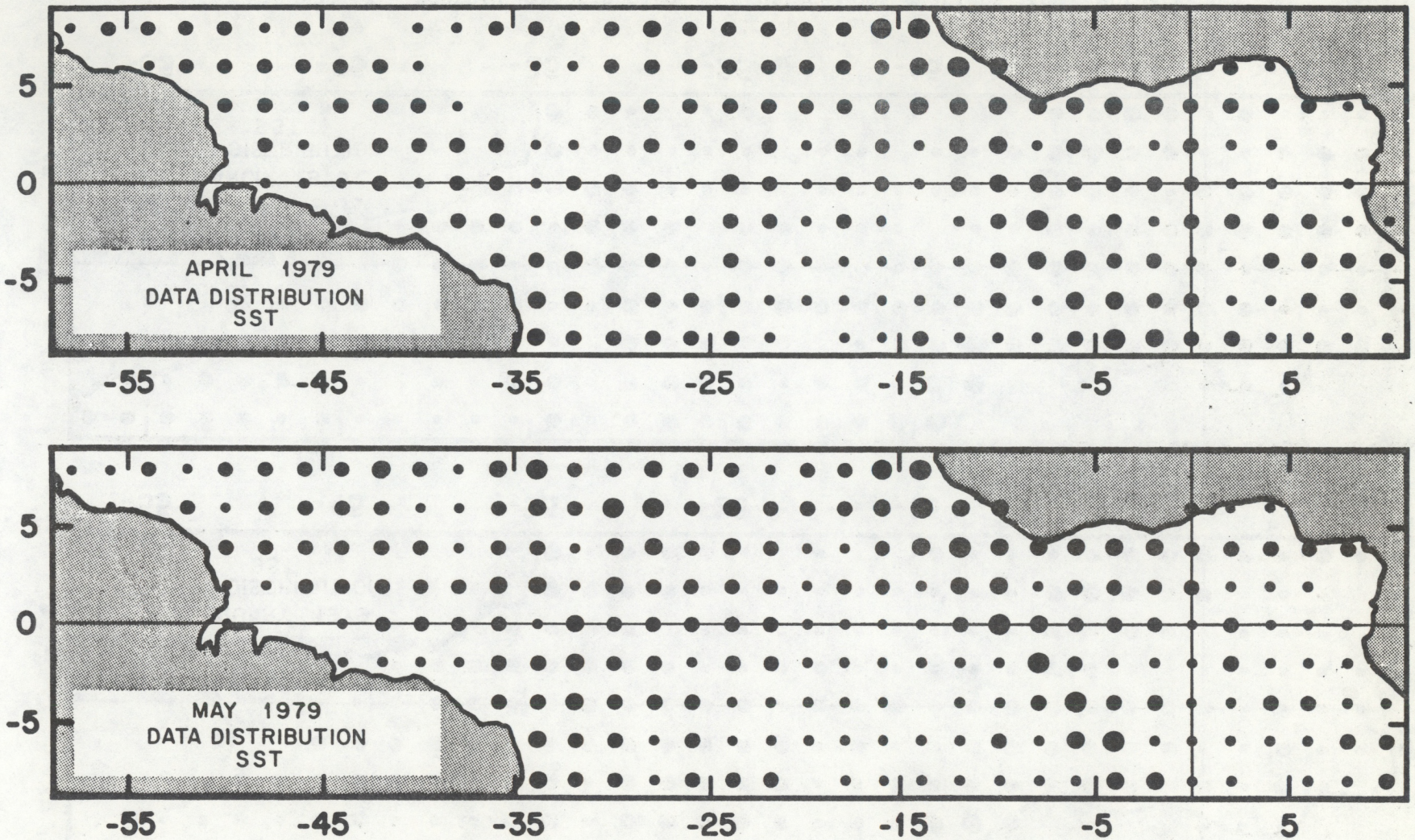

Figure 3. Monthly distribution of surface observations for April and May 1979 (as in Figure 1).

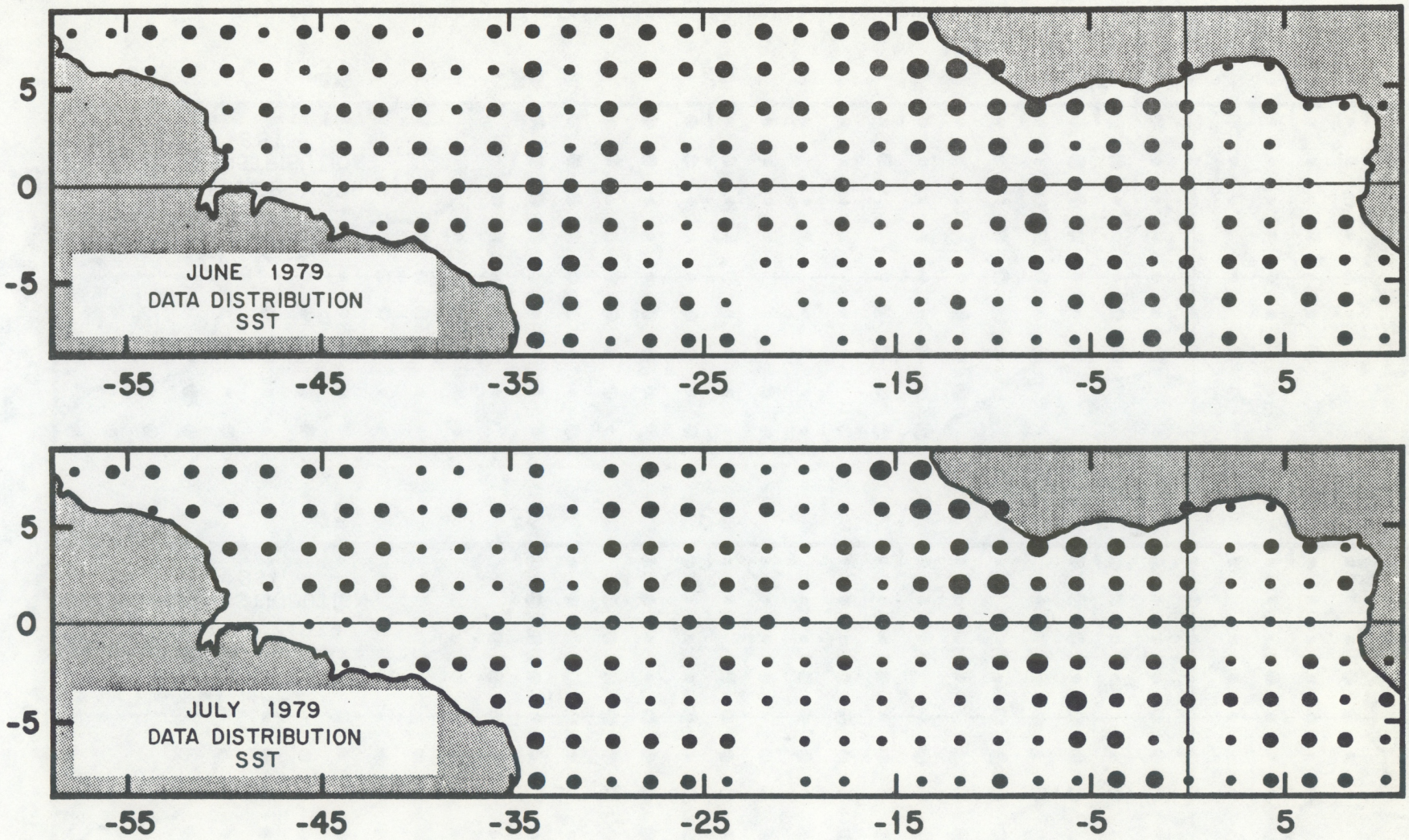

Figure 4. Monthly distribution of surface observations for June and July 1979 (as in Figure 1).

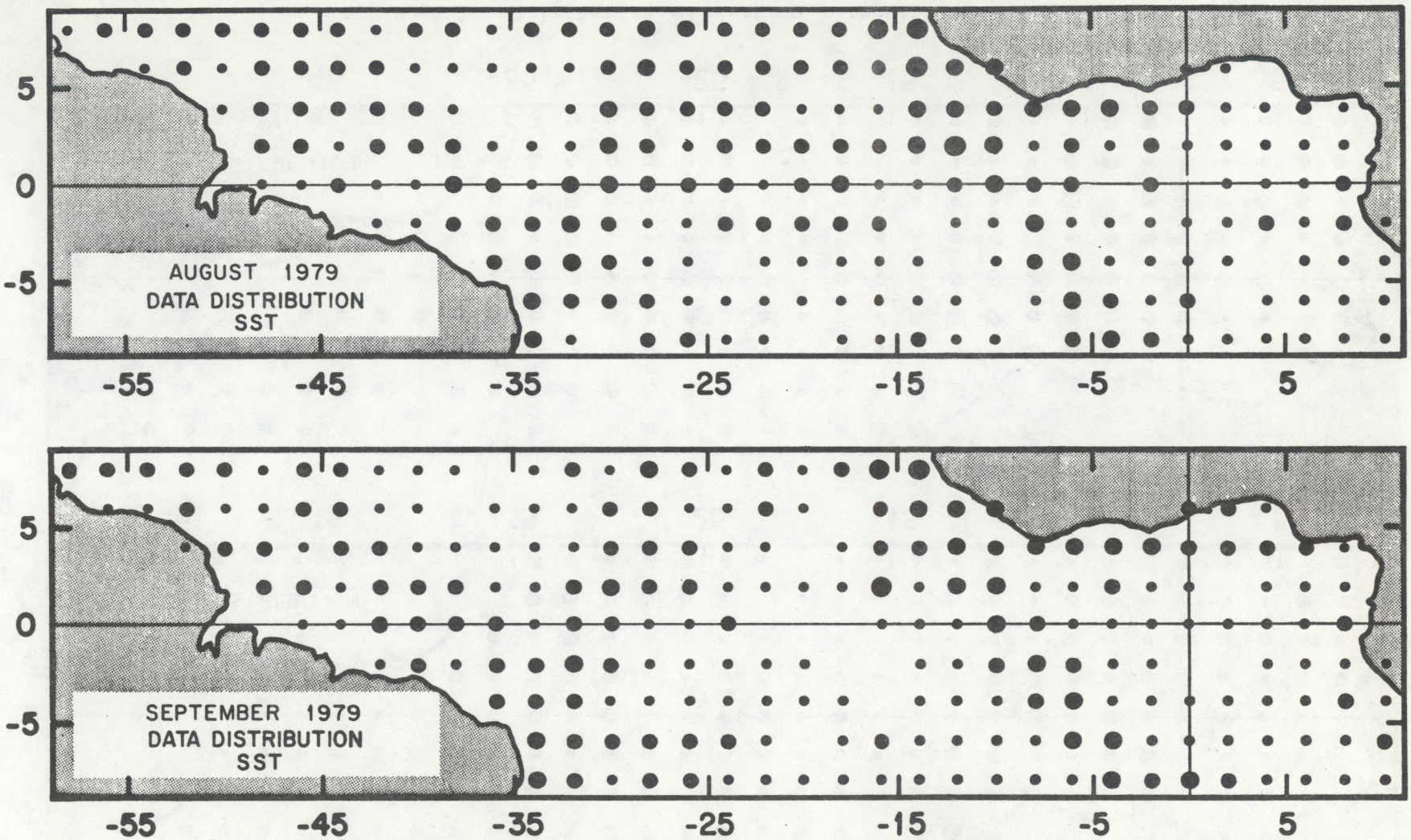

Figure 5. Monthly distribution of surface observations for August and September 1979 (as in Figure 1).

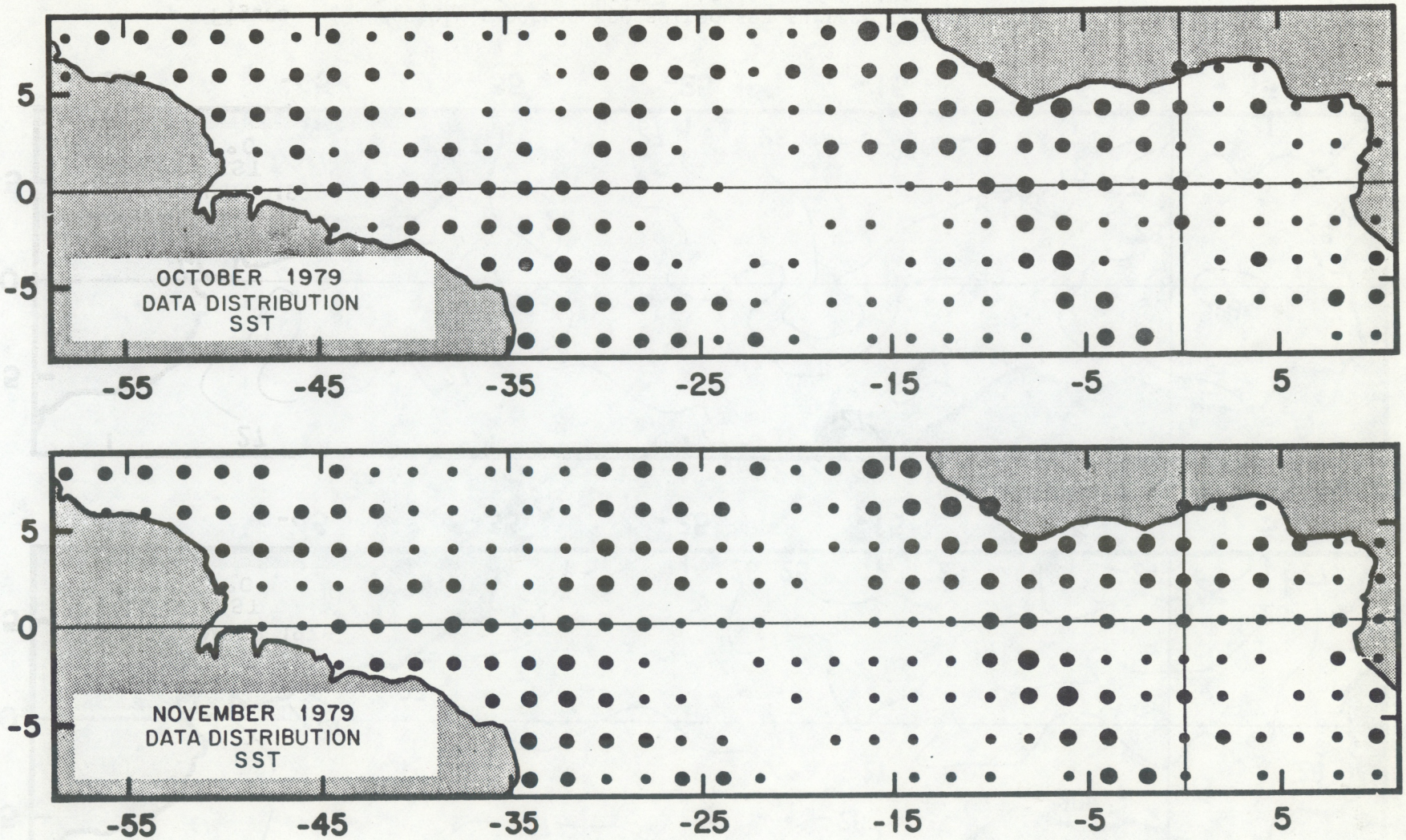

Figure 6. Monthly distribution of surface observations for October and November 1979 (as in Figure 1).

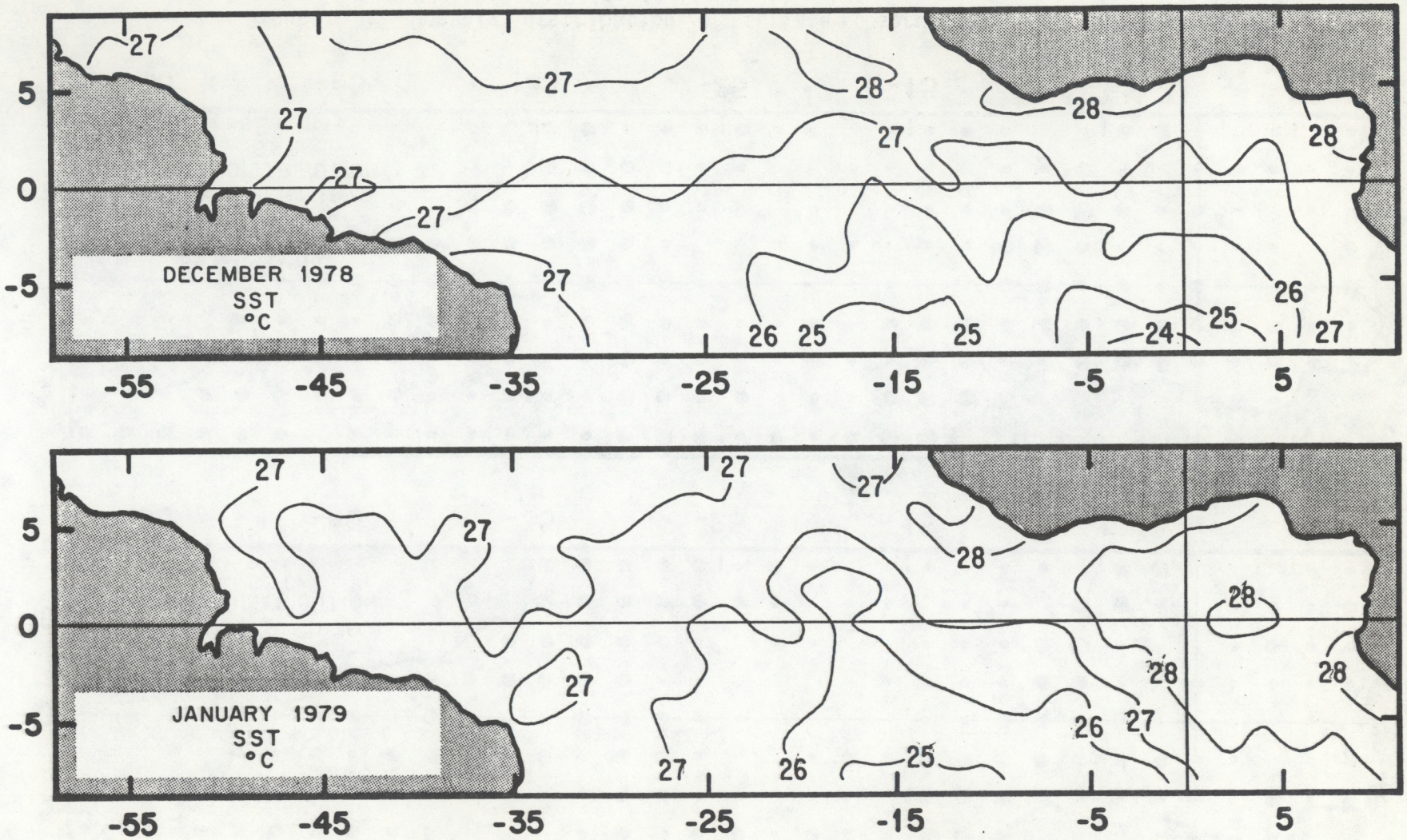

Figure 7. Monthly smoothed and edited sea surface temperatures for December 1978 and January 1979, contoured every 1°C.

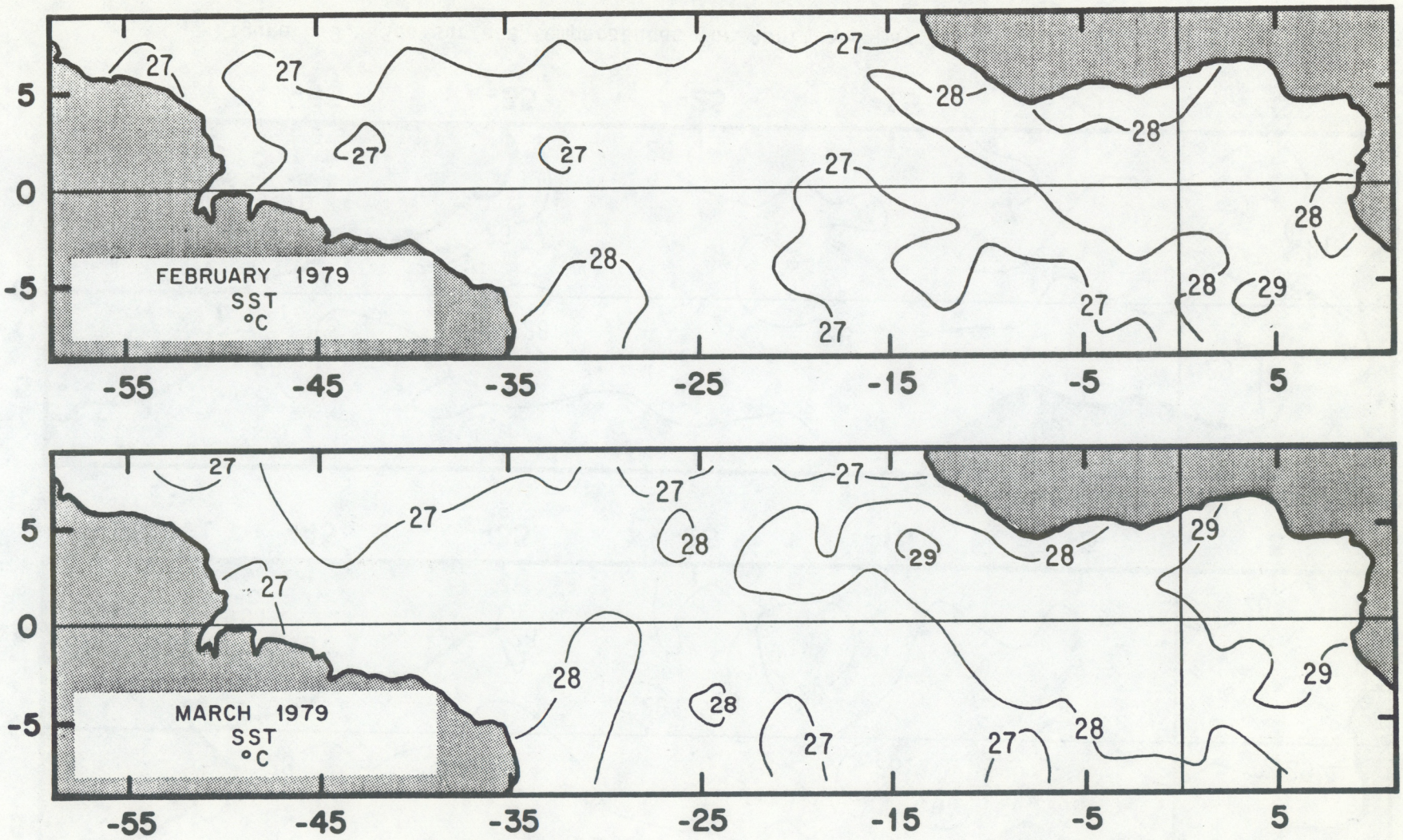

Figure 8. Sea surface temperatures for February and March 1979 (as in Figure 7).

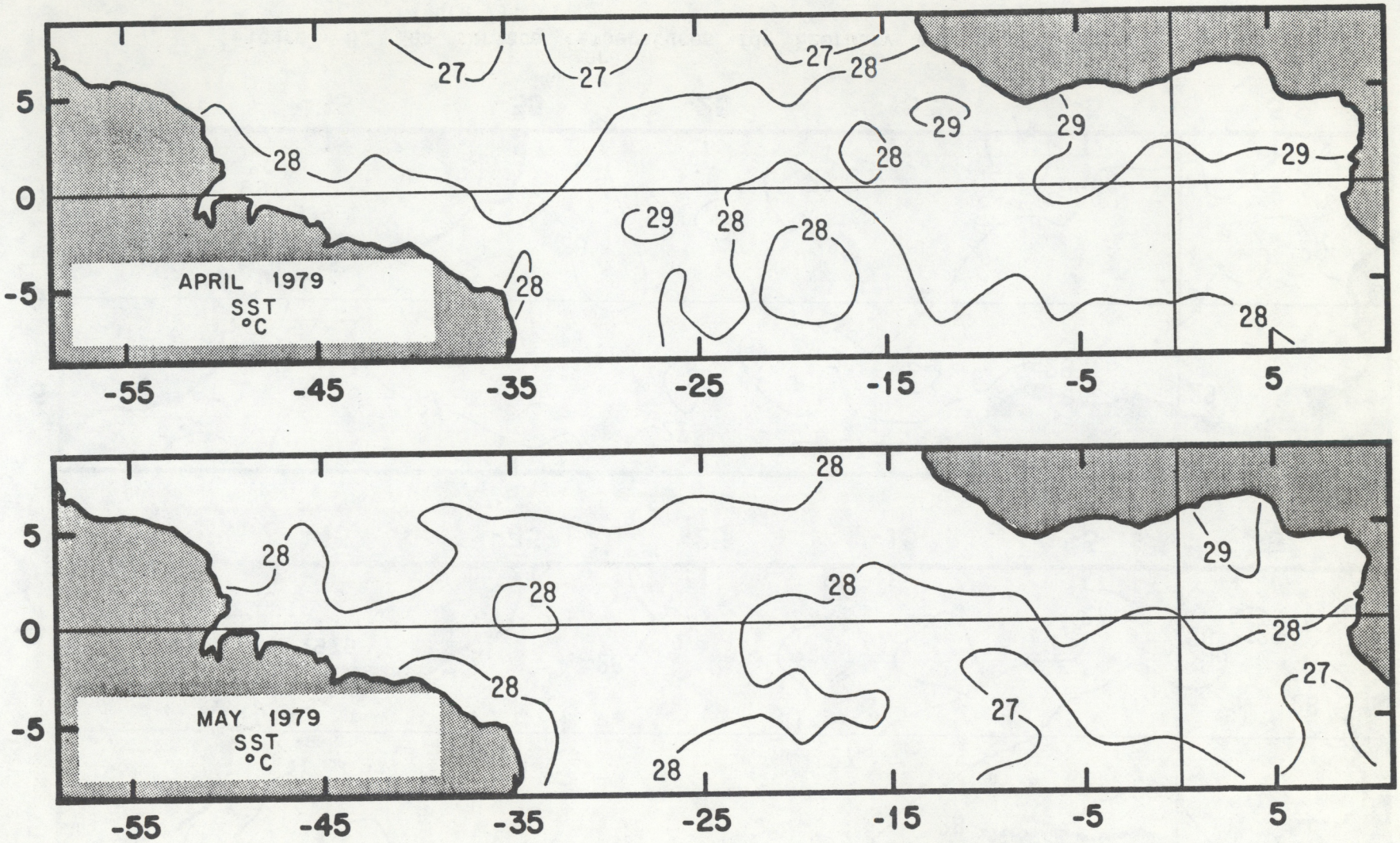

Figure 9. Sea surface temperatures for April and May 1979 (as in Figure 7).

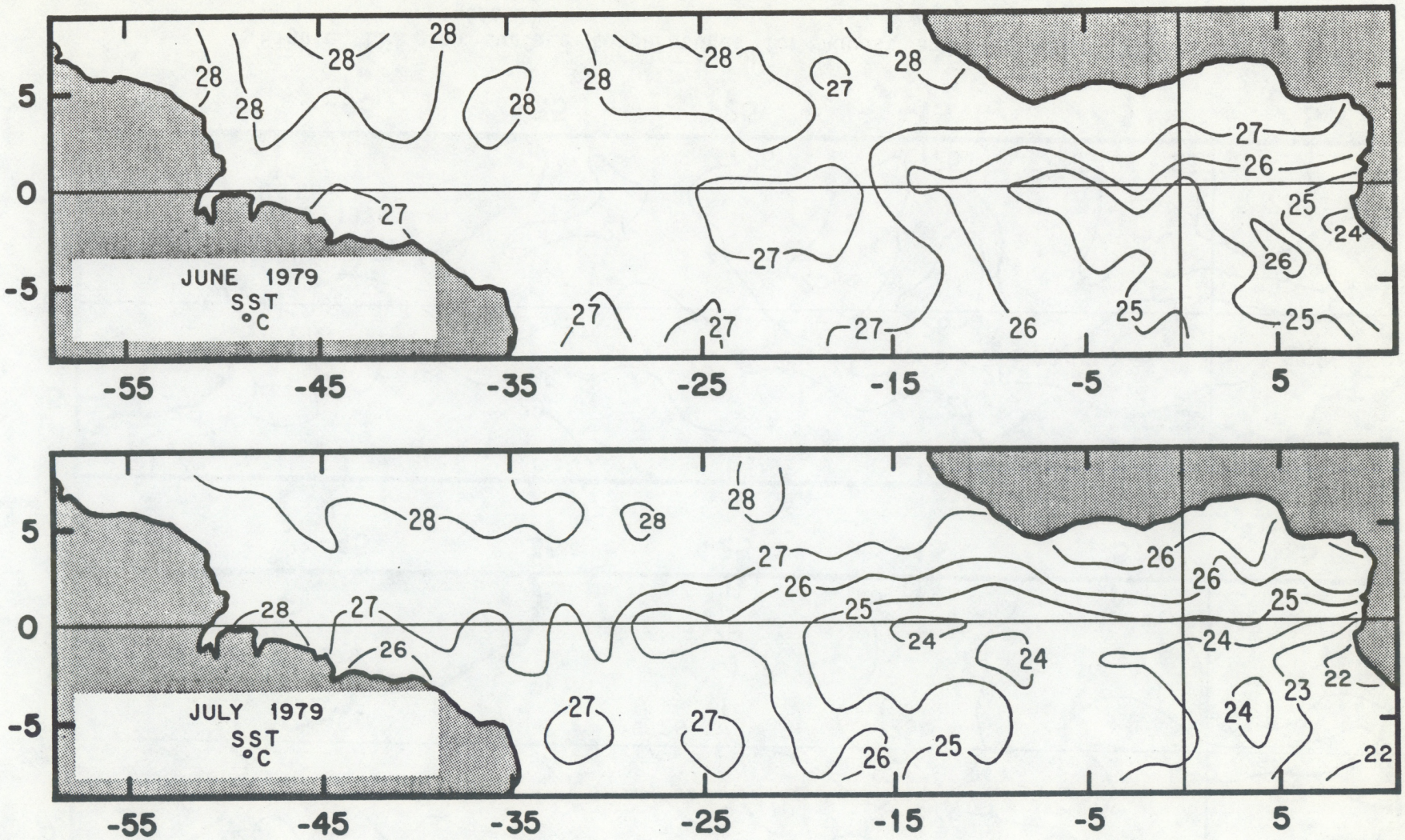

Figure 10. Sea surface temperatures for June and July 1979 (as in Figure 7).

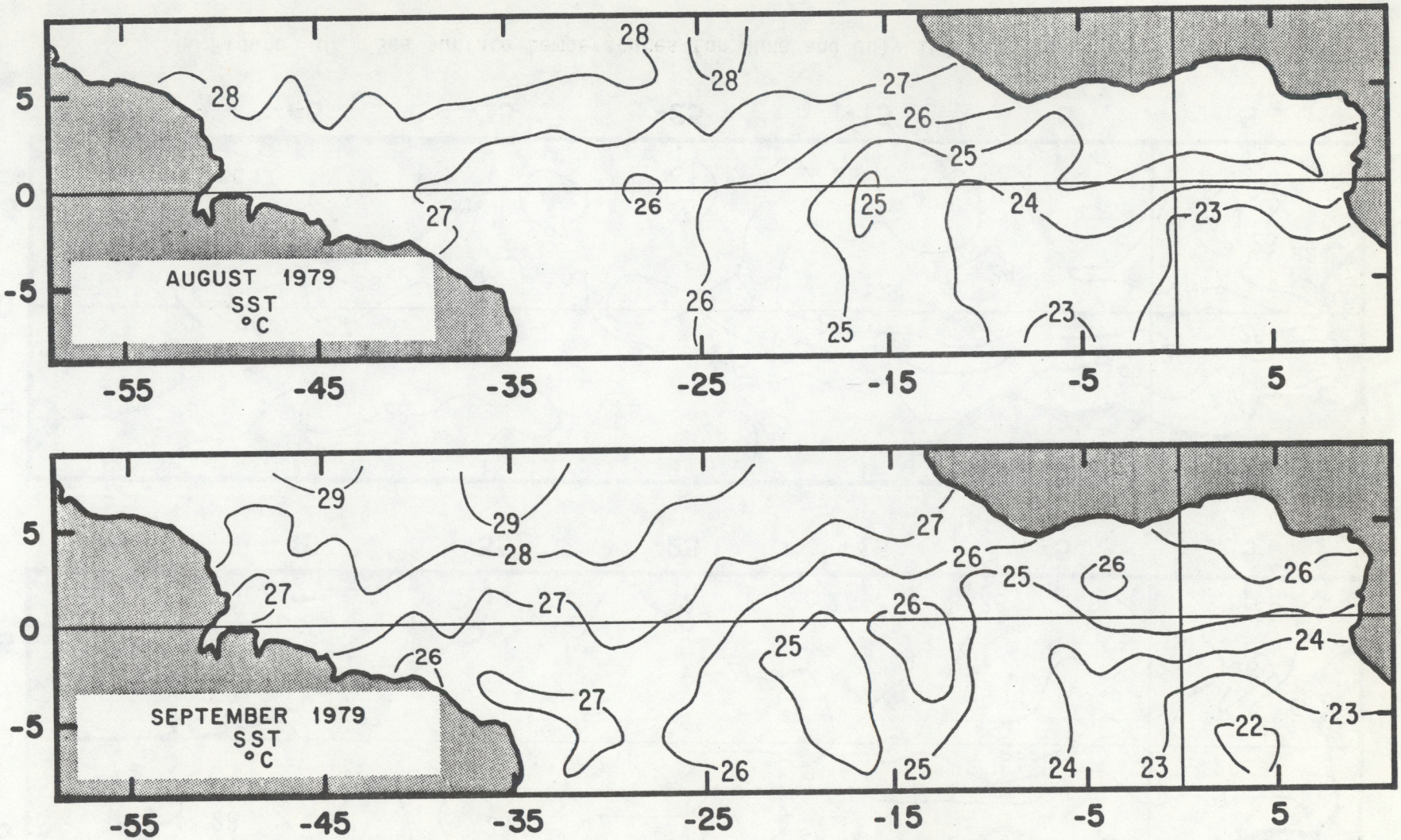

Figure 11. Sea surface temperatures for August and September 1979 (as in Figure 7).

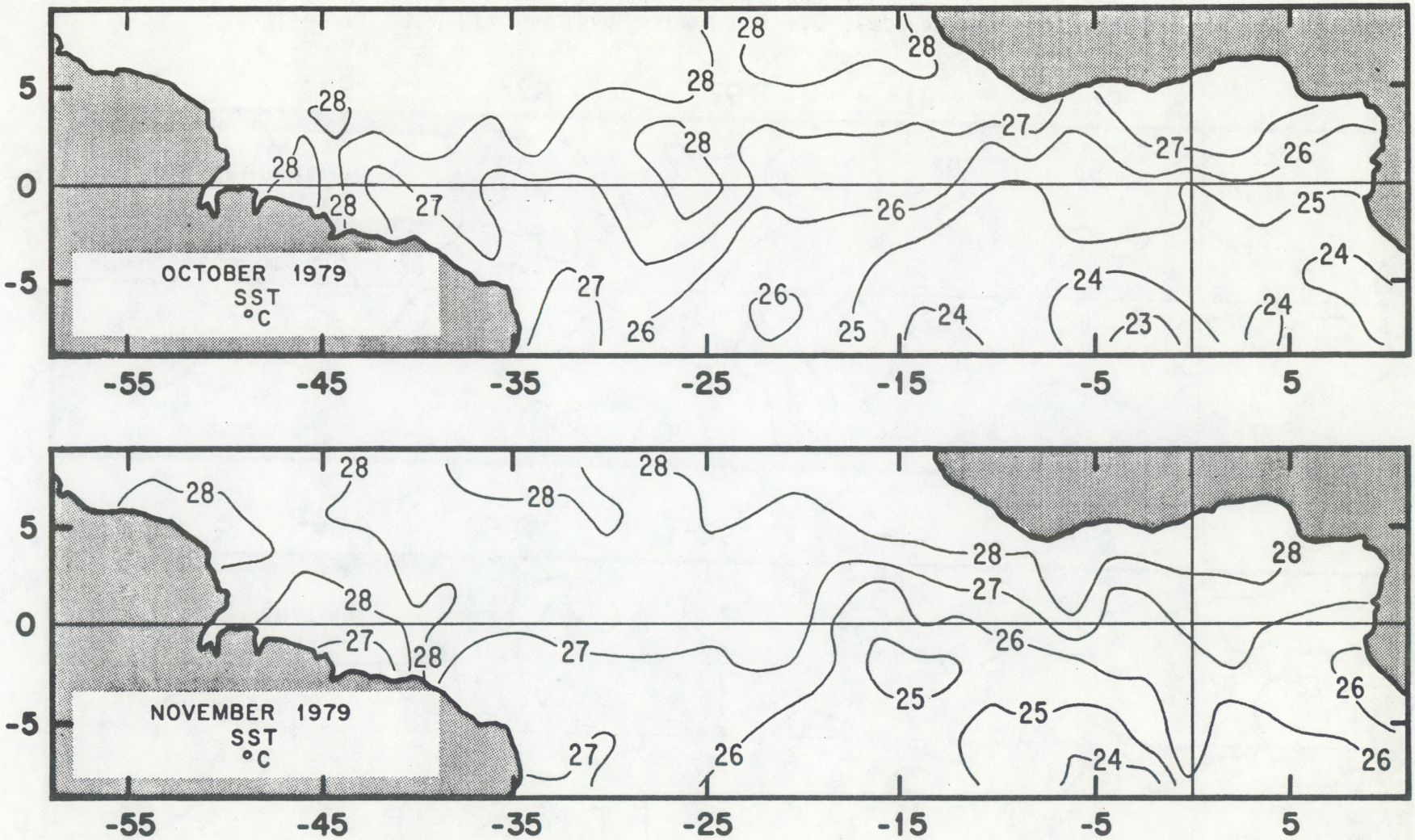

Figure 12. Sea surface temperatures for October and November 1979 (as in Figure 7).

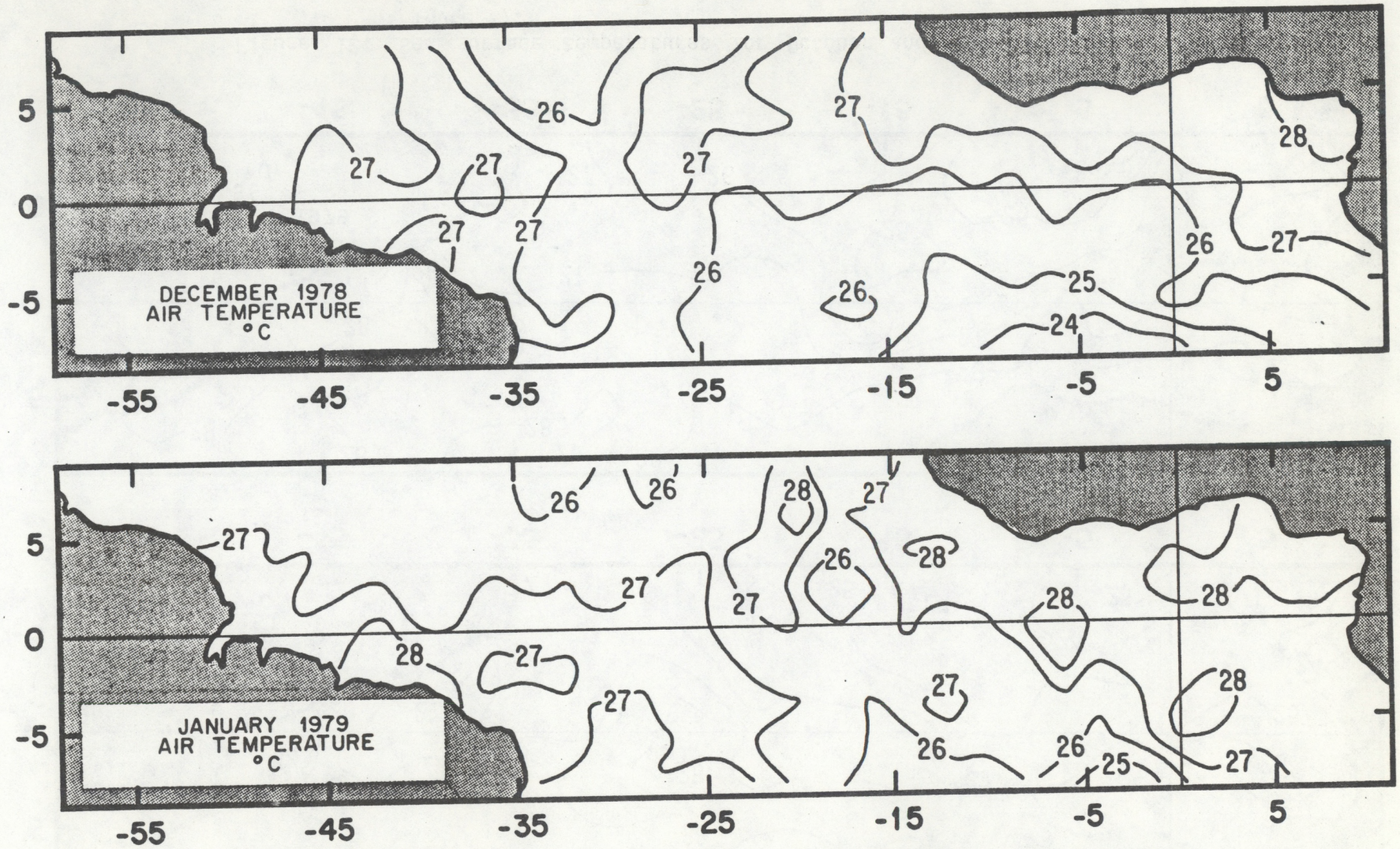

Figure 13. Monthly smoothed and edited air temperatures for December 1978 and January 1979, contoured every 1°C.

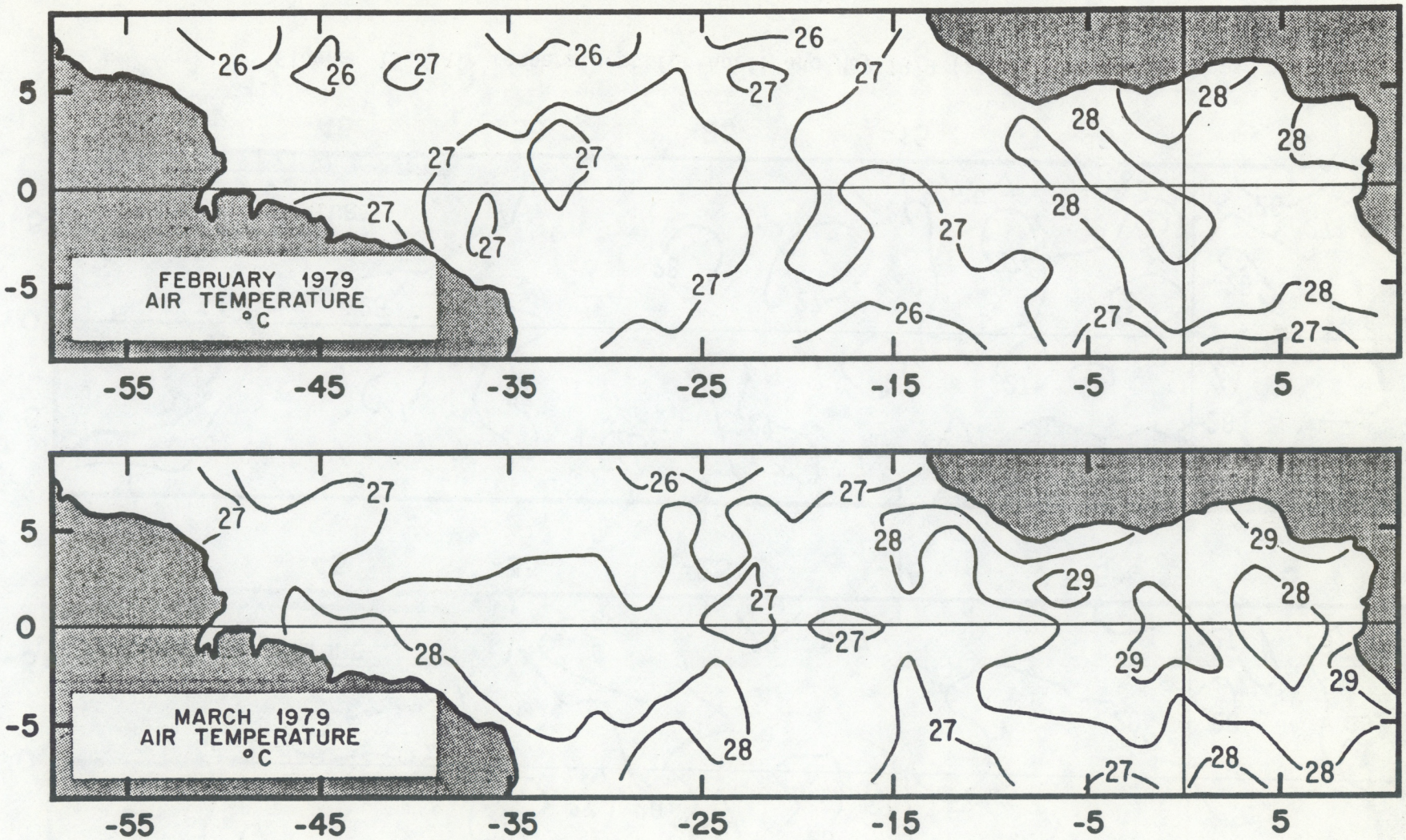

Figure 14. Air temperatures for February and March 1979 (as in Figure 13).

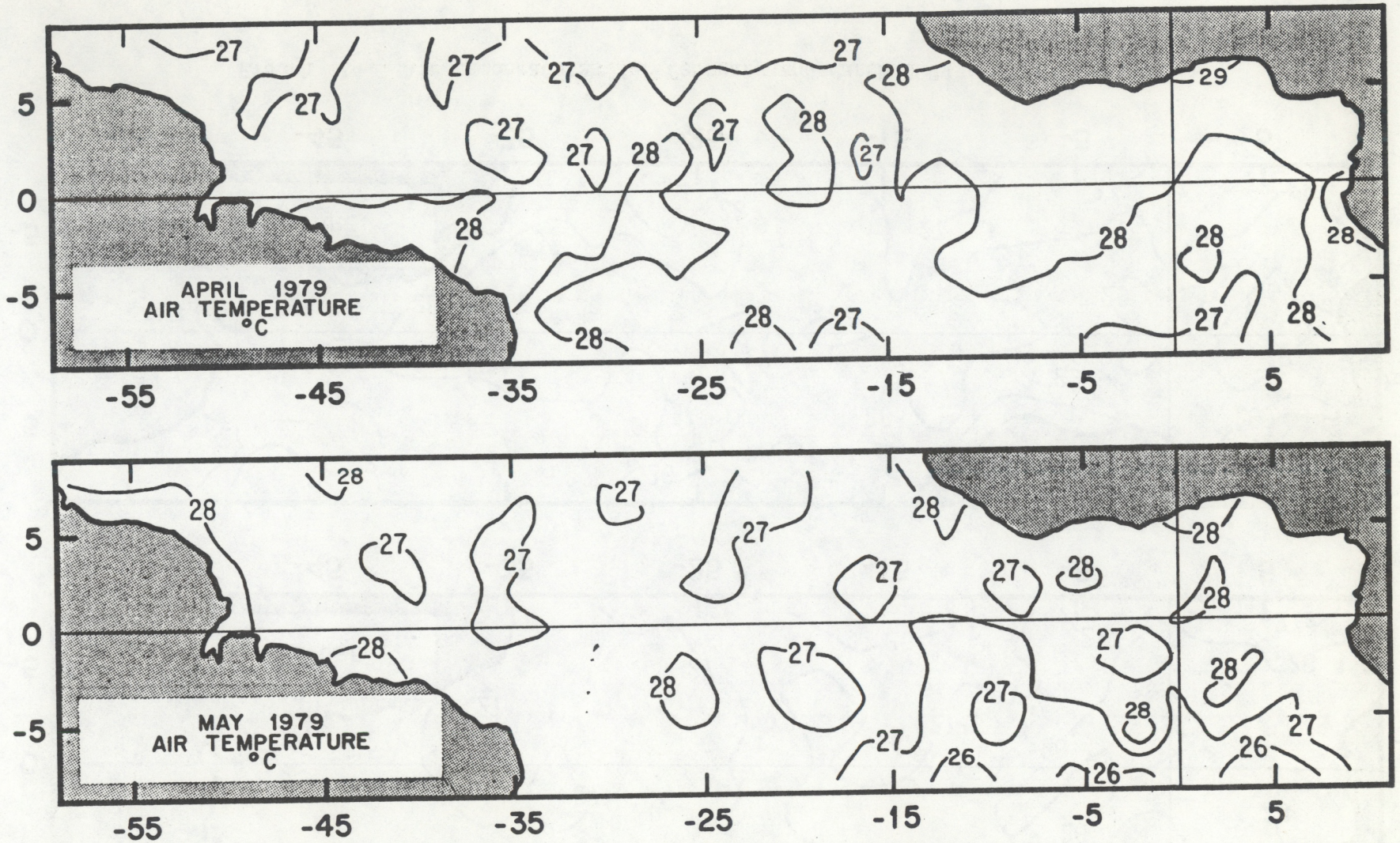

Figure 15. Air temperatures for April and May 1979 (as in Figure 13).

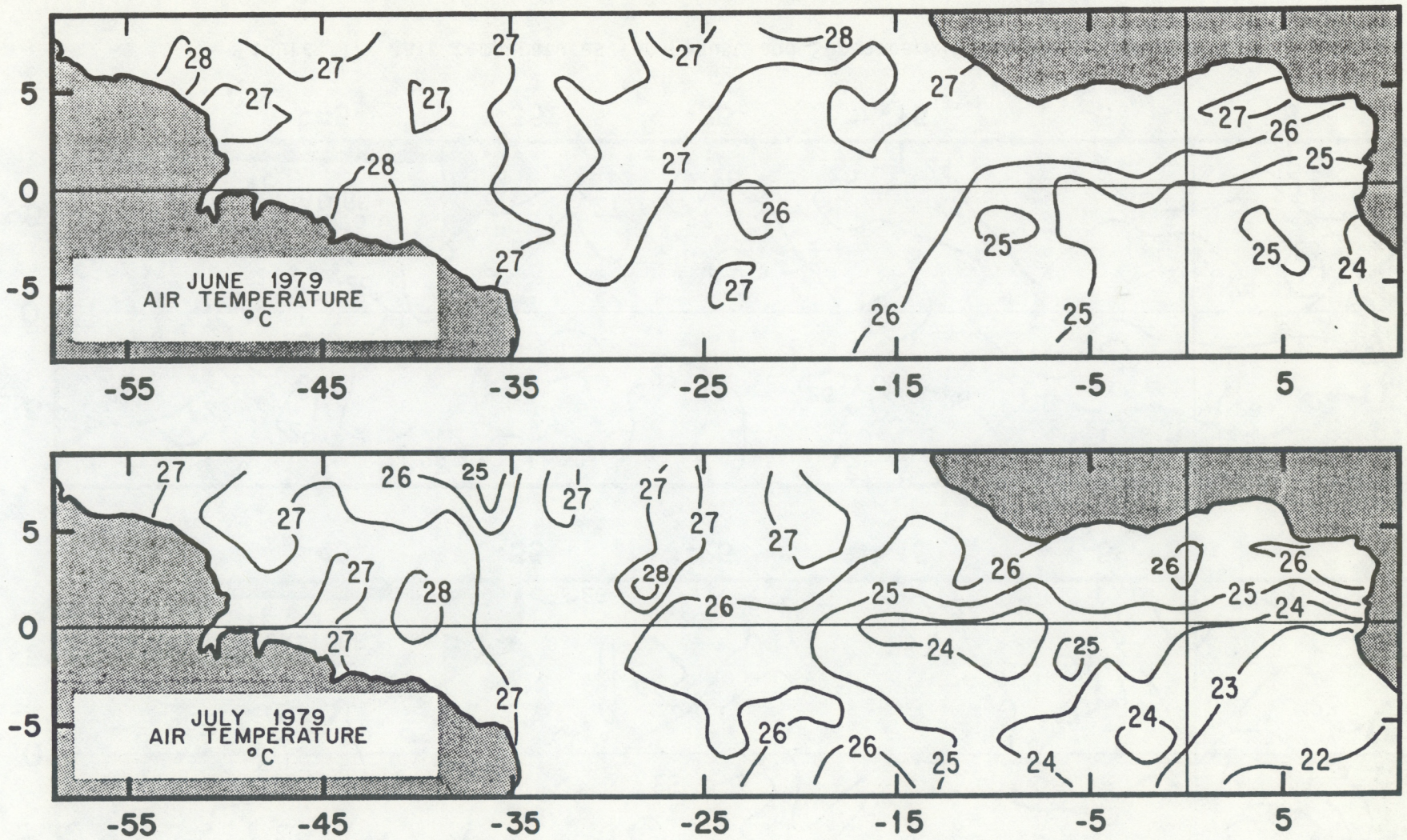

Figure 16. Air temperatures for June and July 1979 (as in Figure 13).

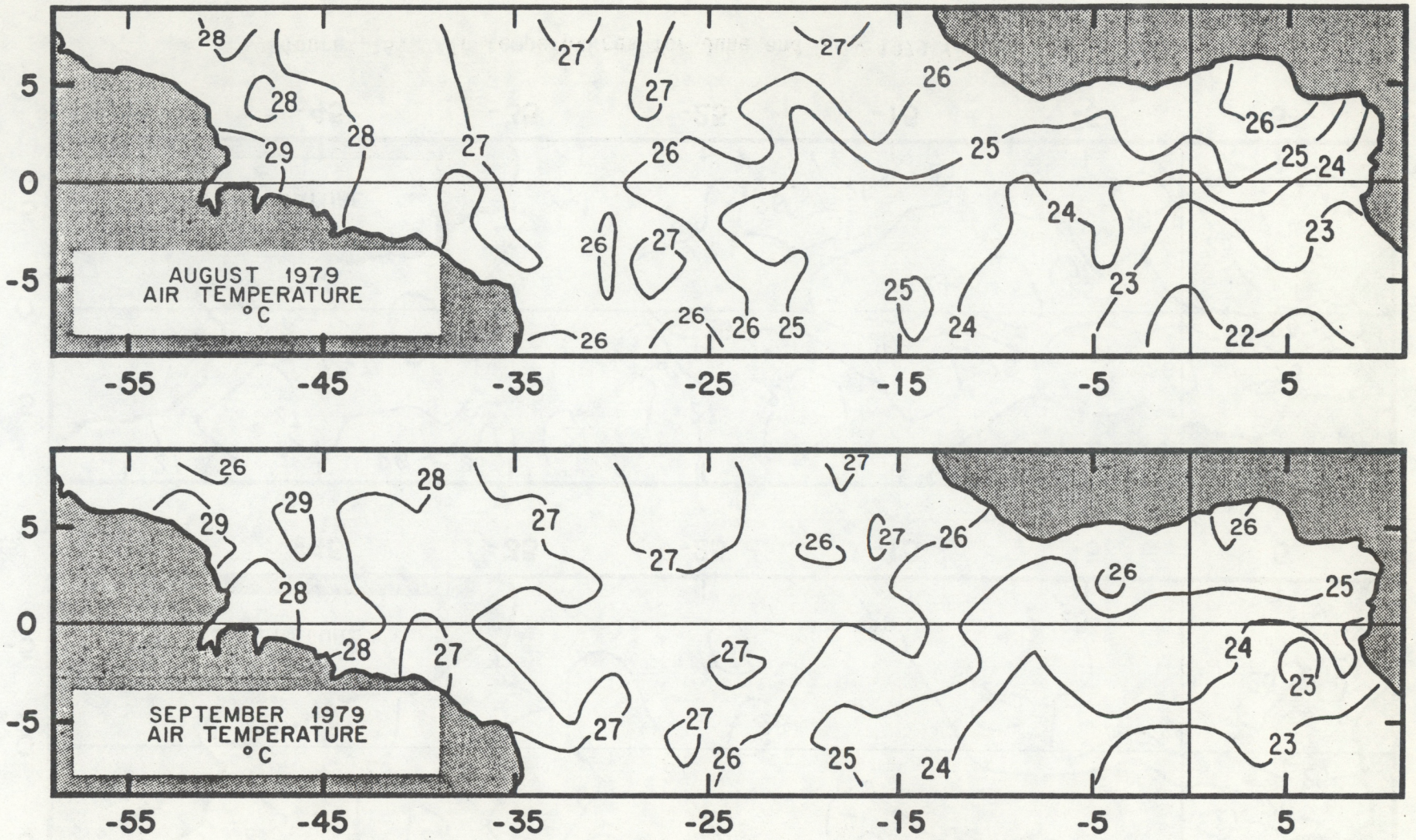

Figure 17. Air temperatures for August and September 1979 (as in Figure 13).

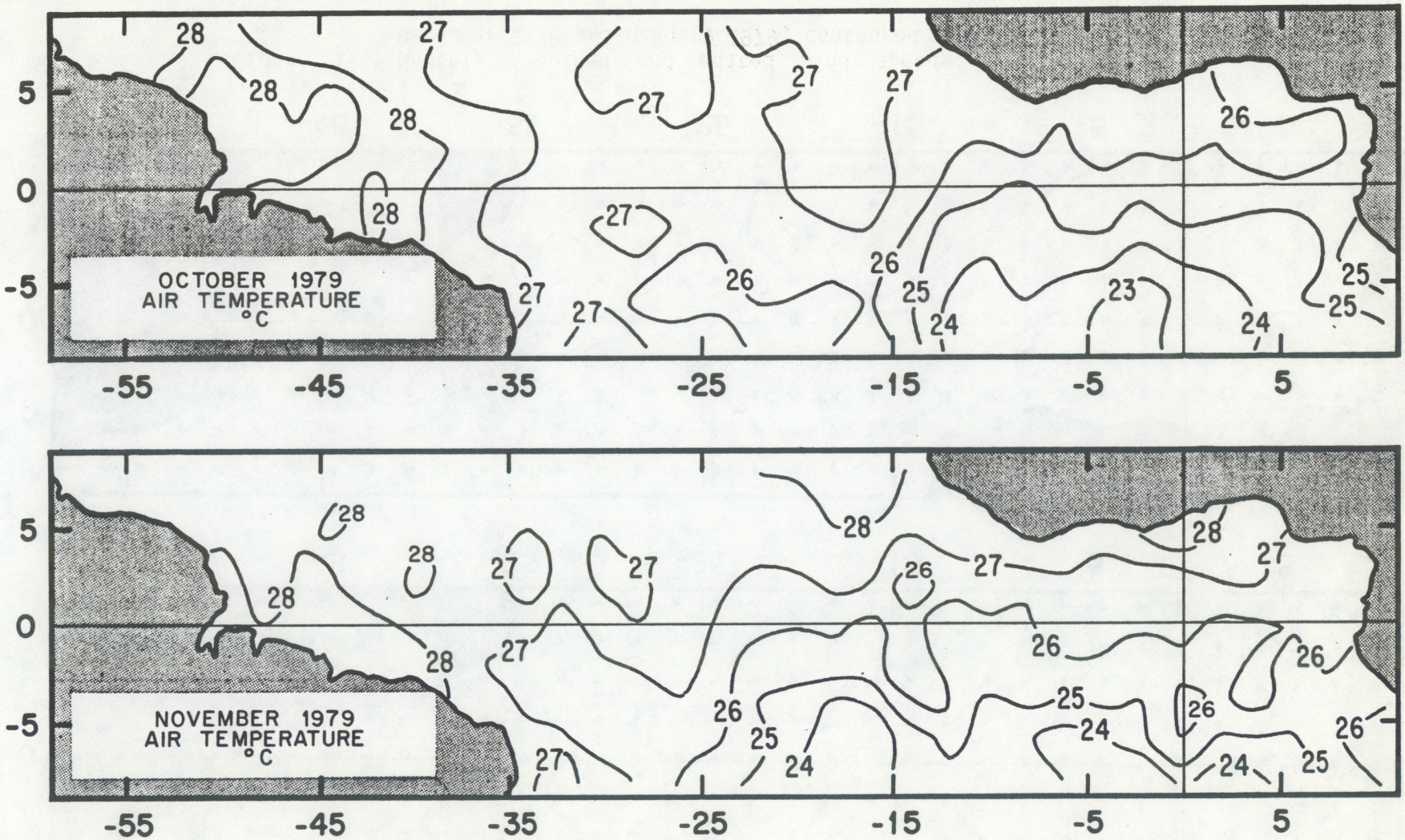

Figure 18. Air temperatures for October and November 1979 (as in Figure 13).

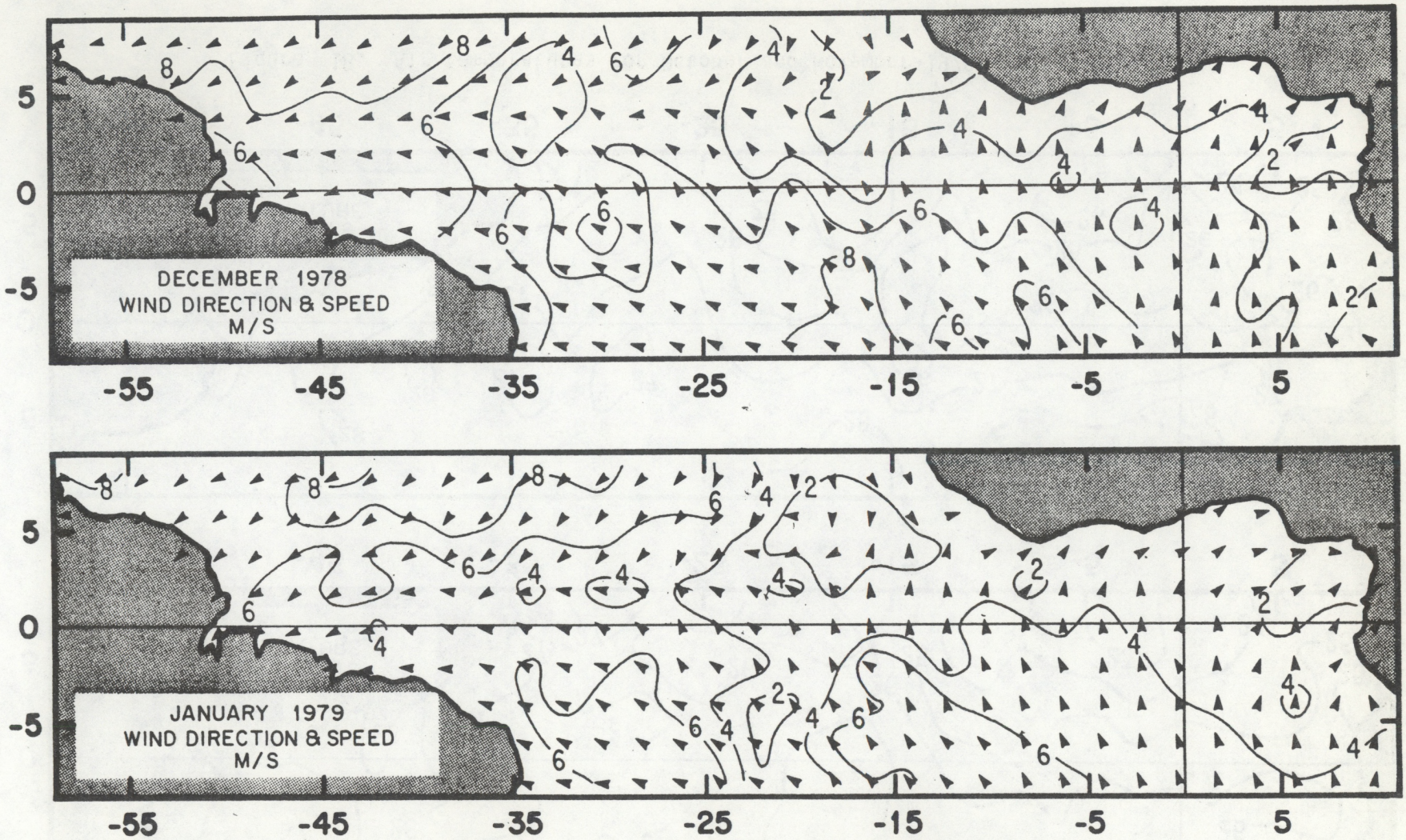

Figure 19. Monthly smoothed and edited wind speeds and directions for December 1978 and January 1979, contoured every 2 m/s.

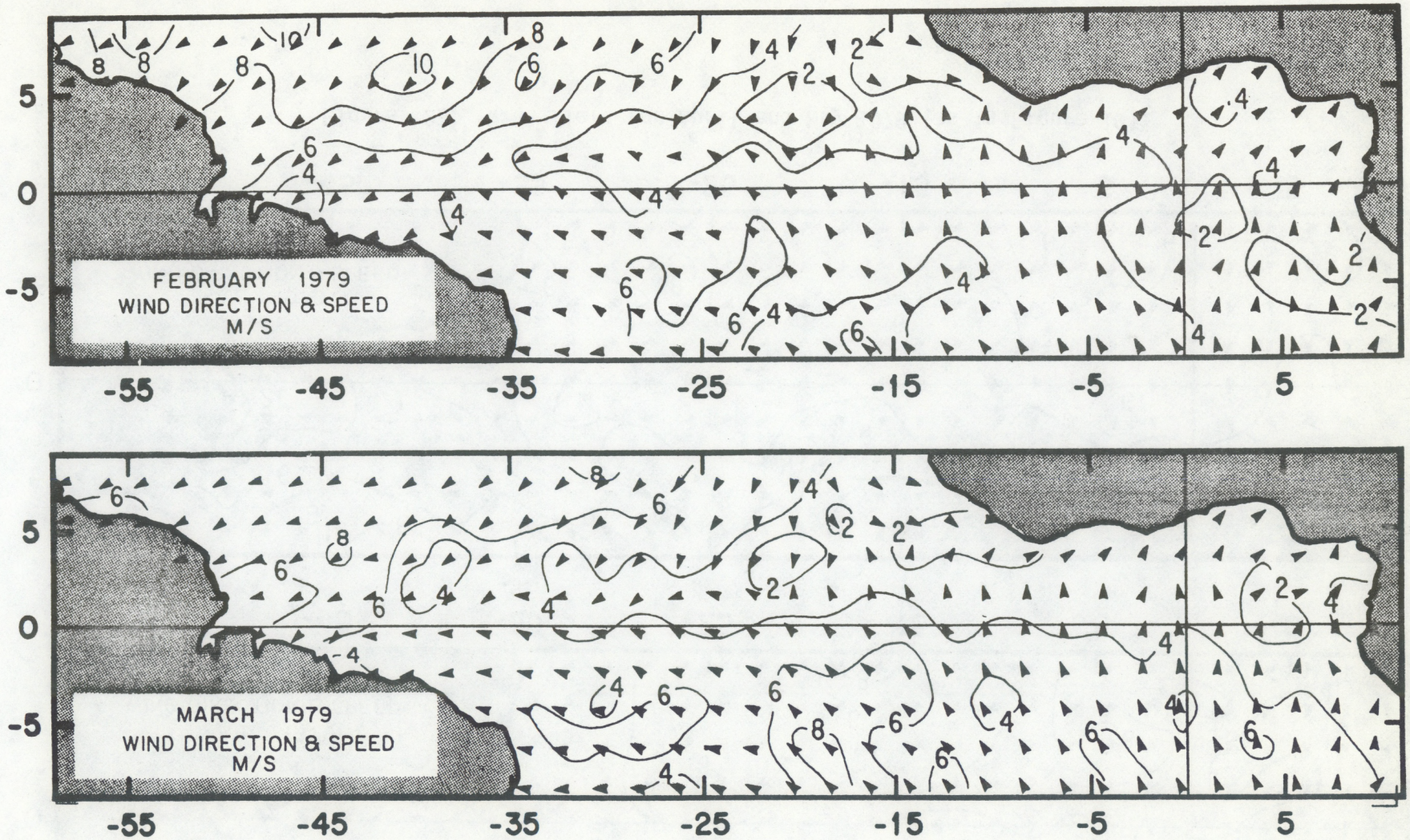

Figure 20. Wind field for February and March 1979 (as in Figure 19).

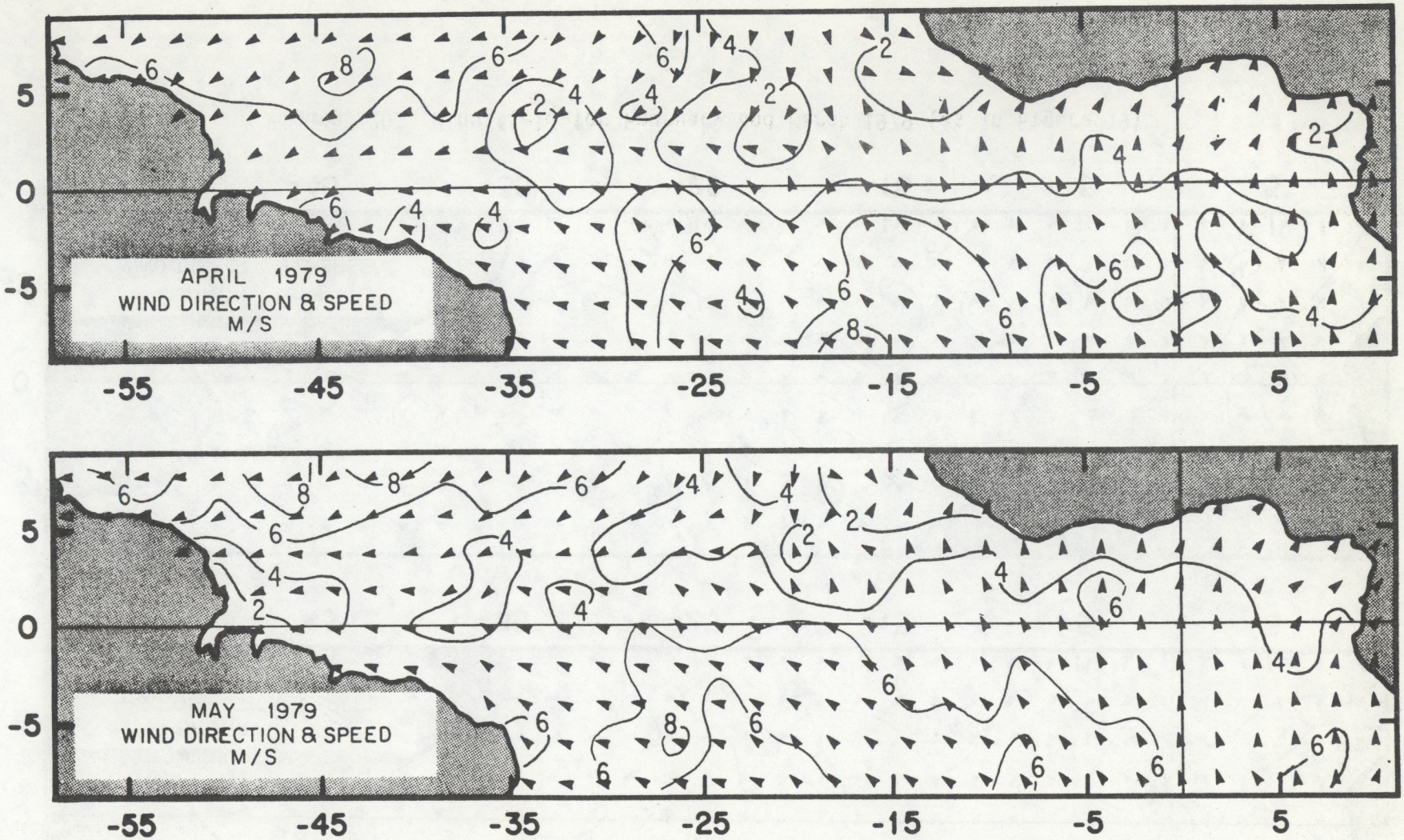

Figure 21. Wind field for April and May 1979 (as in Figure 19).

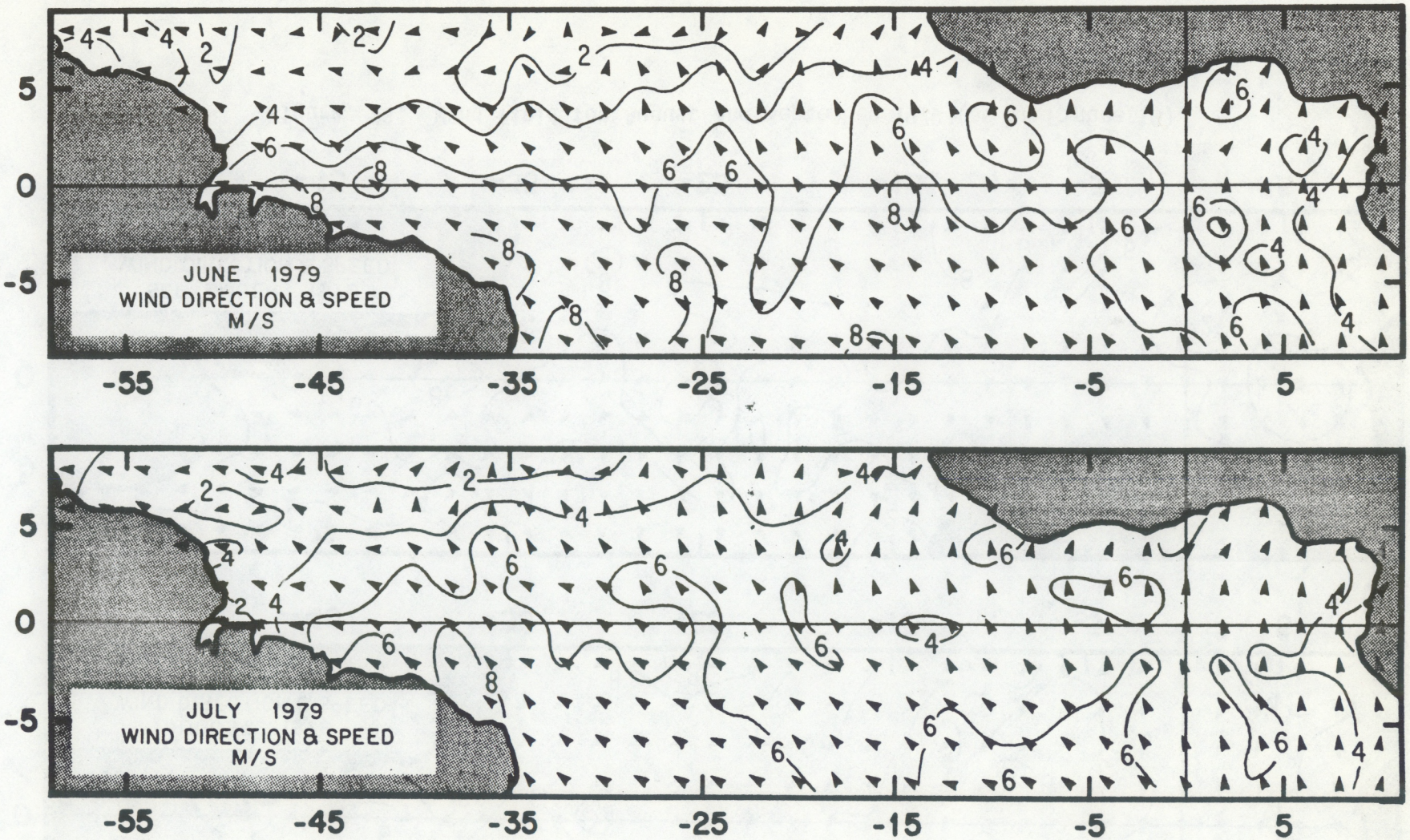

Figure 22. Wind field for June and July 1979 (as in Figure 19).

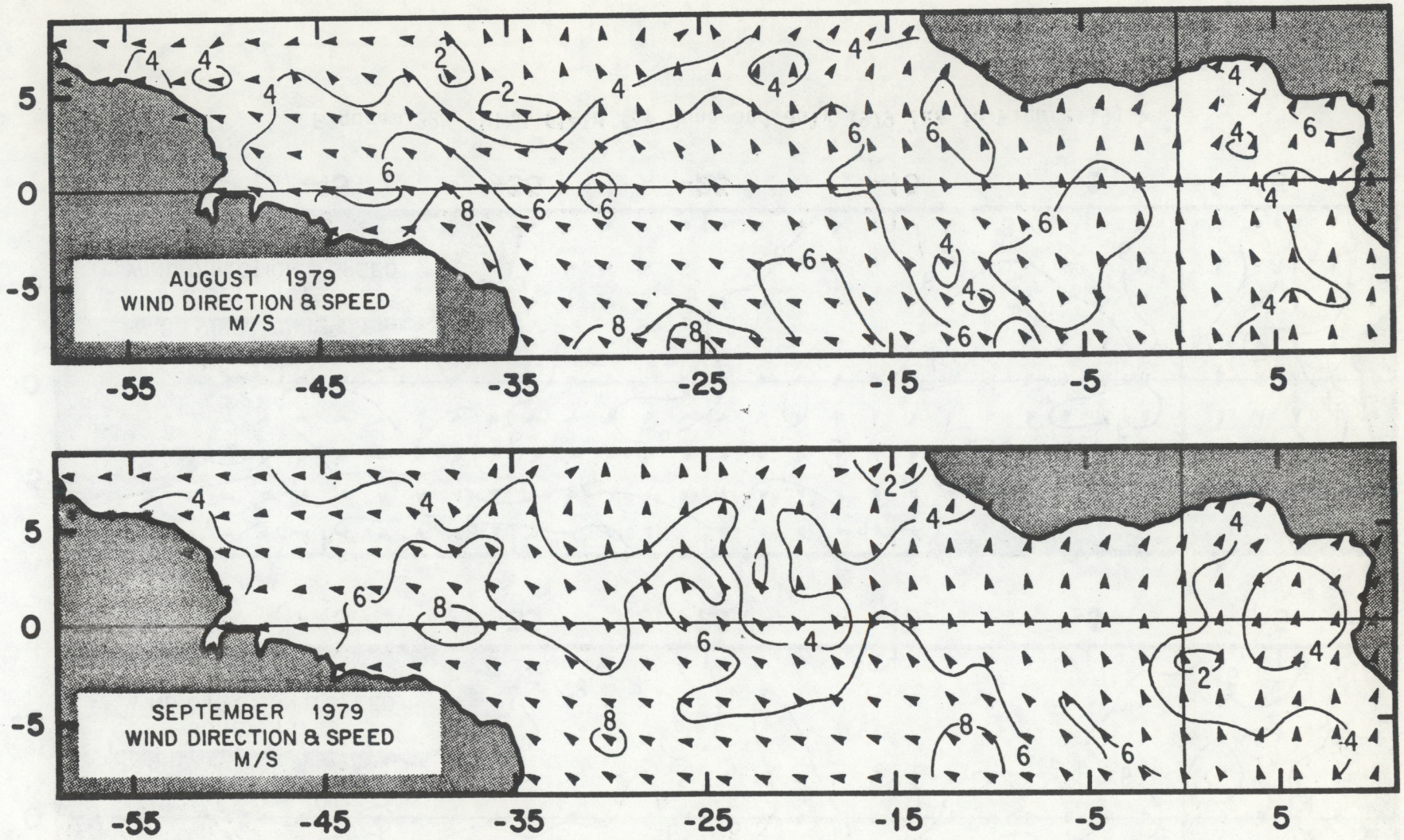

Figure 23. Wind field for August and September 1979 (as in Figure 19).

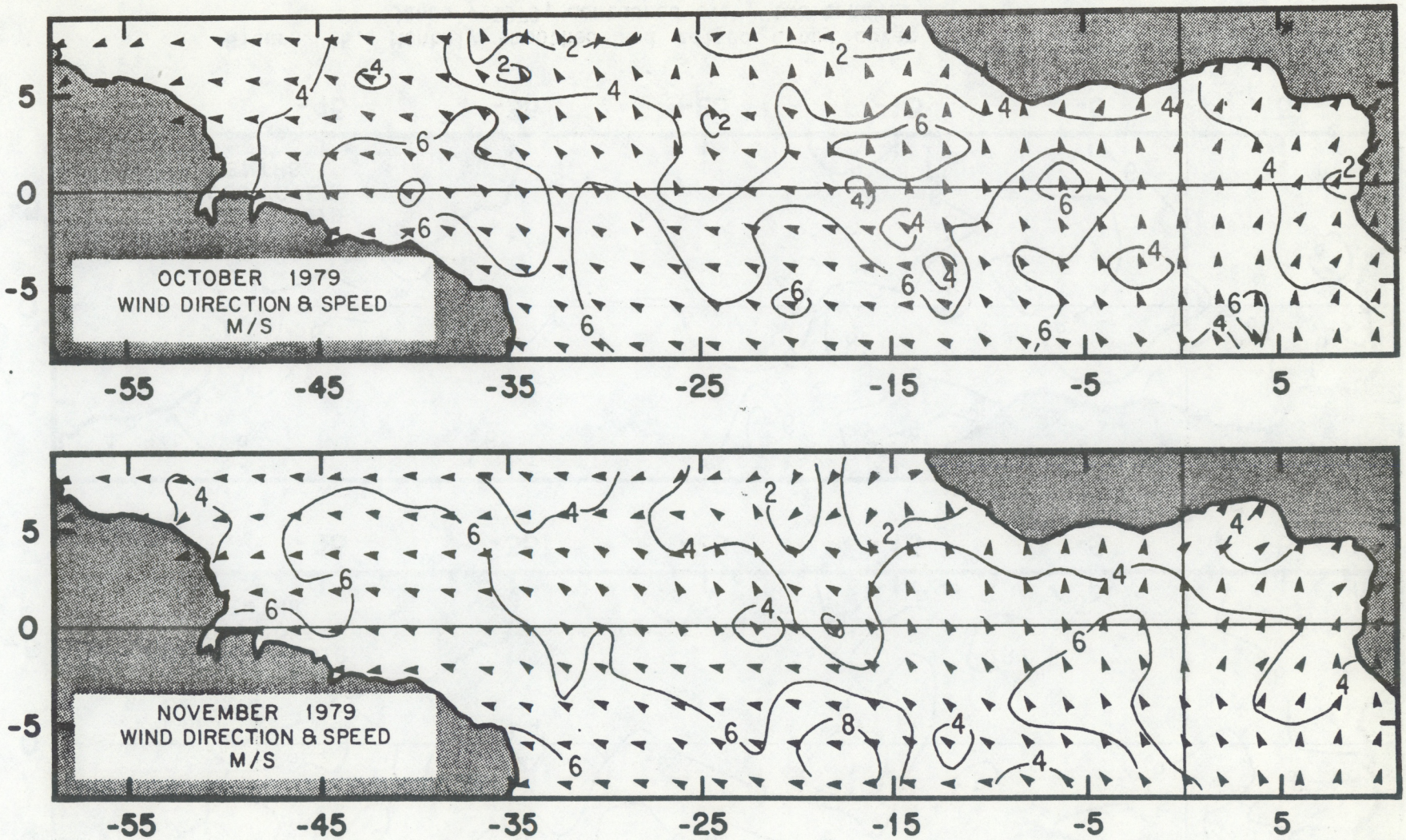

Figure 24. Wind field for October and November 1979 (as in Figure 19).

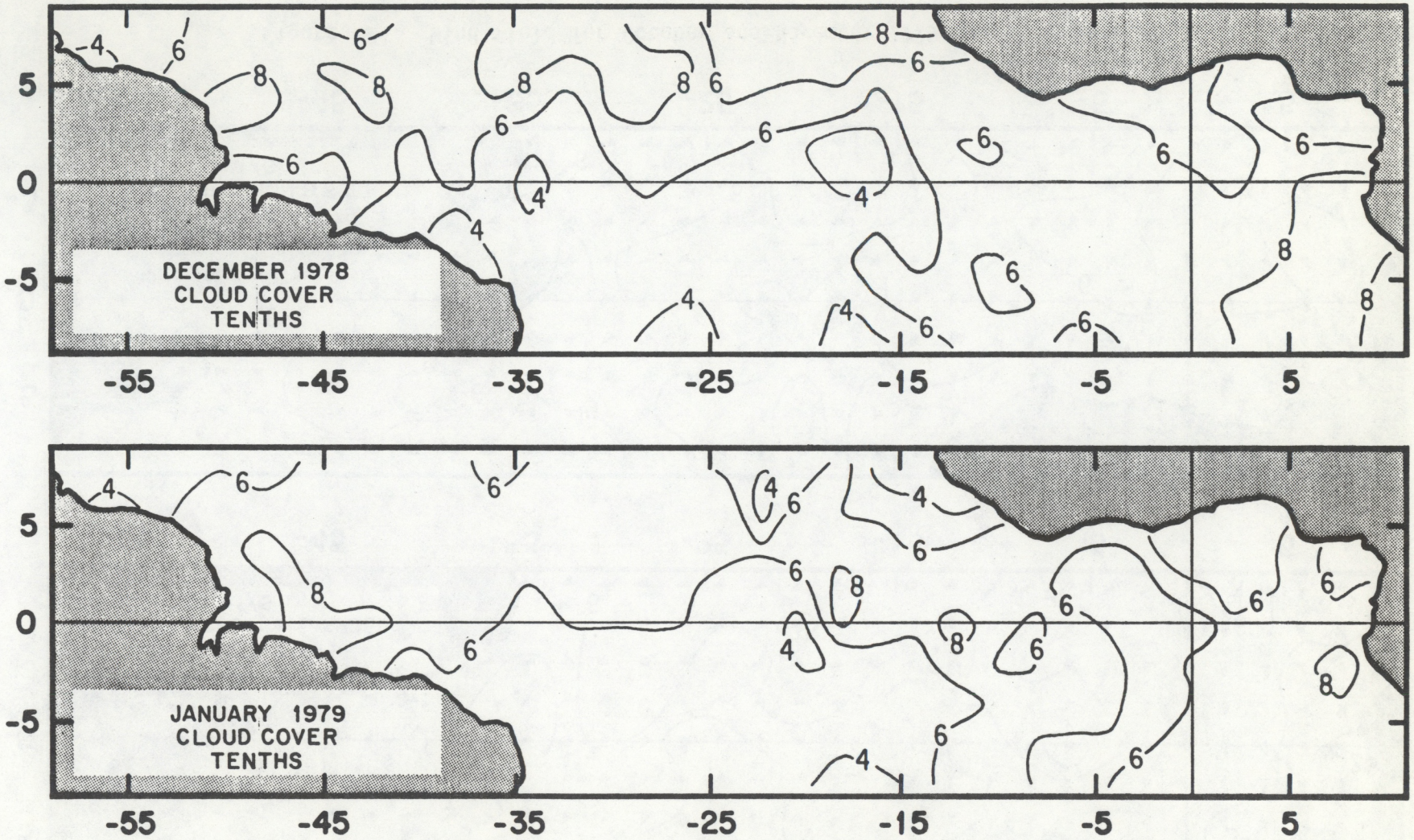

Figure 25. Monthly smoothed and edited cloud cover for December 1978 and January 1979, contoured every two-tenths.

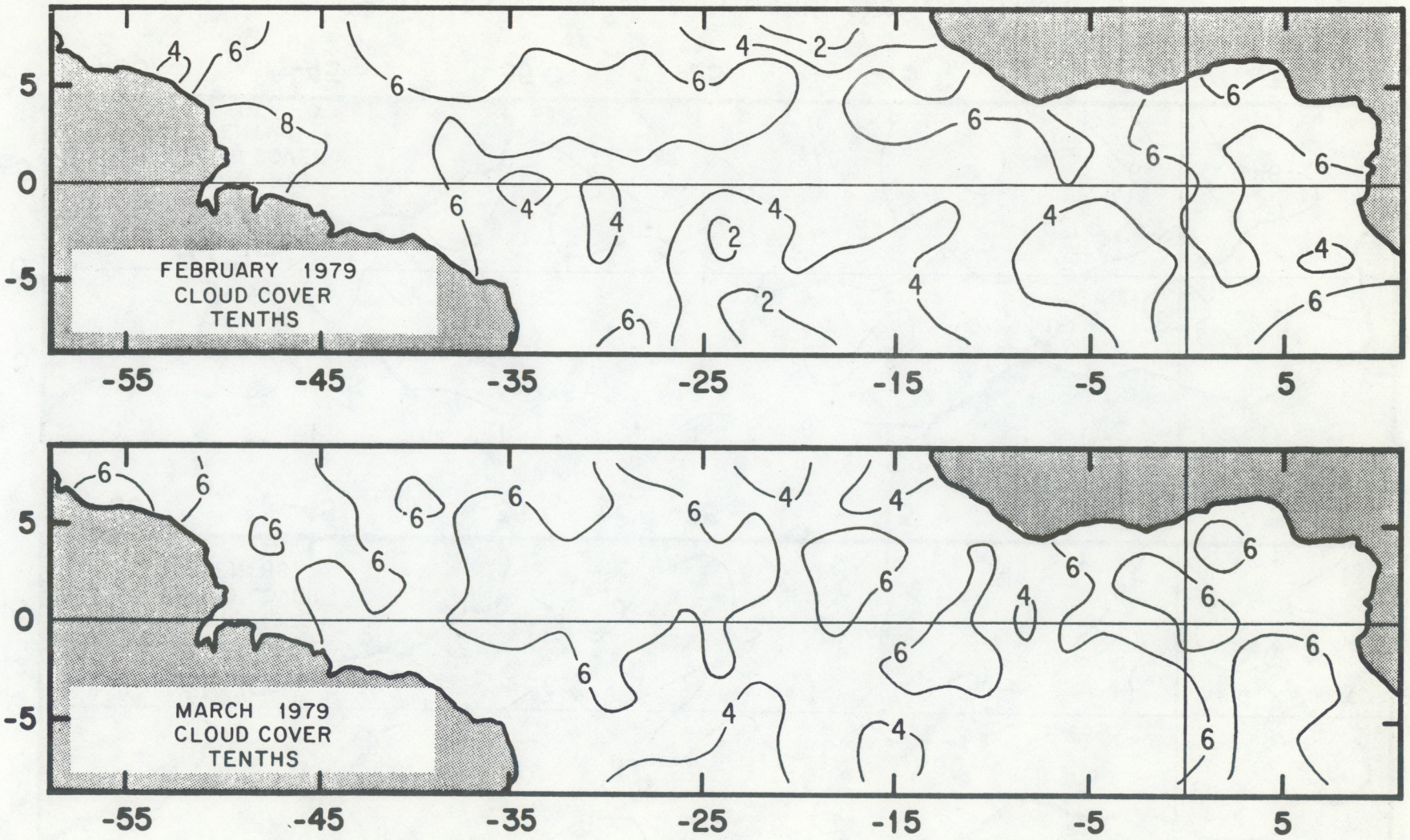

Figure 26. Cloud cover for February and March 1979 (as in Figure 25).

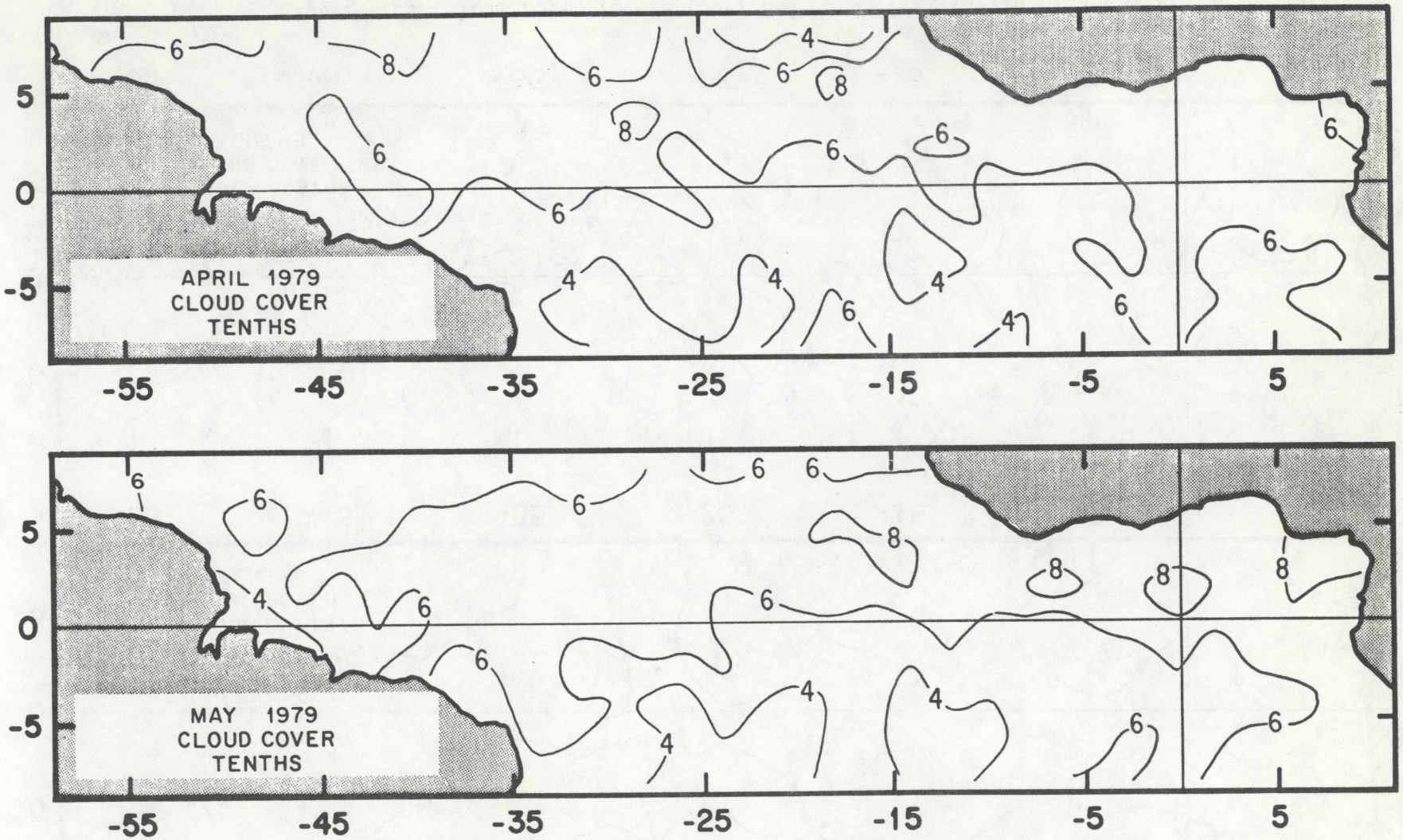

Figure 27. Cloud cover for April and May 1979 (as in Figure 25).

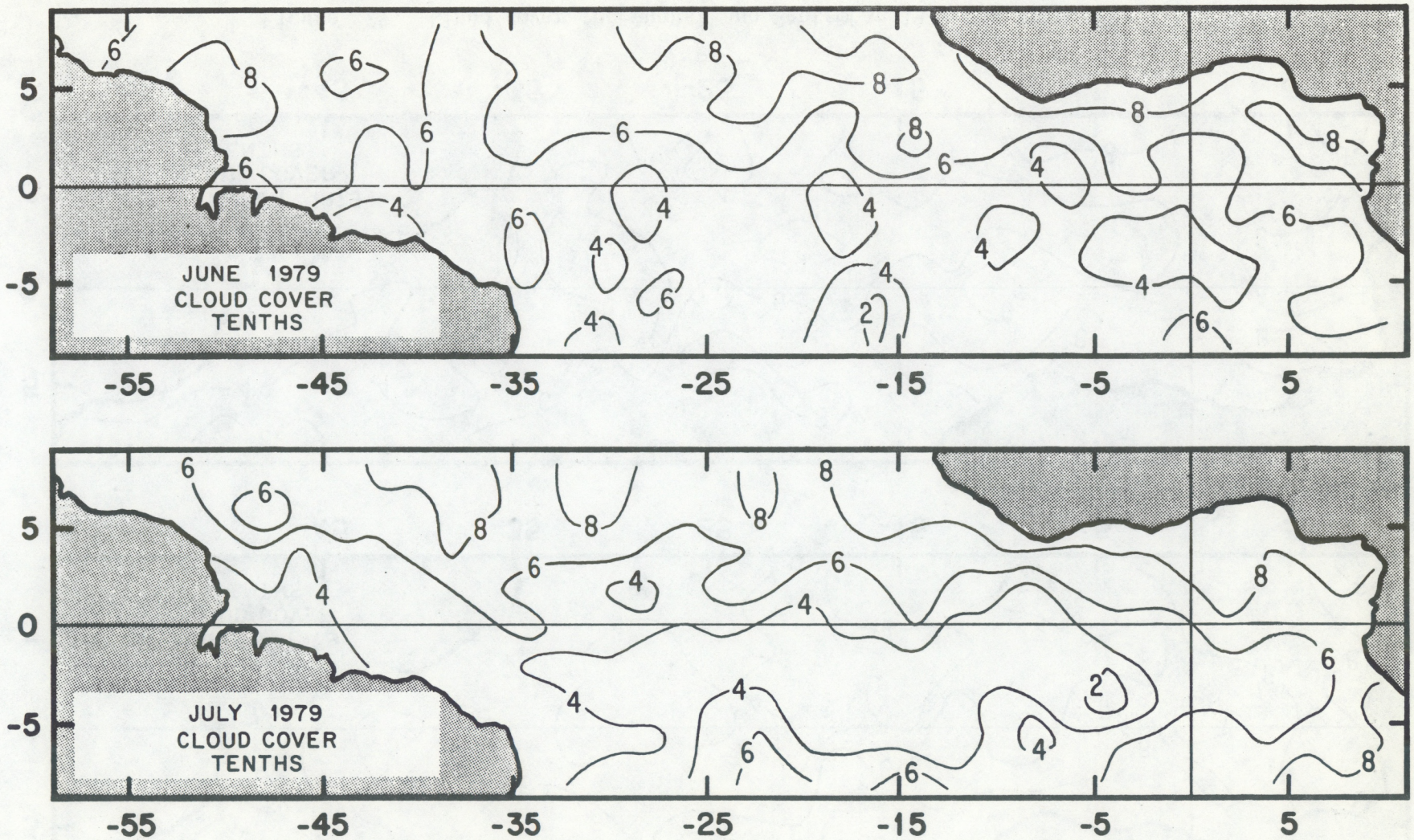

Figure 28. Cloud cover for June and July 1979 (as in Figure 25).

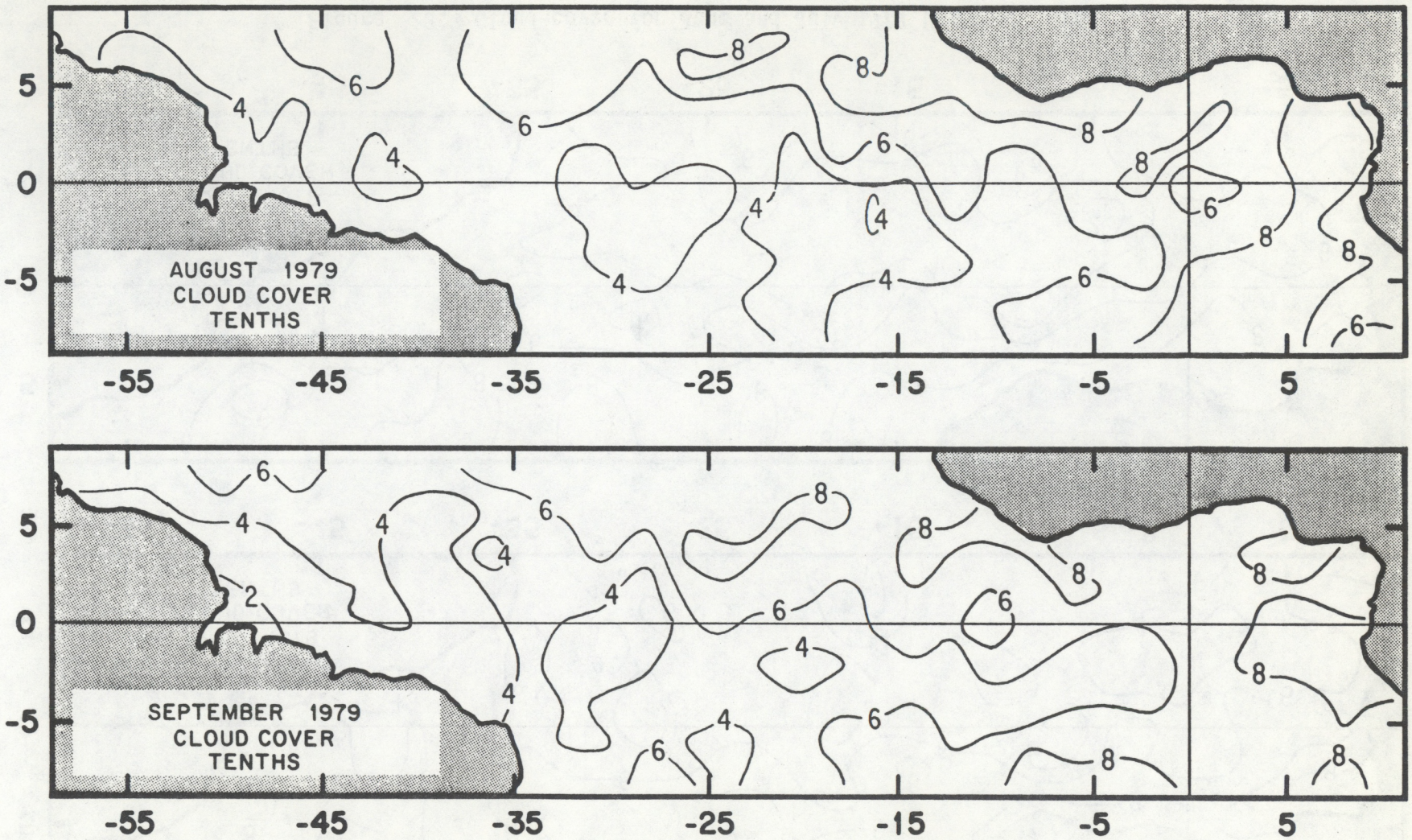

Figure 29. Cloud cover for August and September 1979 (as in Figure 25).

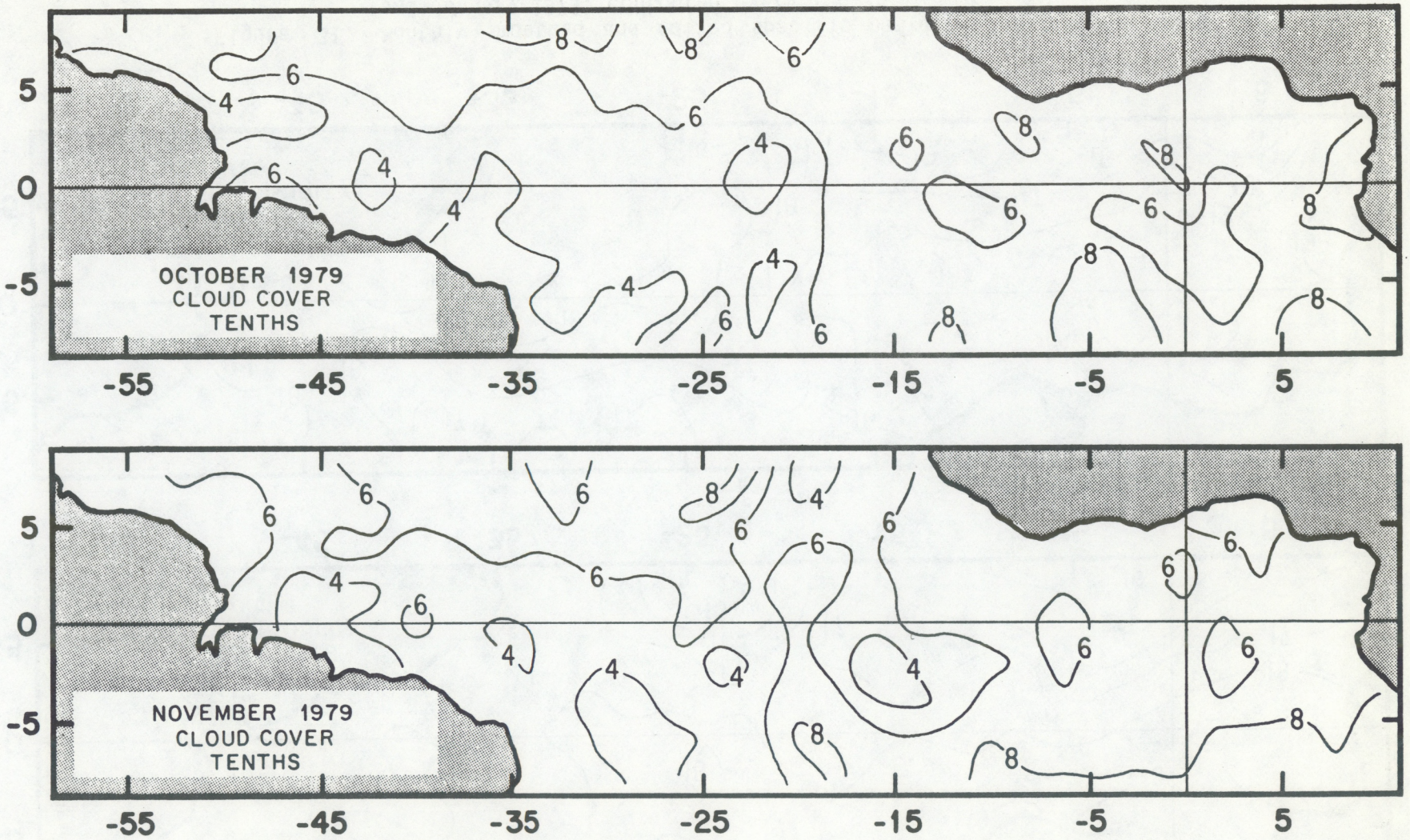

Figure 30. Cloud cover for October and November 1979 (as in Figure 25).

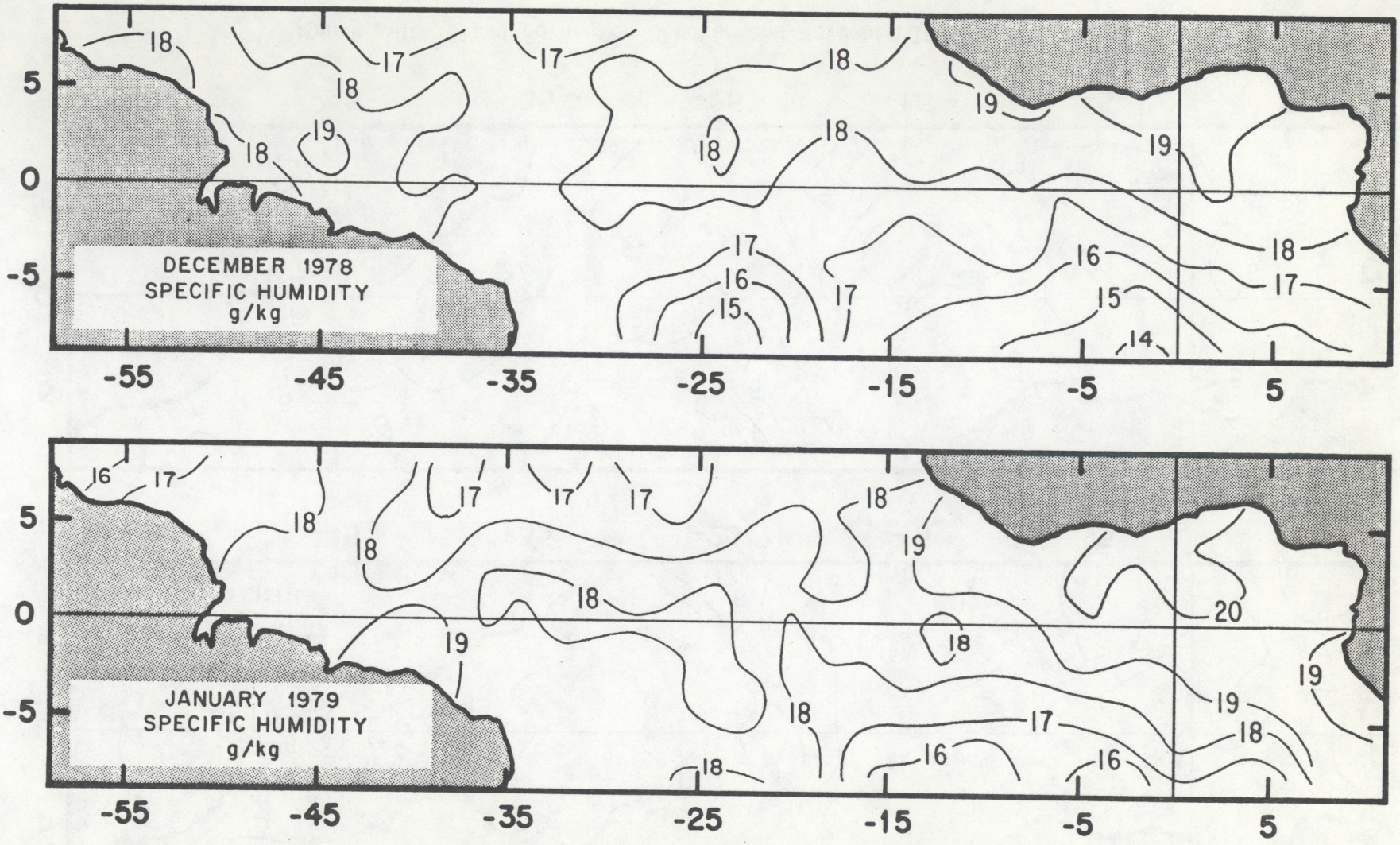

Figure 31. Monthly smoothed and edited specific humidity for December 1978 and January 1979, contoured every 1 g/kg.

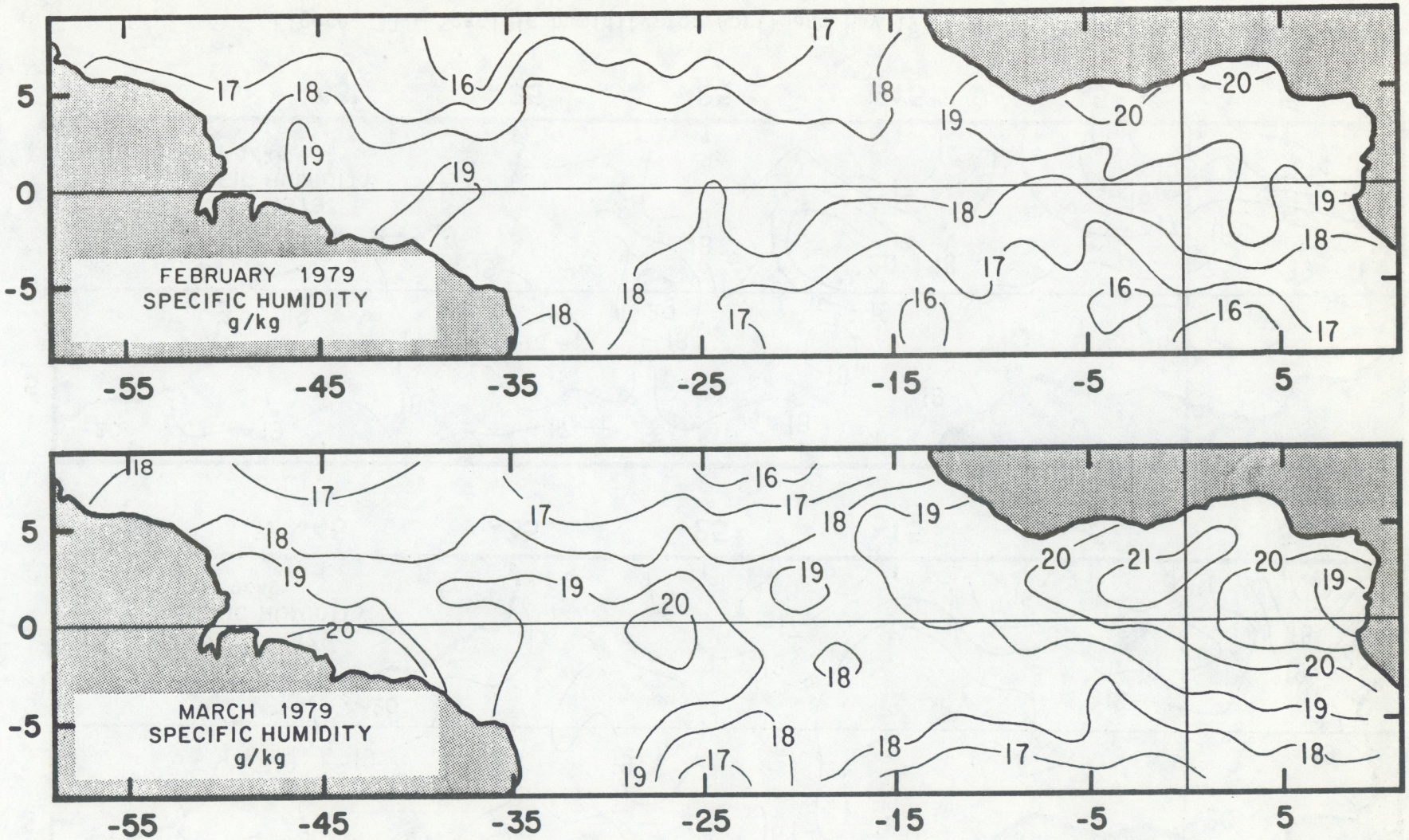

Figure 32. Specific humidity for February and March 1979 (as in Figure 31).

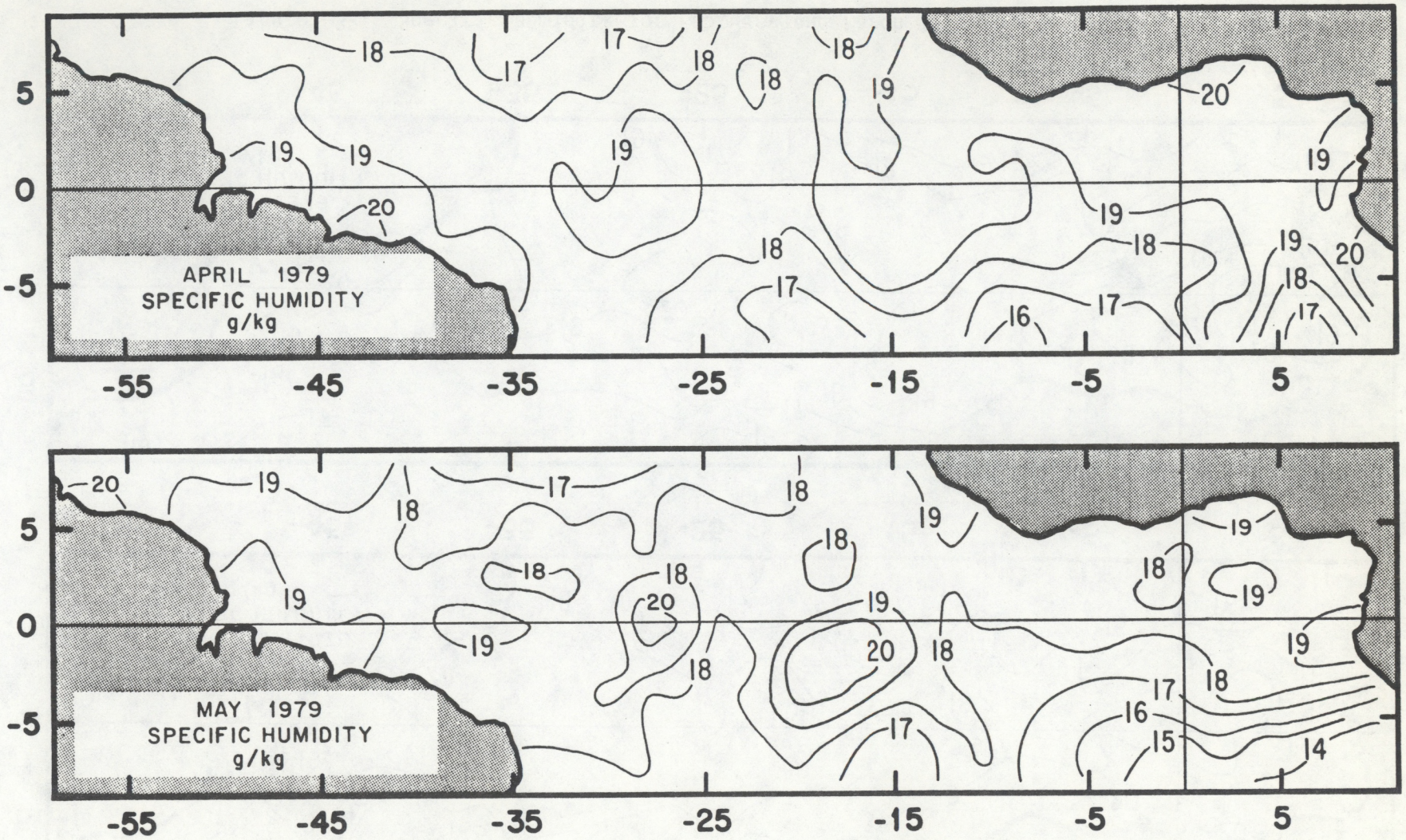

Figure 33. Specific humidity for April and May 1979 (as in Figure 31).

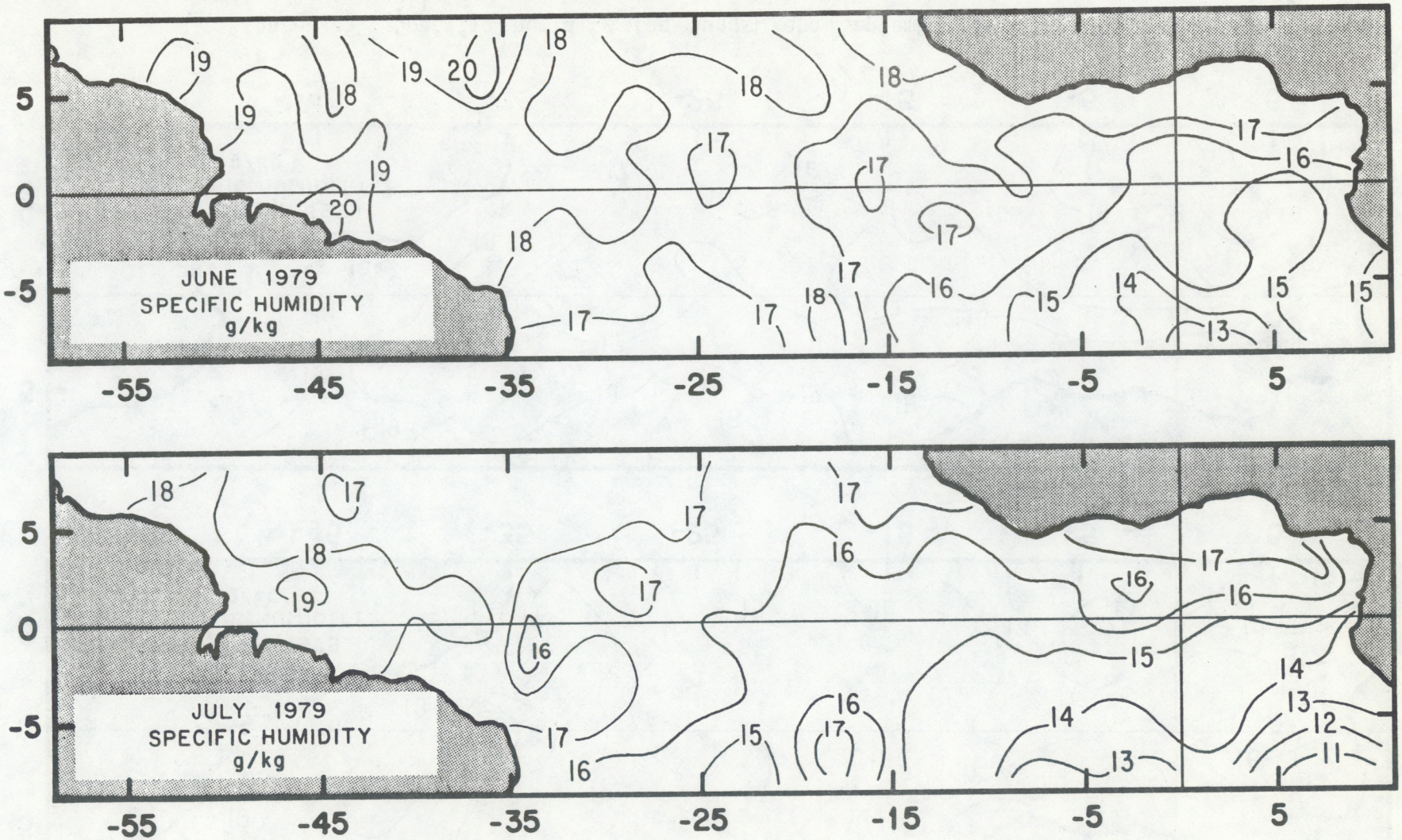

Figure 34. Specific humidity for June and July 1979 (as in Figure 31).

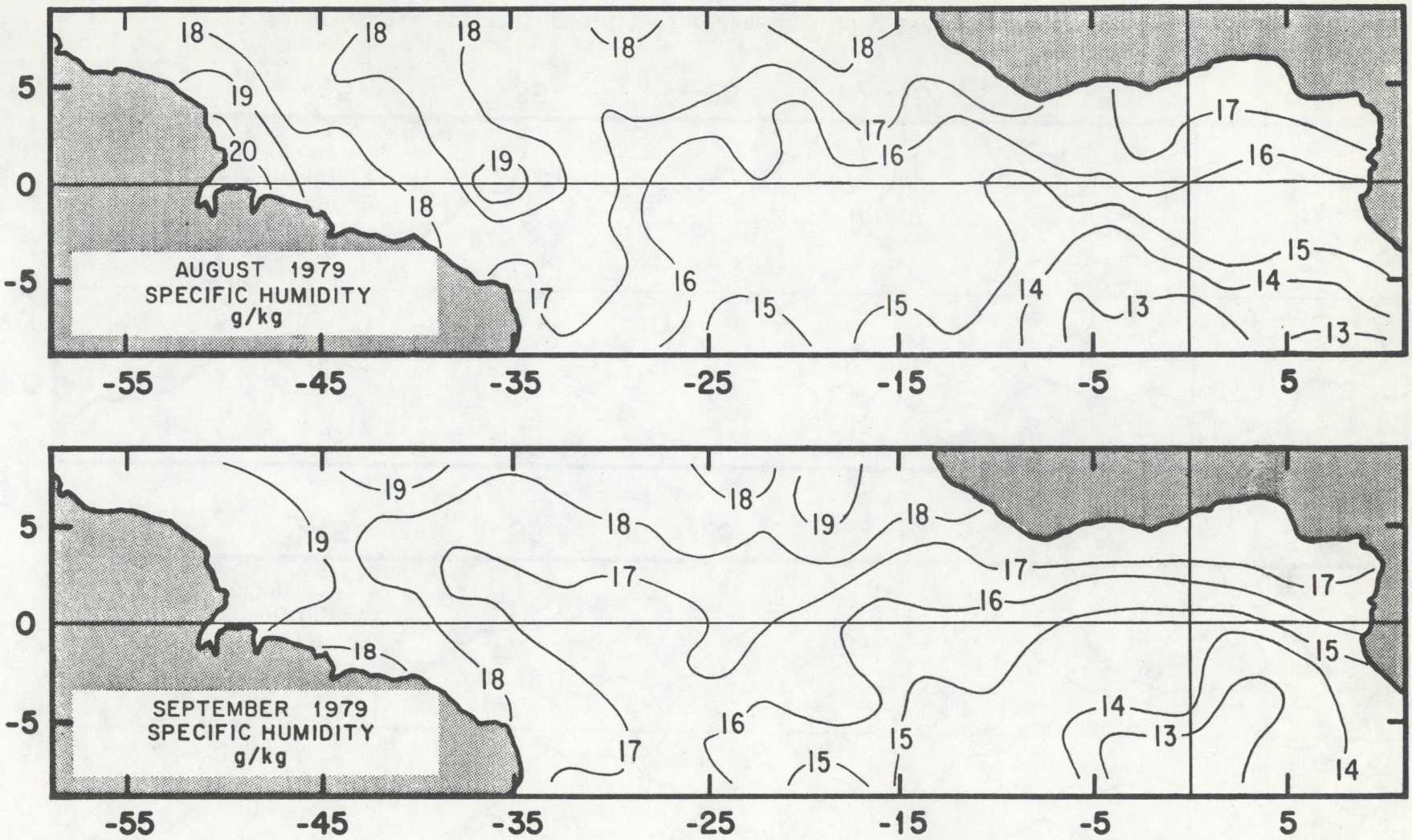

Figure 35. Specific humidity for August and September 1979 (as in Figure 31).

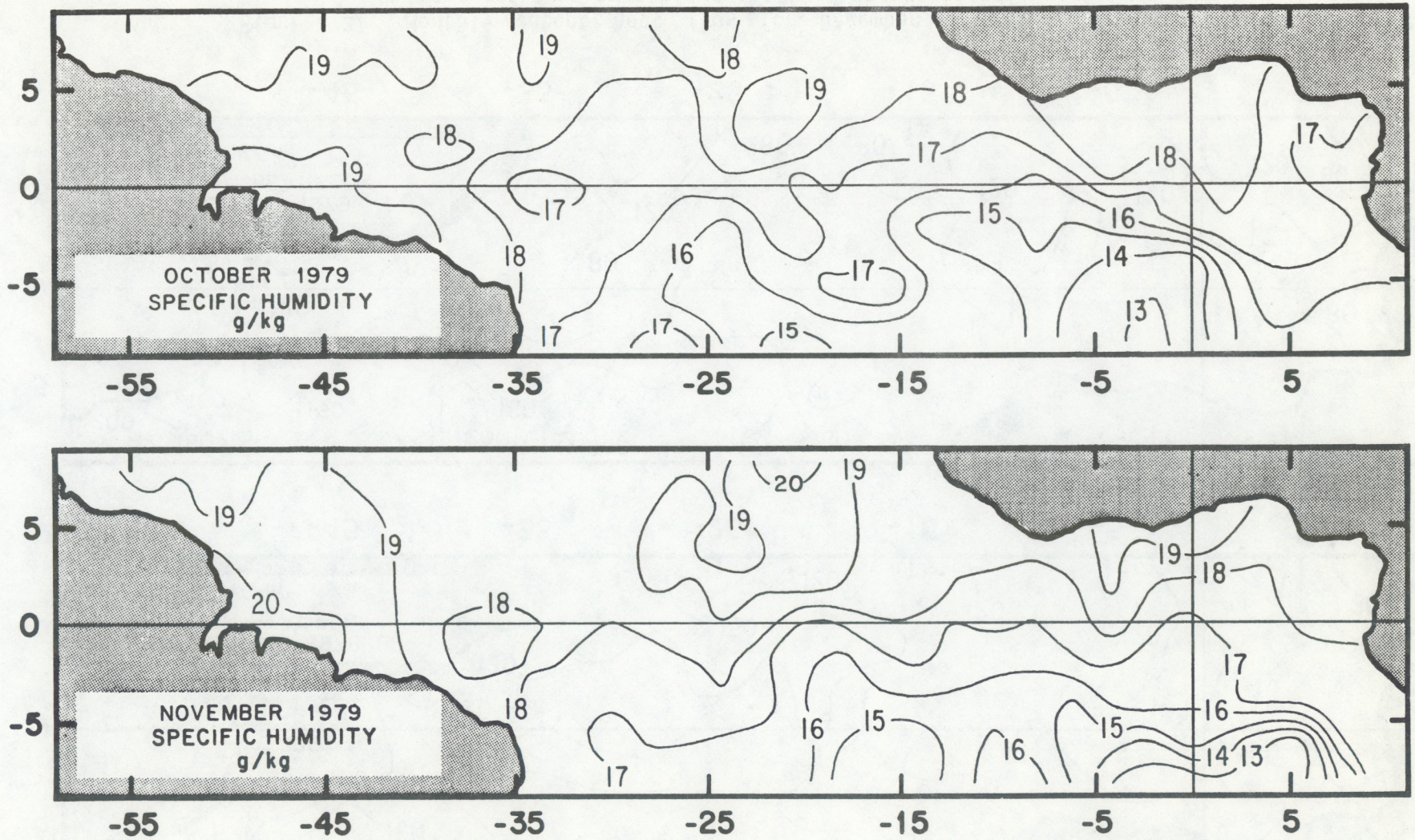

Figure 36. Specific humidity for October and November 1979 (as in Figure 31).

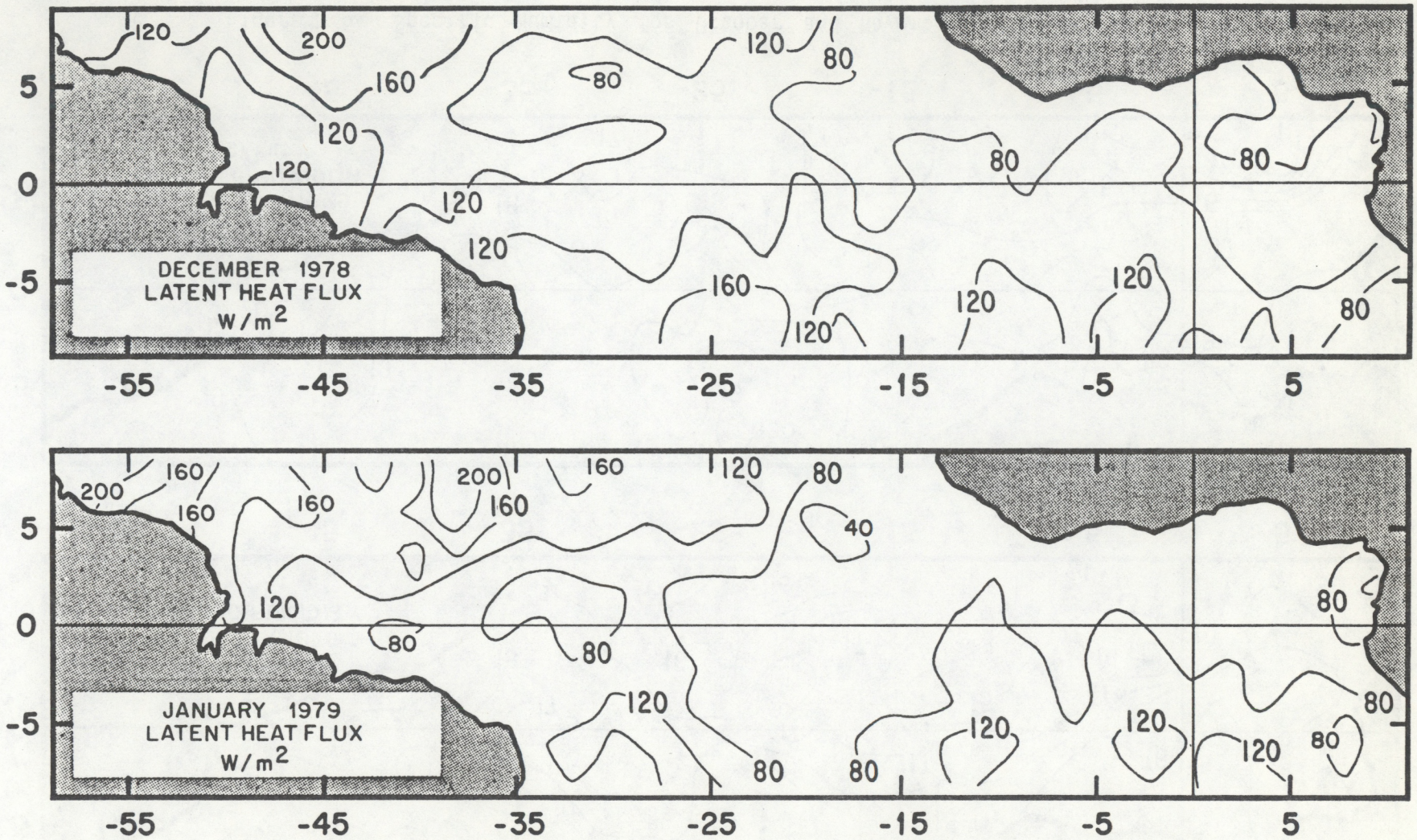

Figure 37. Monthly latent heat flux for December 1978 and January 1979 (computed from smoothed and edited observations), contoured every 40 W/m^2.

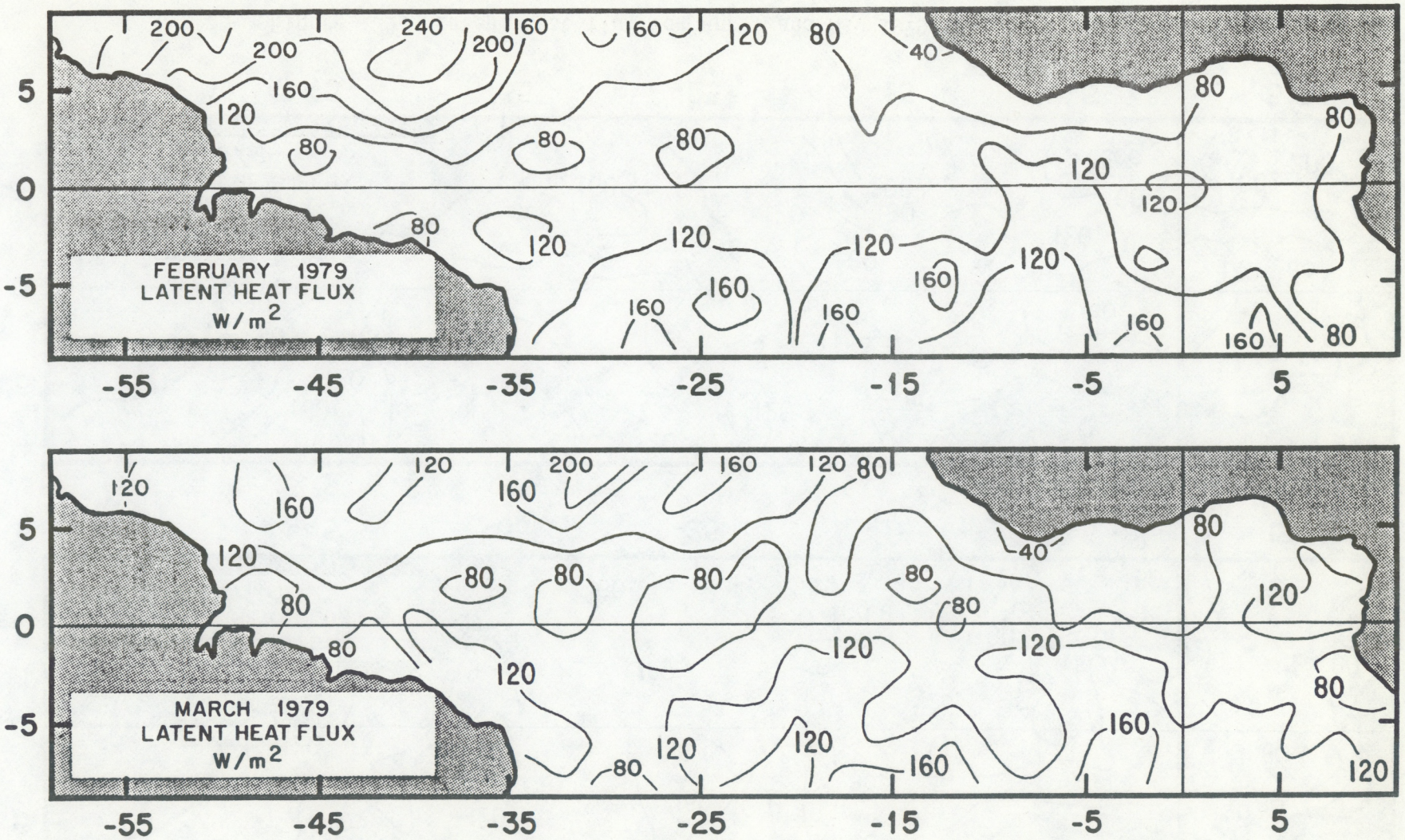

Figure 38. Latent heat flux for February and March 1979 (as in Figure 37).

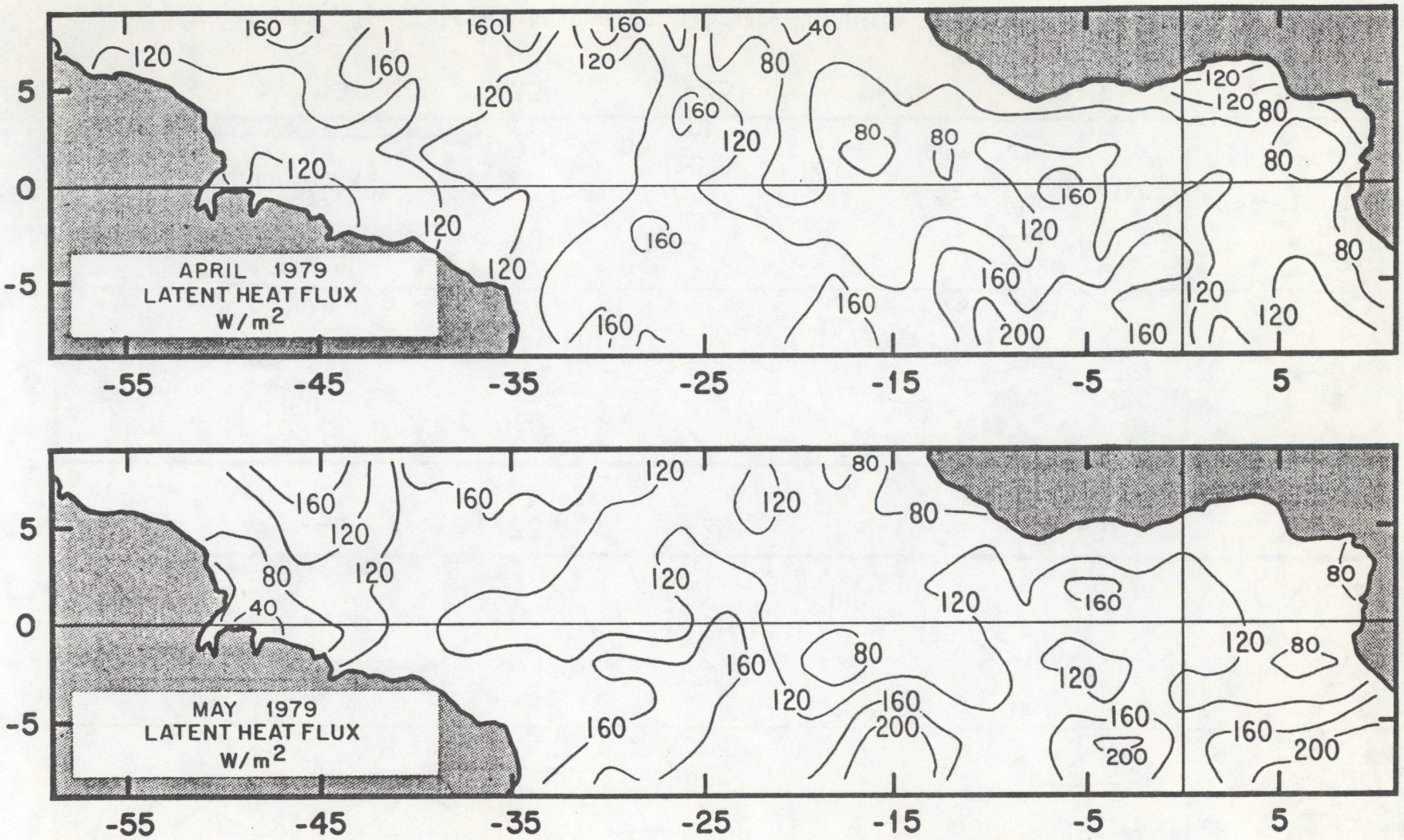

Figure 39. Latent heat flux for April and May 1979 (as in Figure 37).

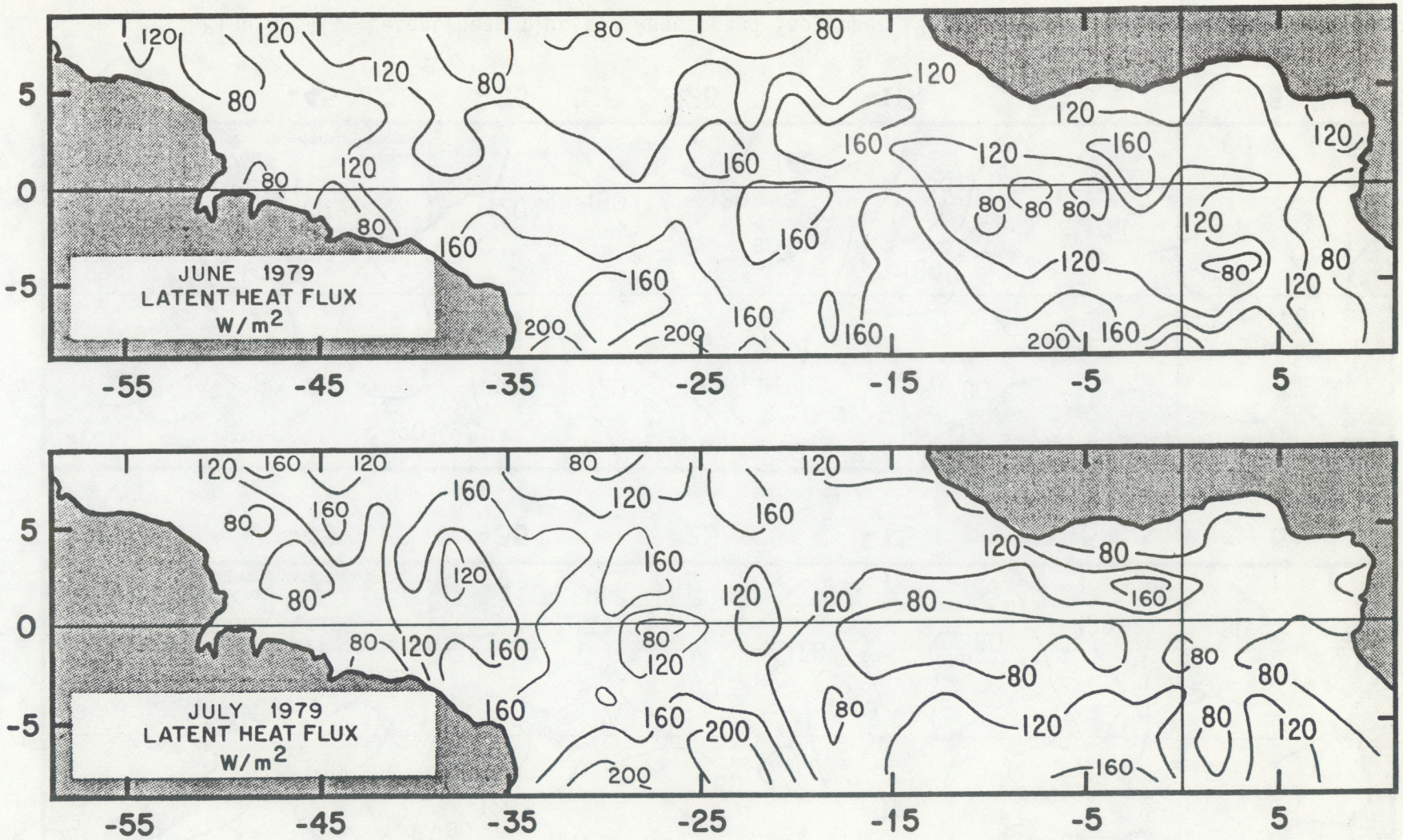

Figure 40. Latent heat flux for June and July 1979 (as in Figure 37).

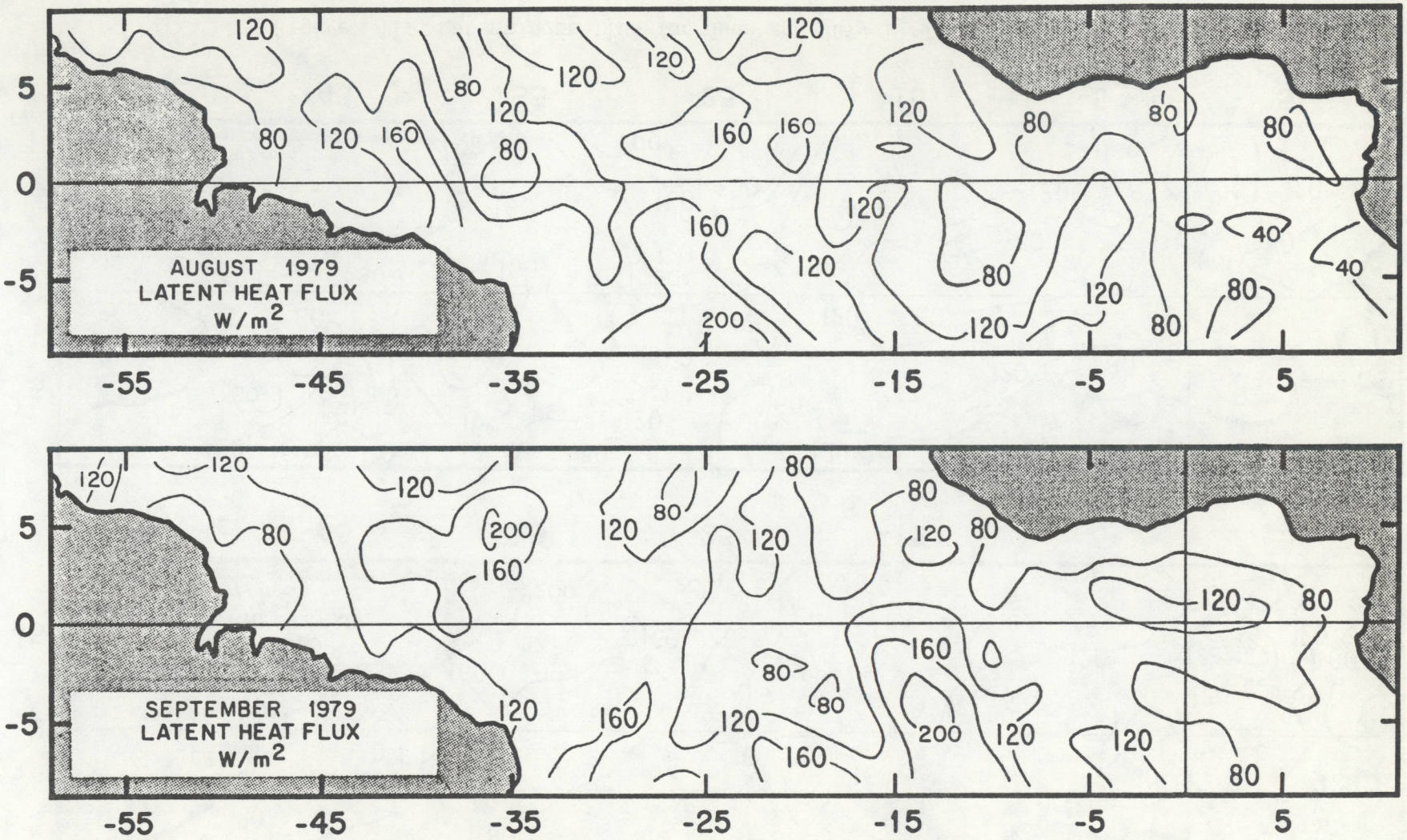

Figure 41. Latent heat flux for August and September 1979 (as in Figure 37).

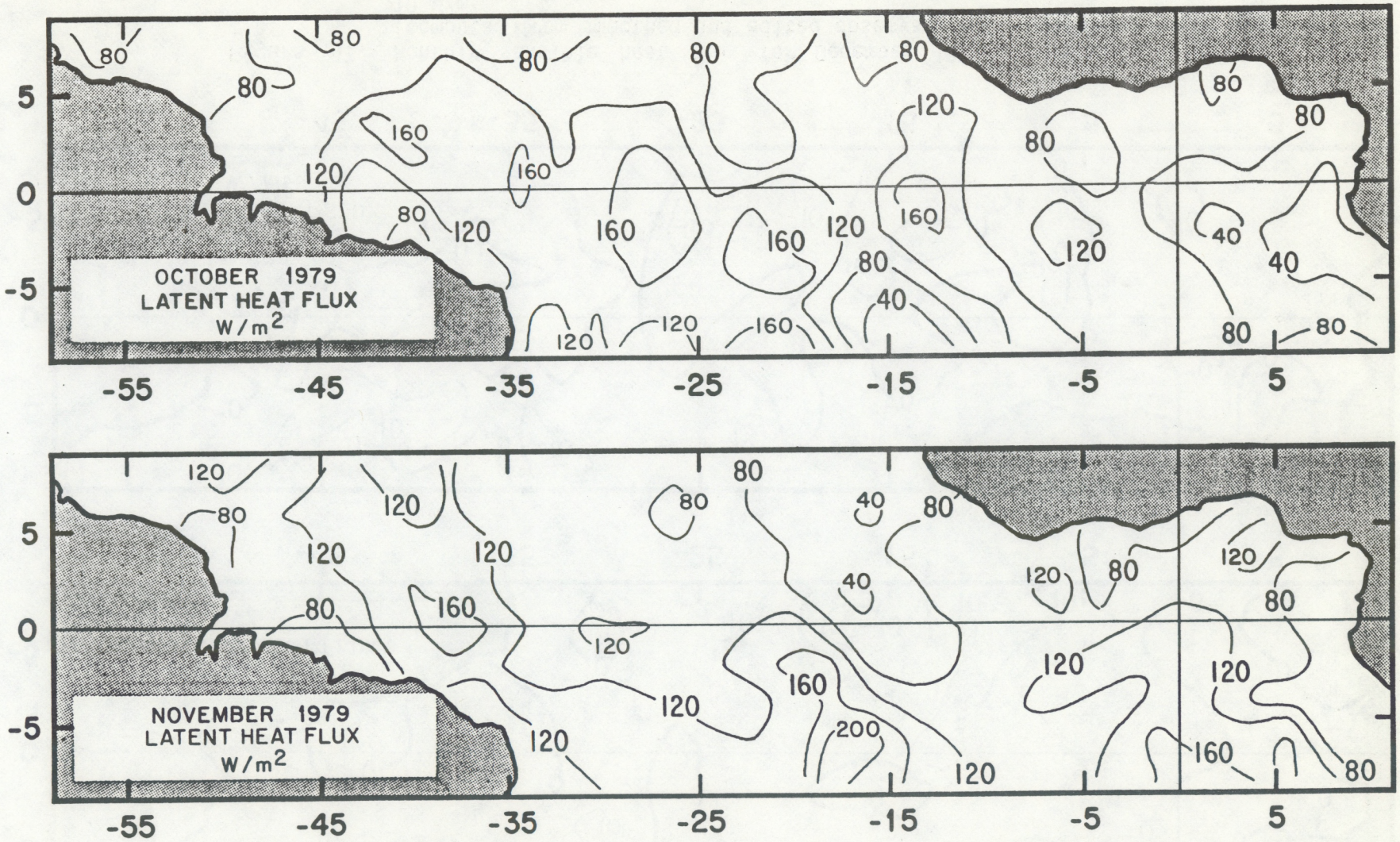

Figure 42. Latent heat flux for October and November 1979 (as in Figure 37).

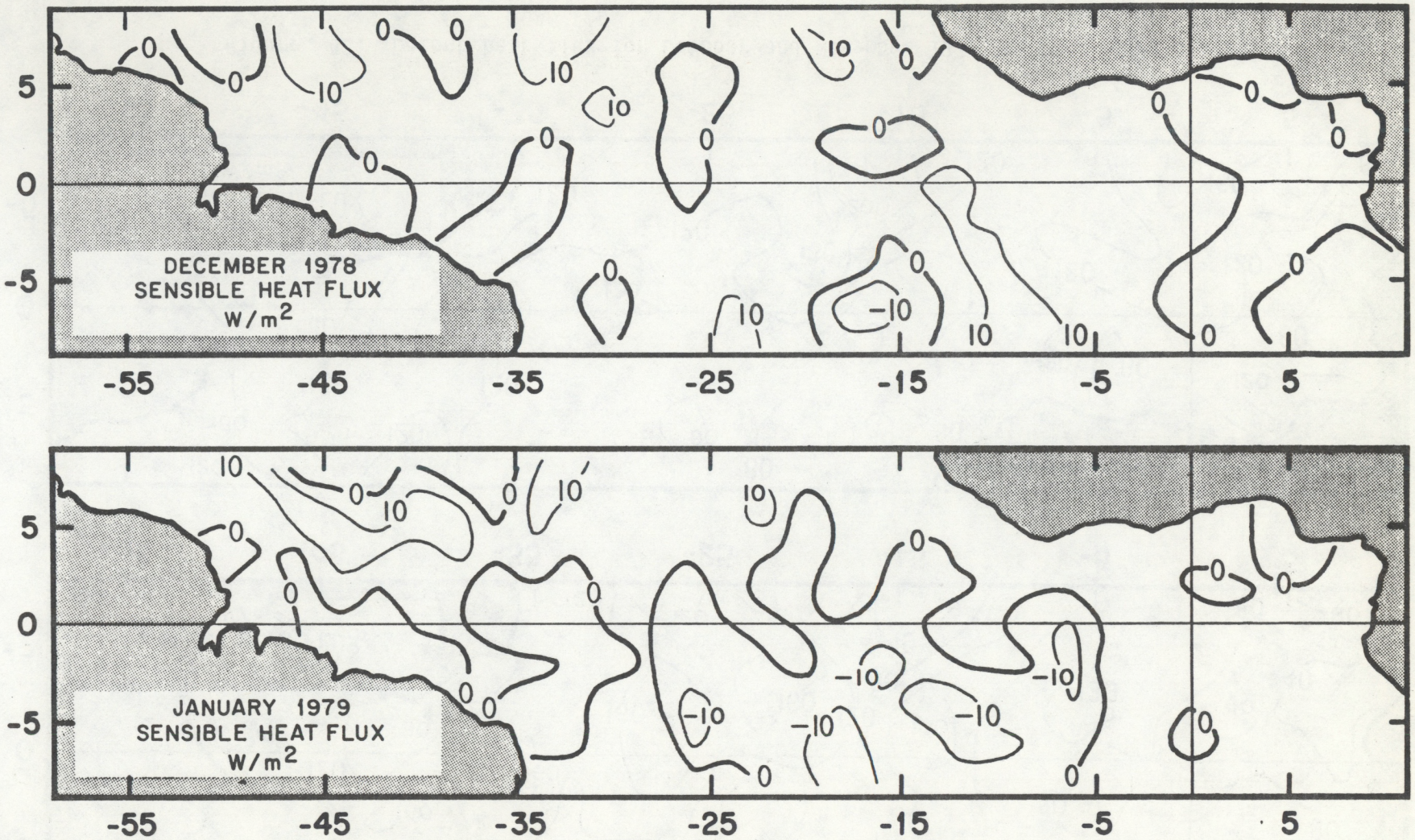

Figure 43. Monthly sensible heat flux for December 1978 and January 1979 (computed from smoothed and edited observations), contoured every 10 W/m^2.

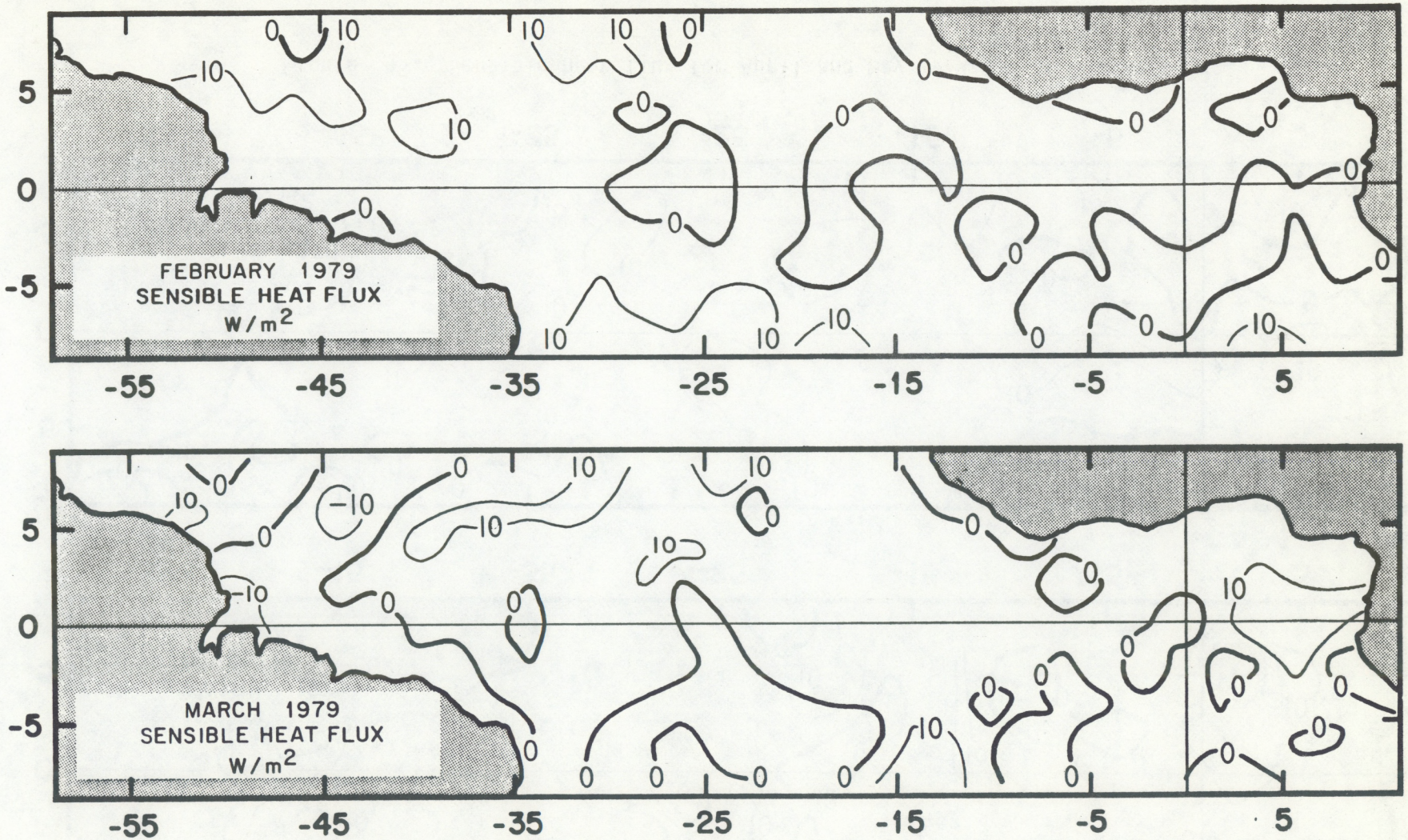

Figure 44. Sensible heat flux for February and March 1979 (as in Figure 43).

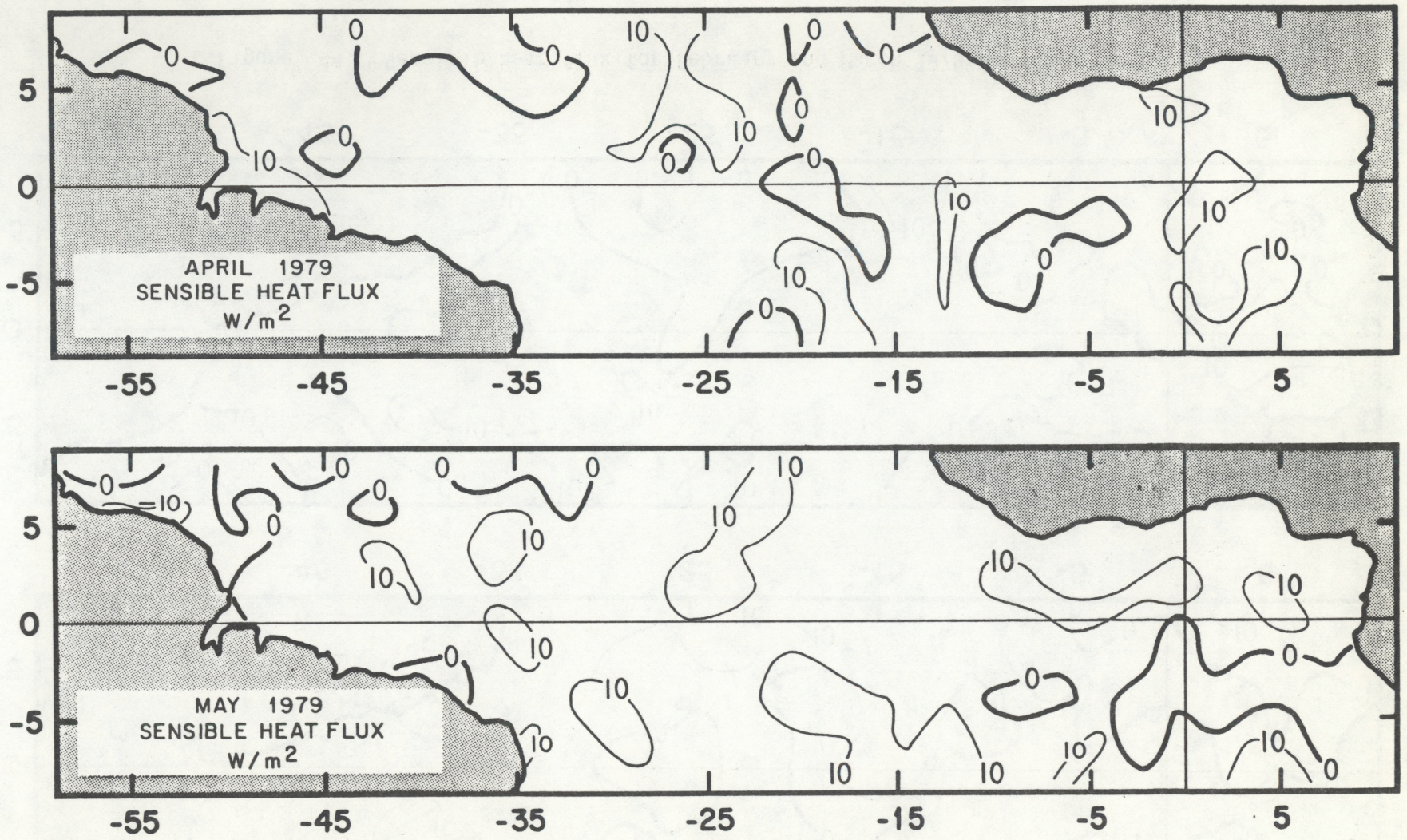

Figure 45. Sensible heat flux for April and May 1979 (as in Figure 43).

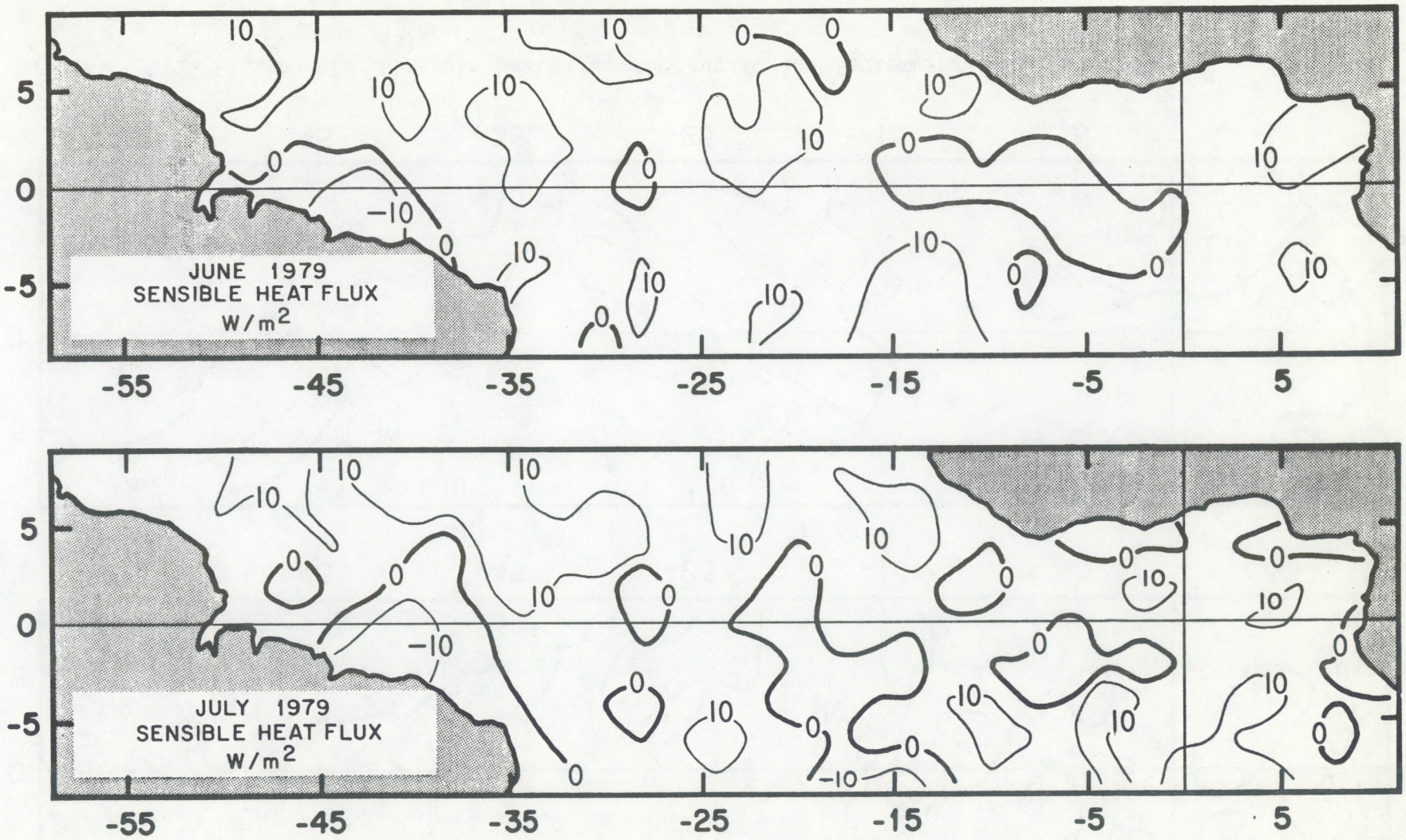

Figure 46. Sensible heat flux for June and July 1979 (as in Figure 43).

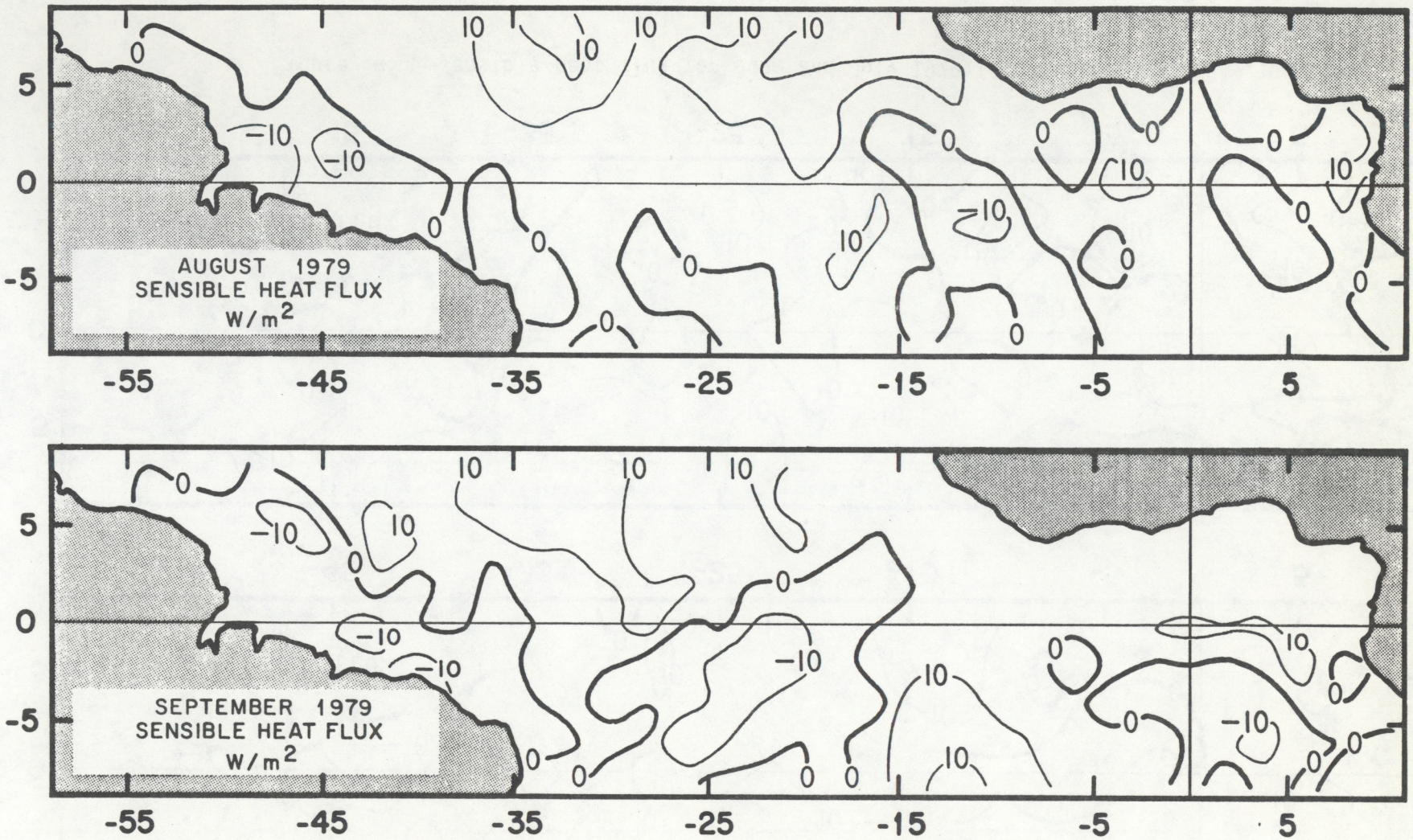

Figure 47. Sensible heat flux for August and September 1979 (as in Figure 43).

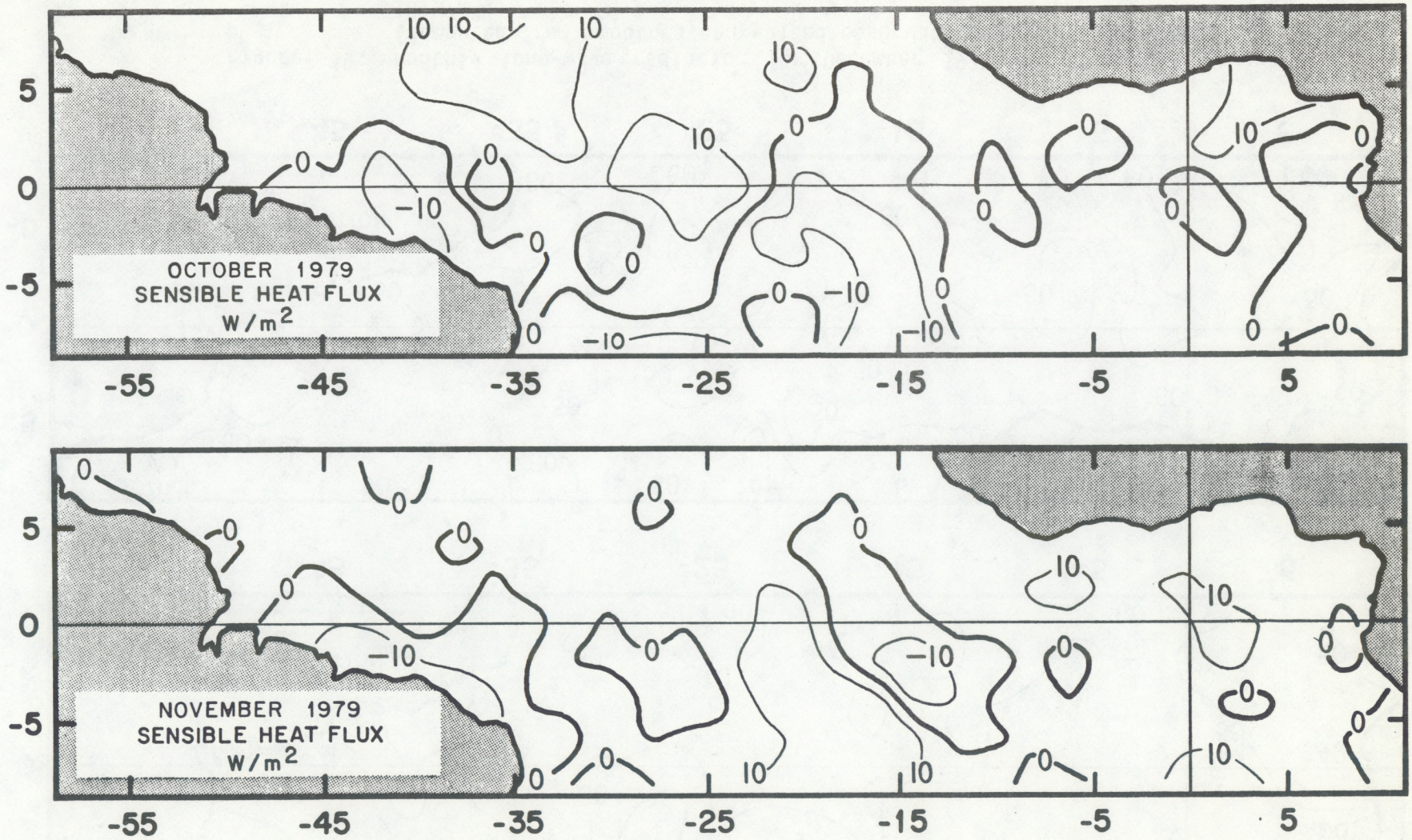

Figure 48. Sensible heat flux for October and November 1979 (as in Figure 43).

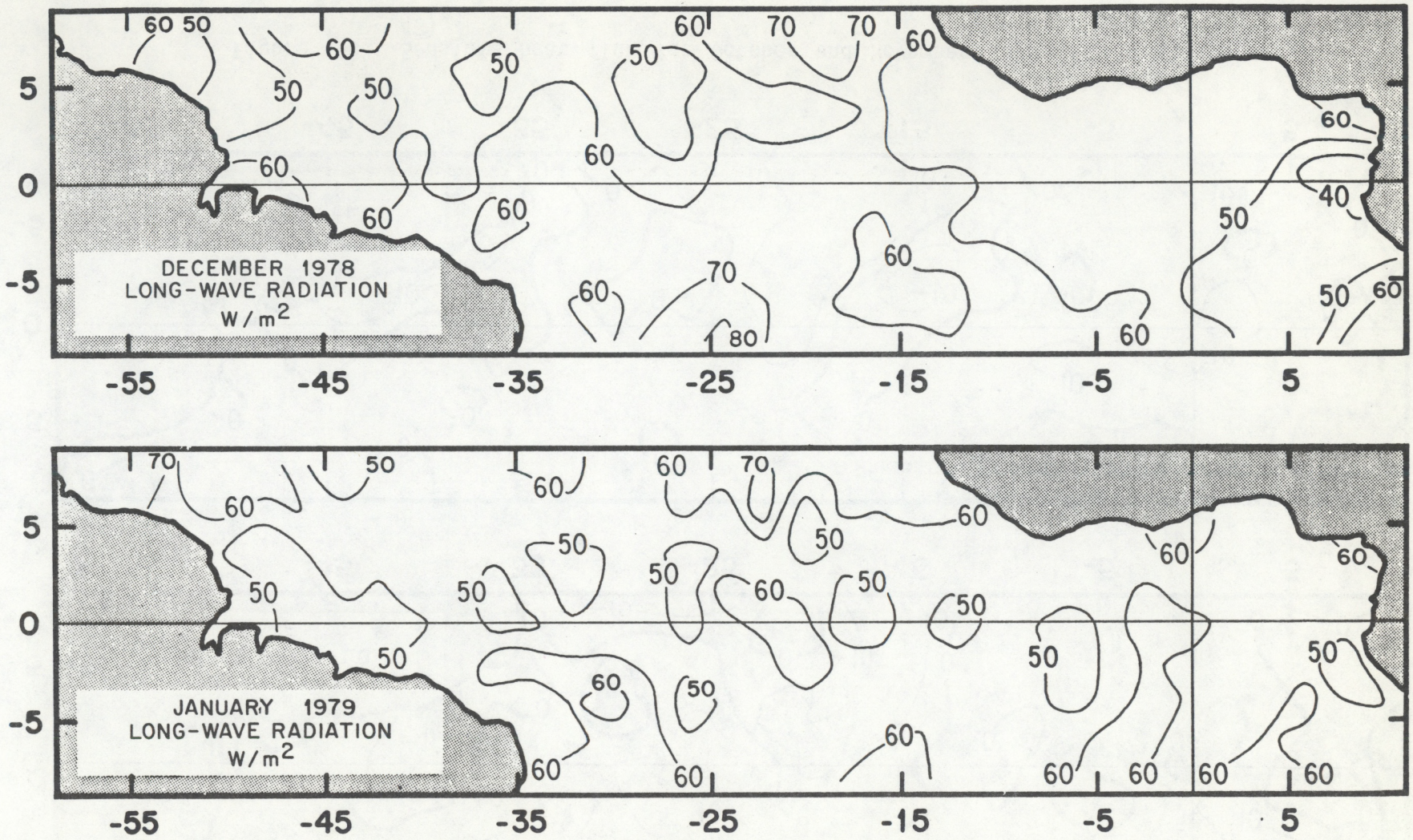

Figure 49. Monthly long-wave radiation for December 1978 and January 1979 (computed from smoothed and edited observations), contoured every 10 W/m^2.

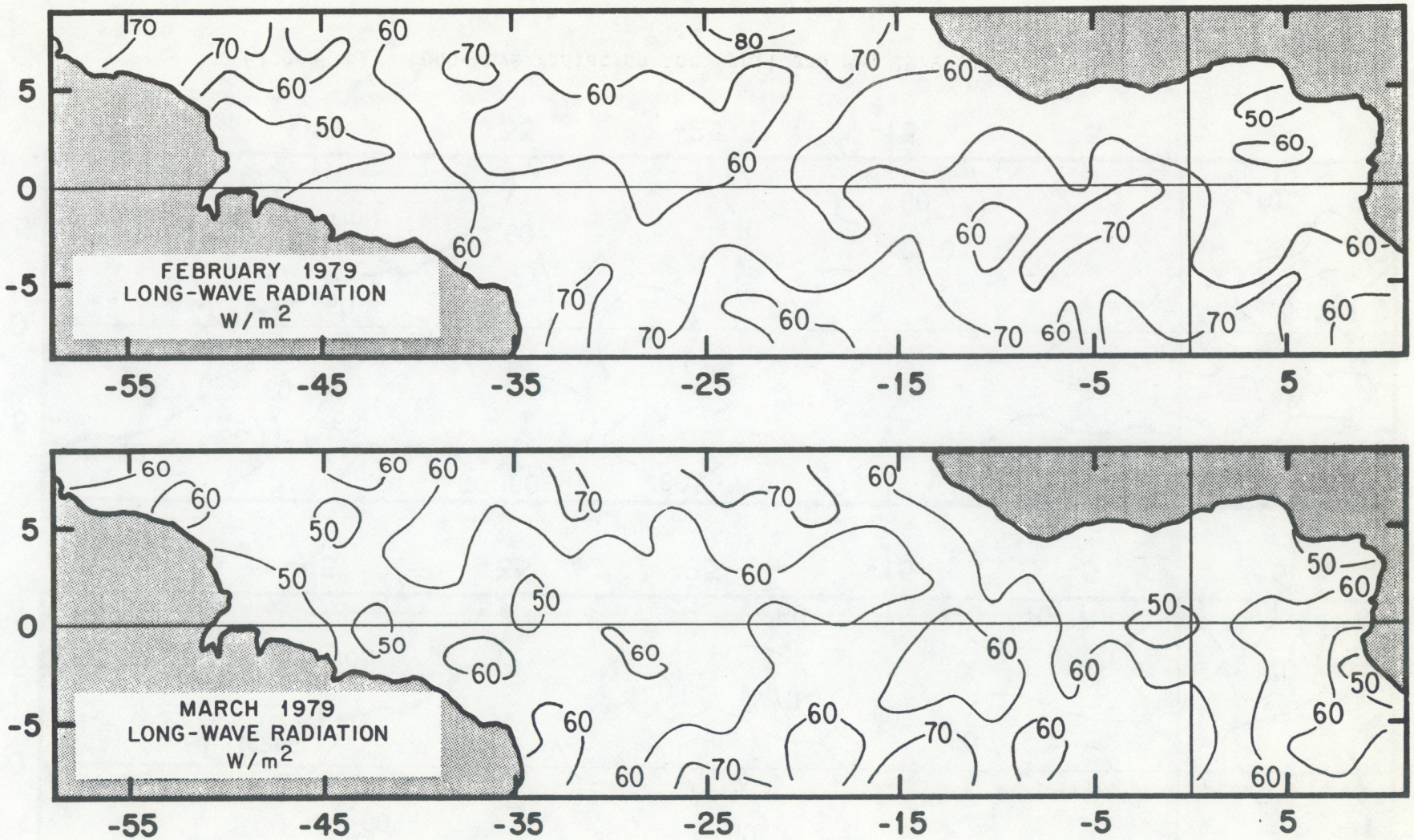

Figure 50. Long-wave radiation for February and March 1979 (as in Figure 49).

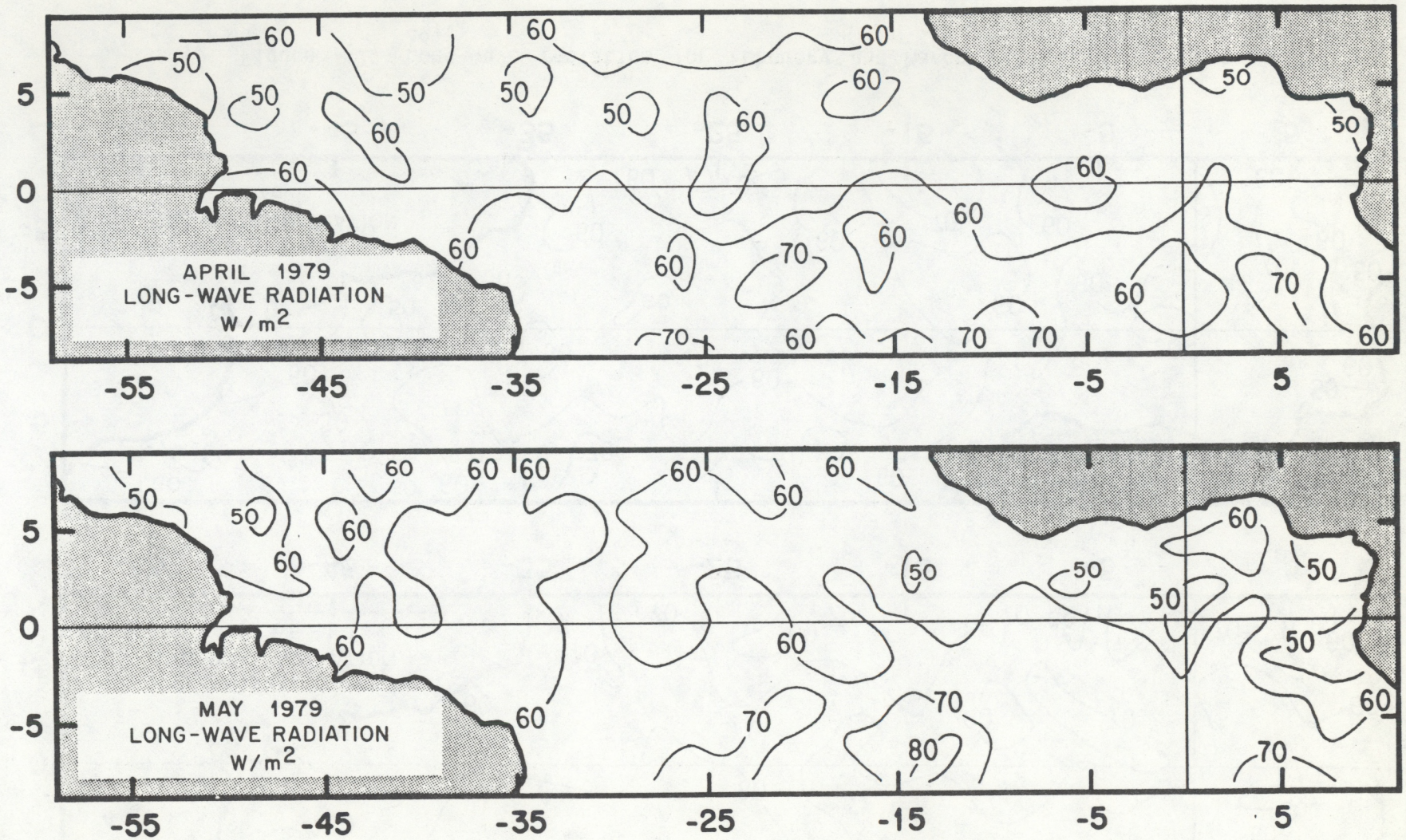

Figure 51. Long-wave radiation for April and May 1979 (as in Figure 49).

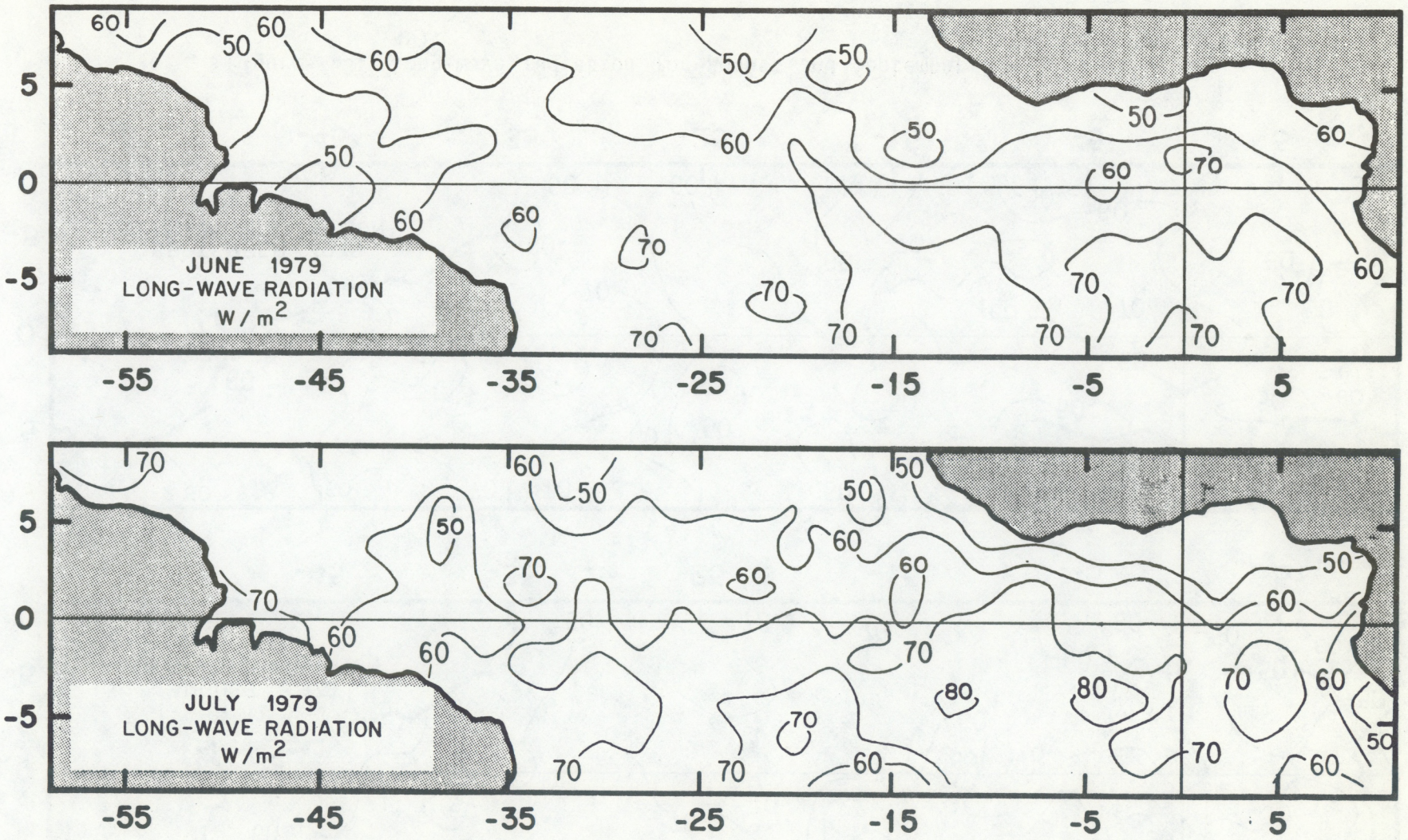

Figure 52. Long-wave radiation for June and July 1979 (as in Figure 49).

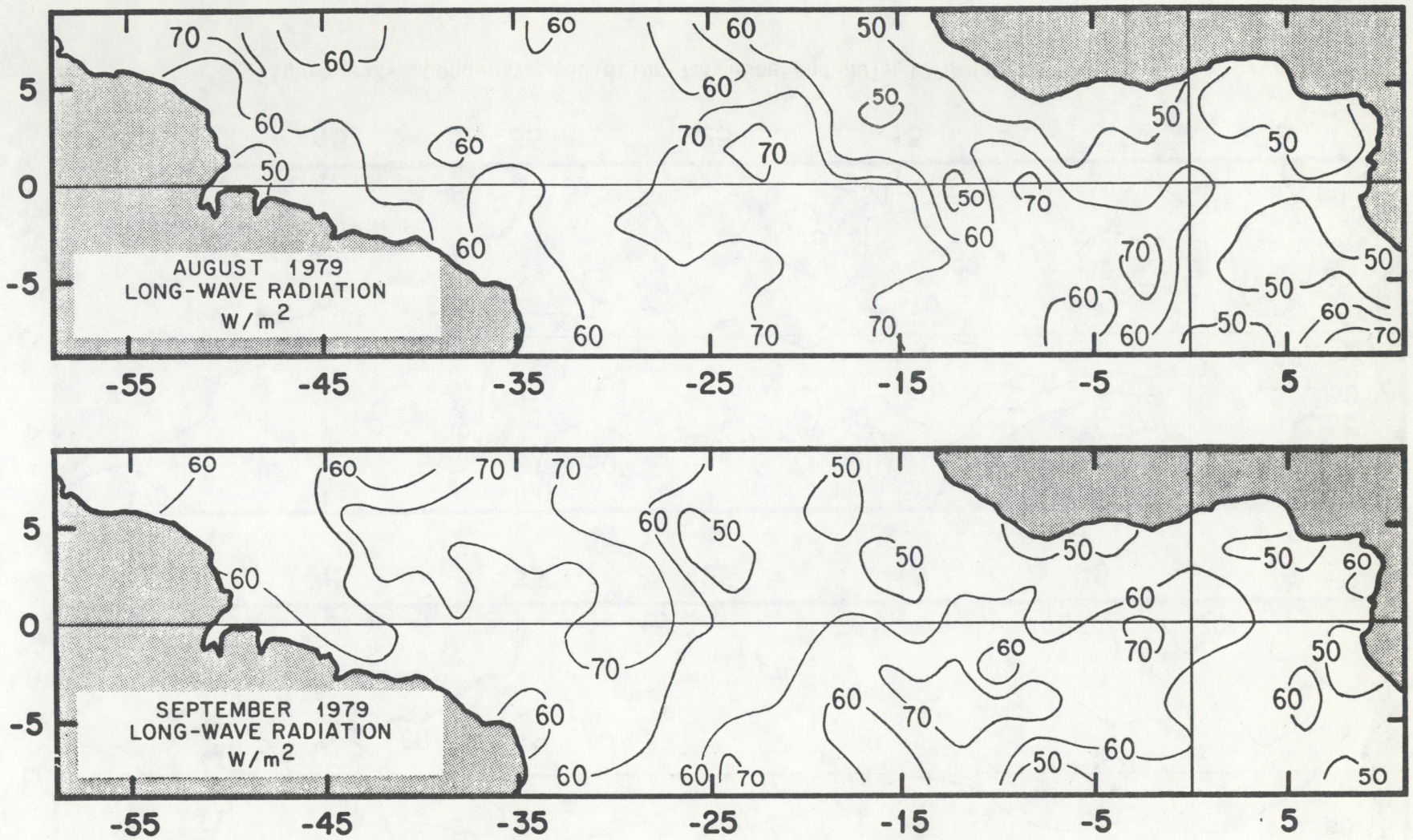

Figure 53. Long-wave radiation for August and September 1979 (as in Figure 49).

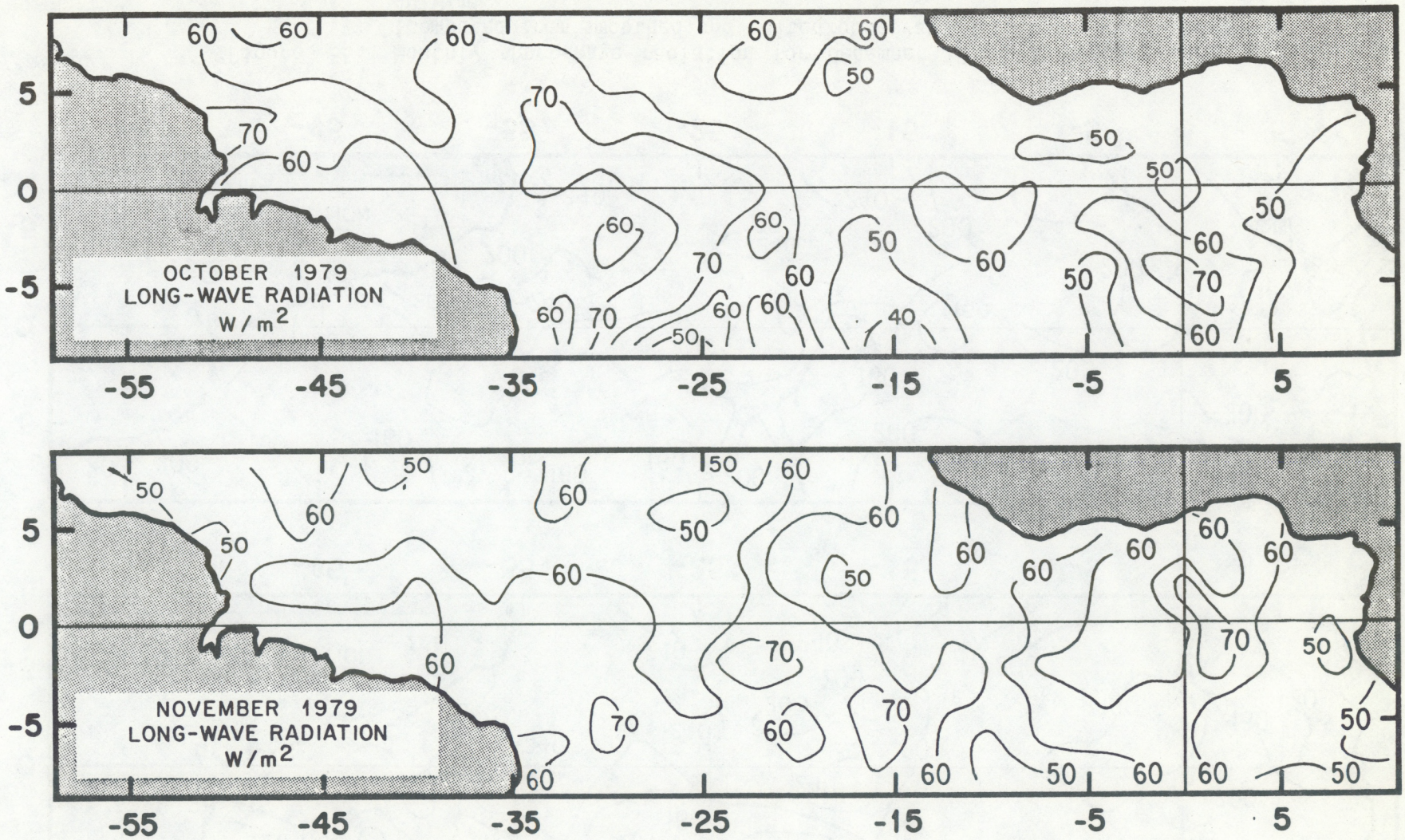

Figure 54. Long-wave radiation for October and November 1979 (as in Figure 49).

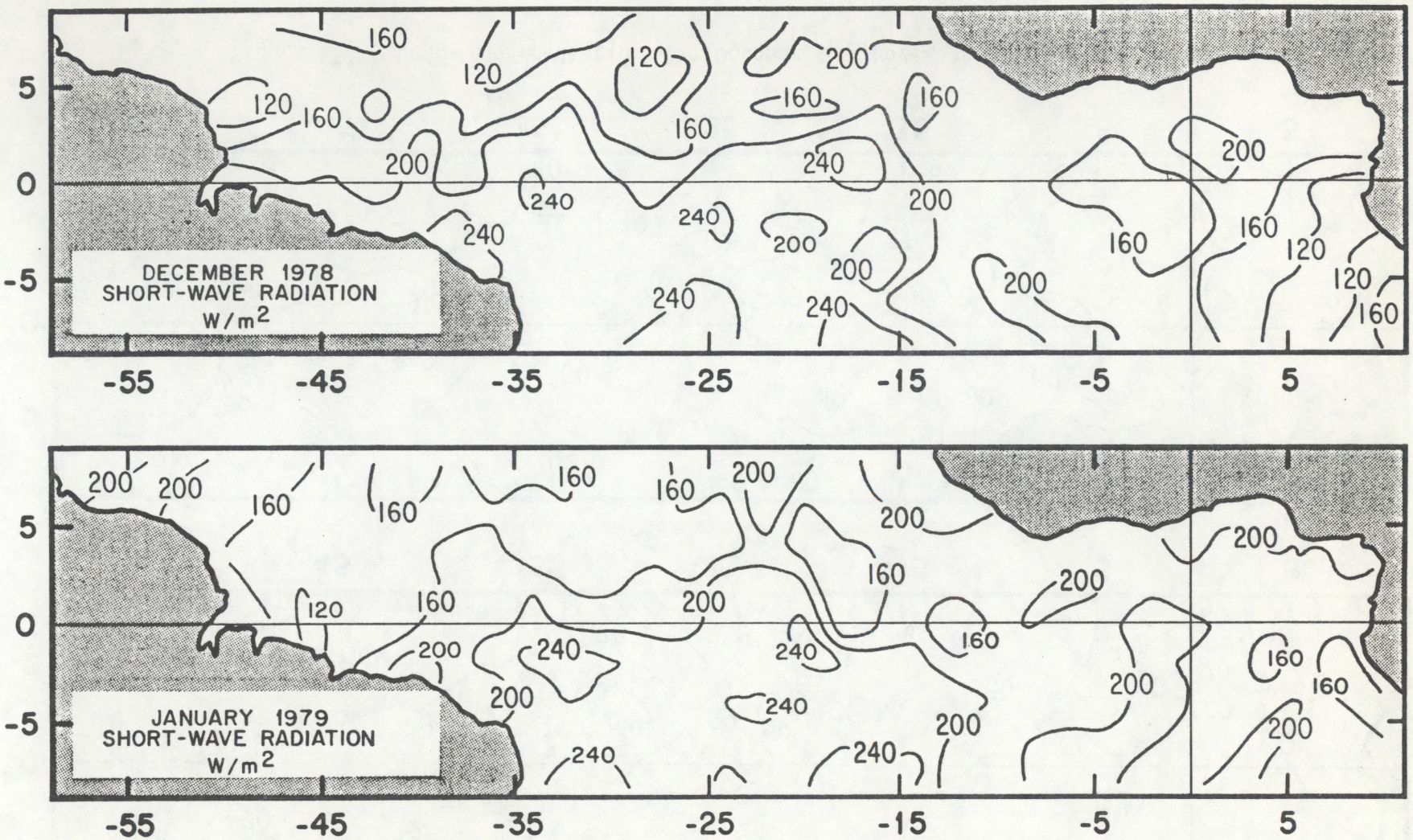

Figure 55. Monthly short-wave radiation for December 1978 and January 1979 (computed from smoothed and edited observations), contoured every 40 W/m^2.

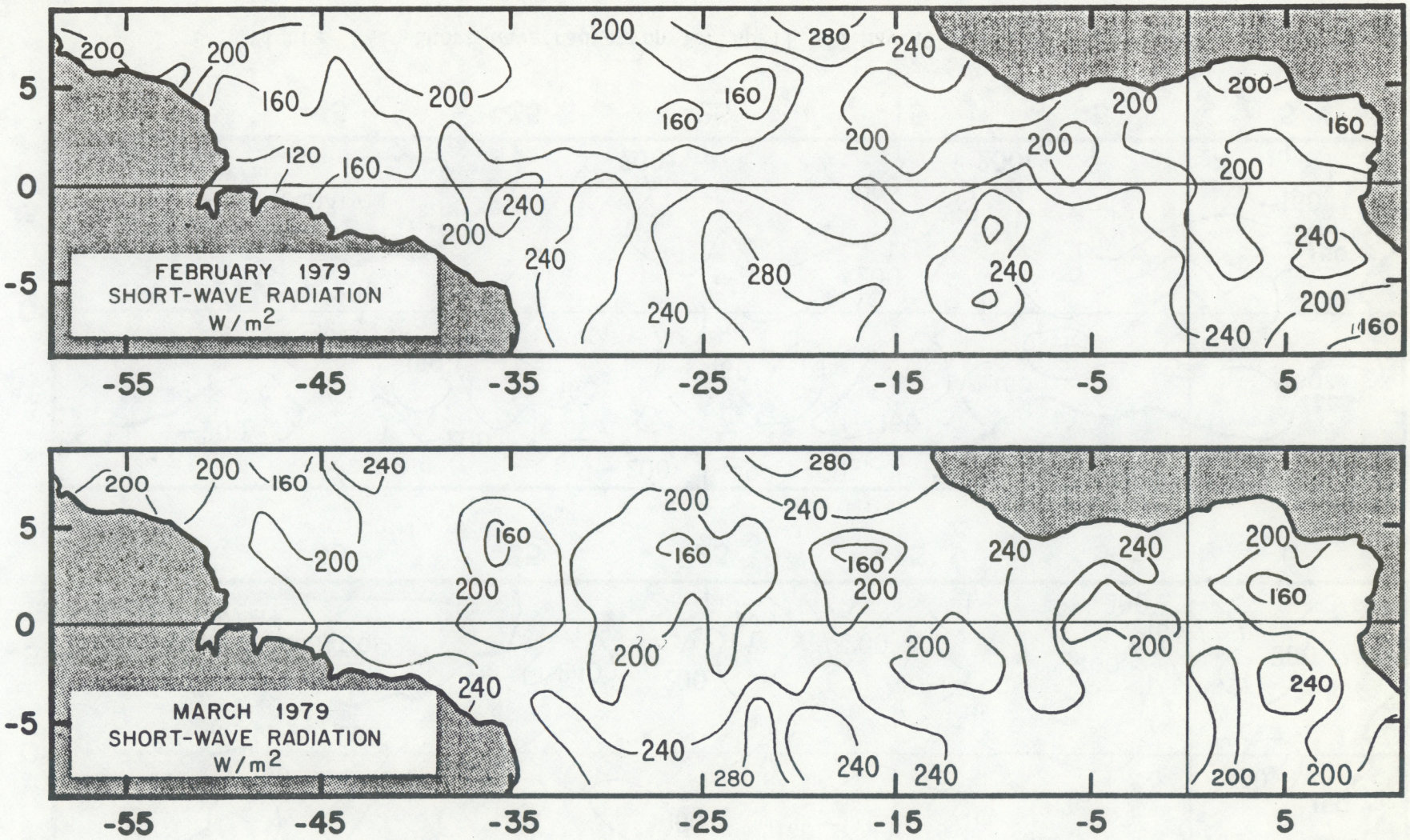

Figure 56. Short-wave radiation for February and March 1979 (as in Figure 55).

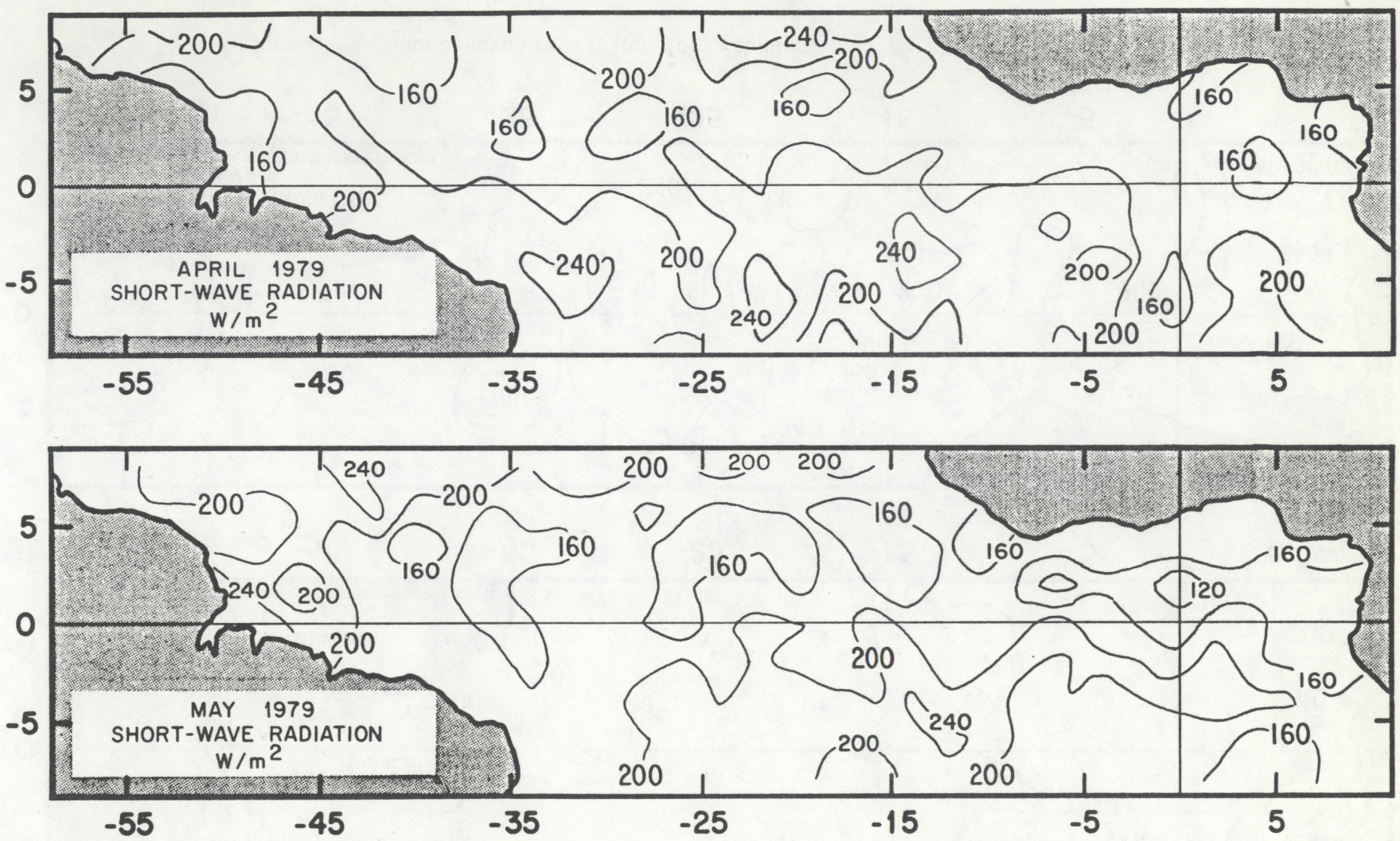

Figure 57. Short-wave radiation for April and May 1979 (as in Figure 55).

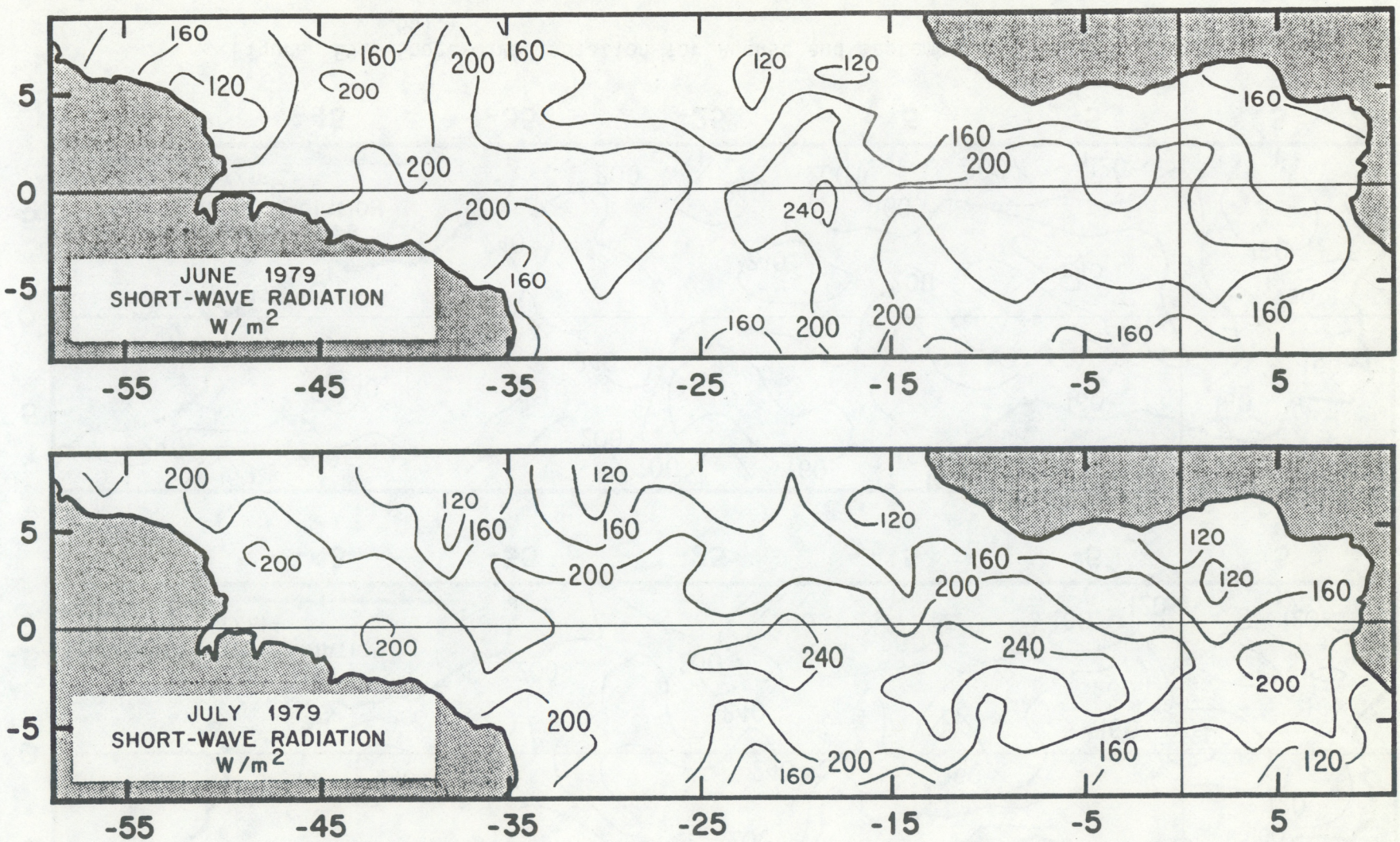

Figure 58. Short-wave radiation for June and July 1979 (as in Figure 55).

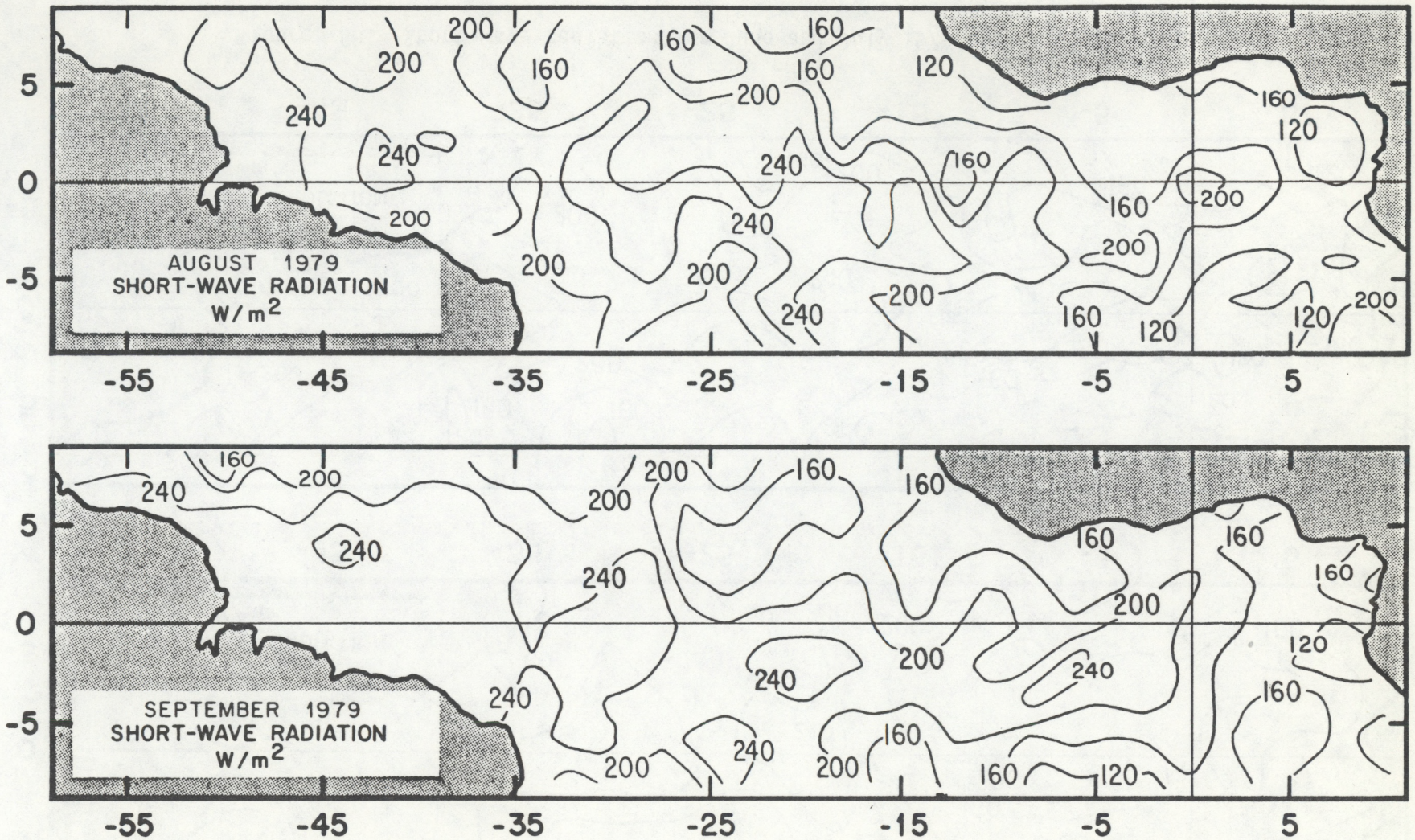

Figure 59. Short-wave radiation for August and September 1979 (as in Figure 55).

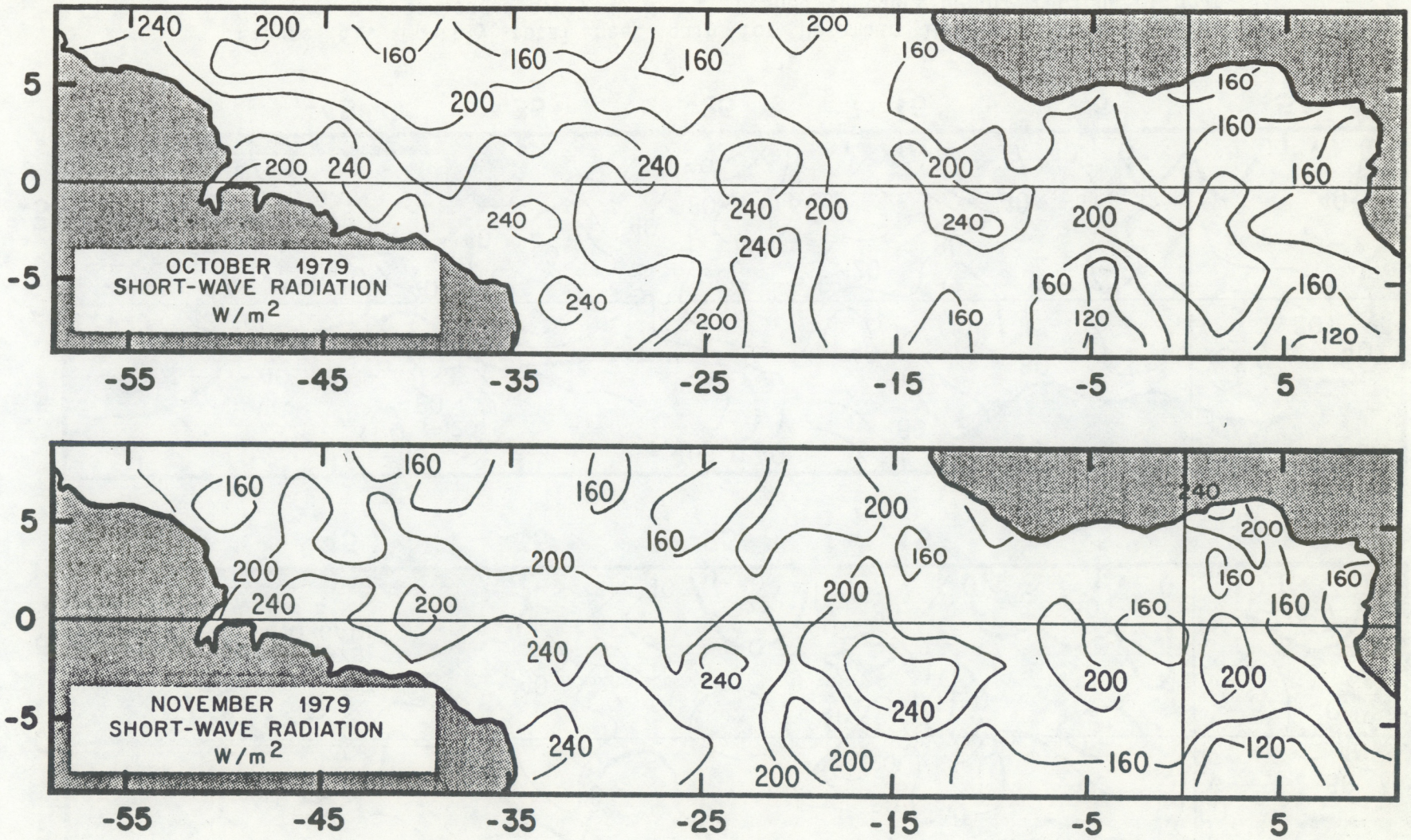

Figure 60. Short-wave radiation for October and November 1979 (as in Figure 55).

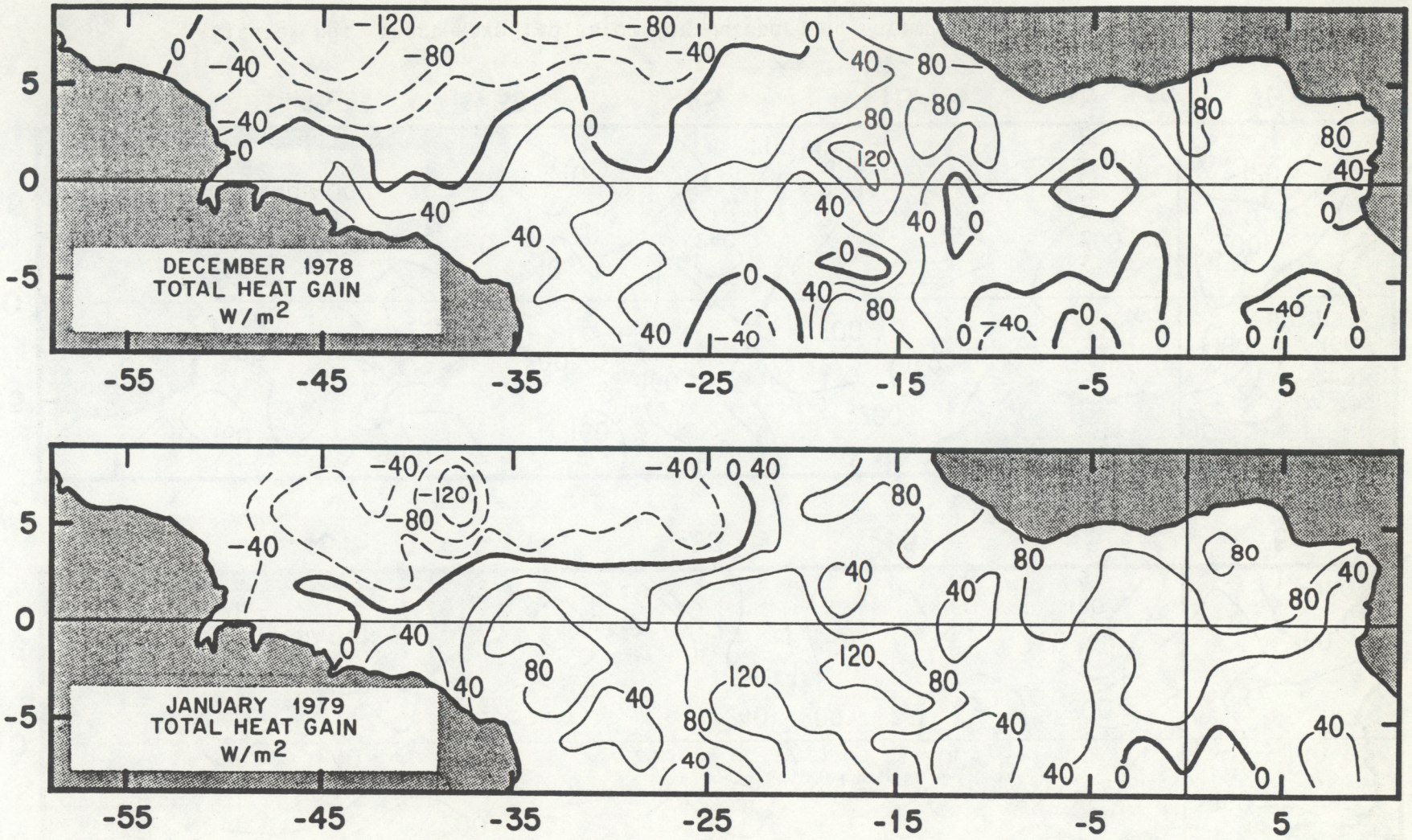

Figure 61. Monthly total heat gain for December 1978 and January 1979, contoured every 40 W/m^2. Dashed contours denote regions of heat loss.

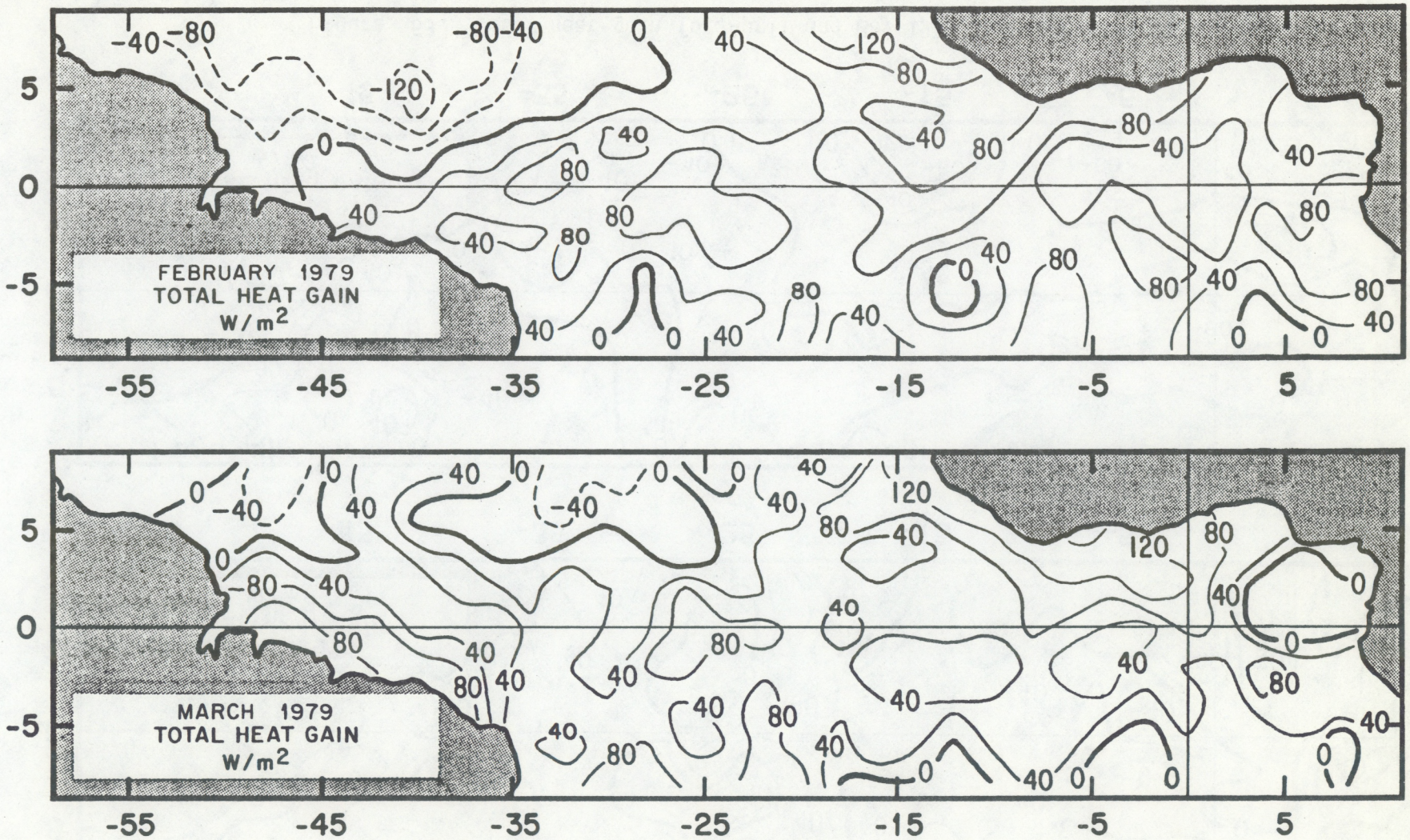

Figure 62. Total heat gain for February and March 1979 (as in Figure 61).

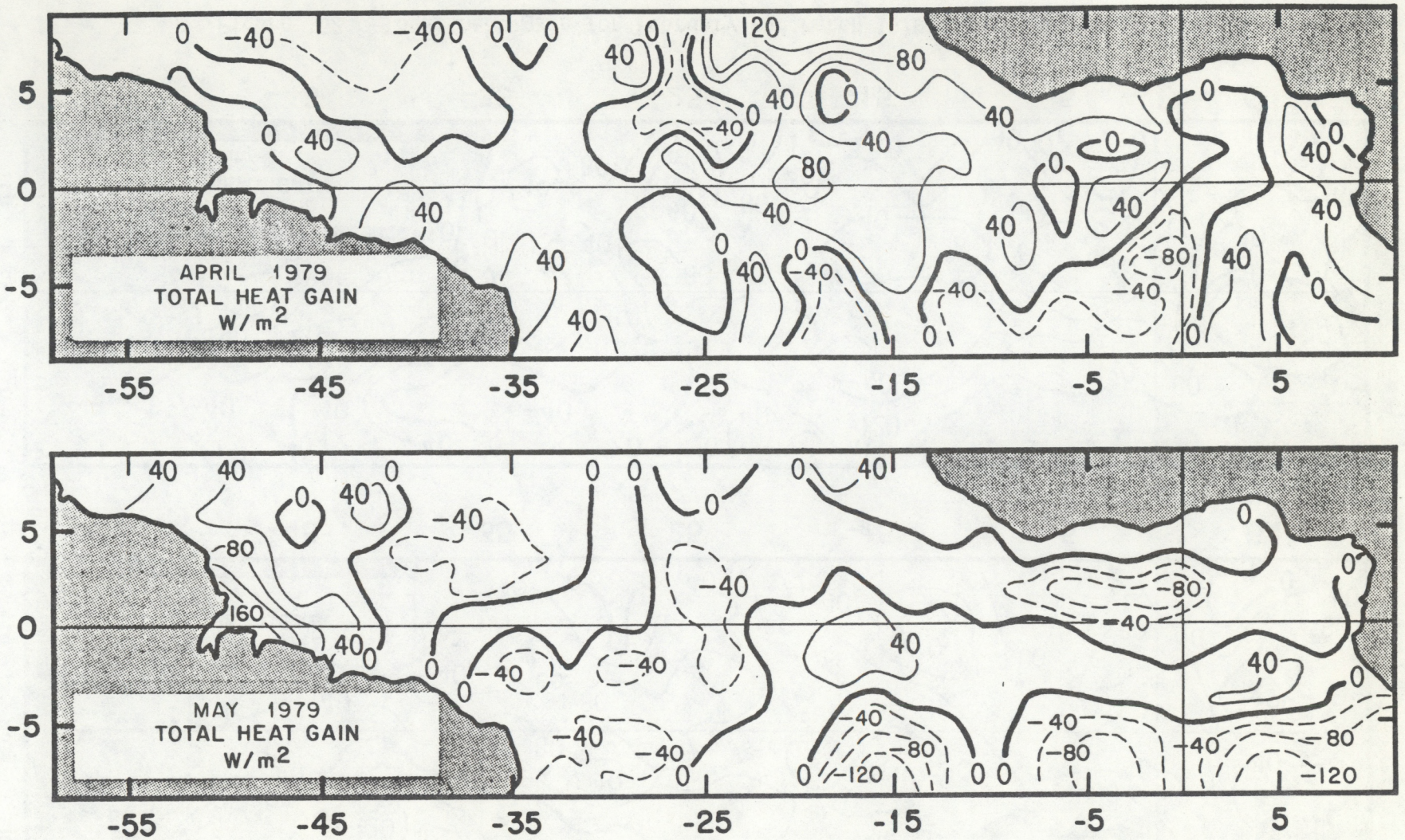

Figure 63. Total heat gain for April and May 1979 (as in Figure 61).

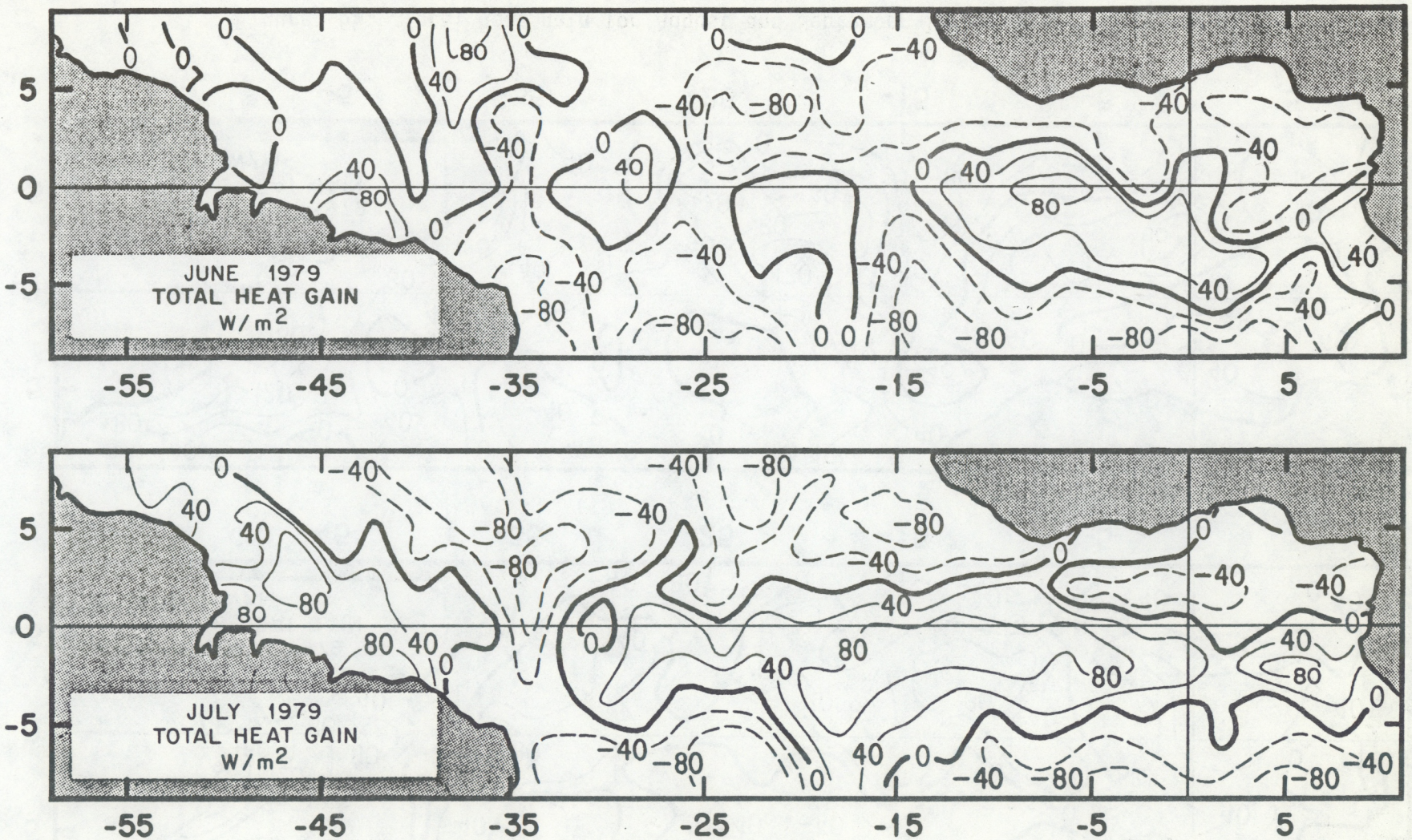

Figure 64. Total heat gain for June and July 1979 (as in Figure 61).

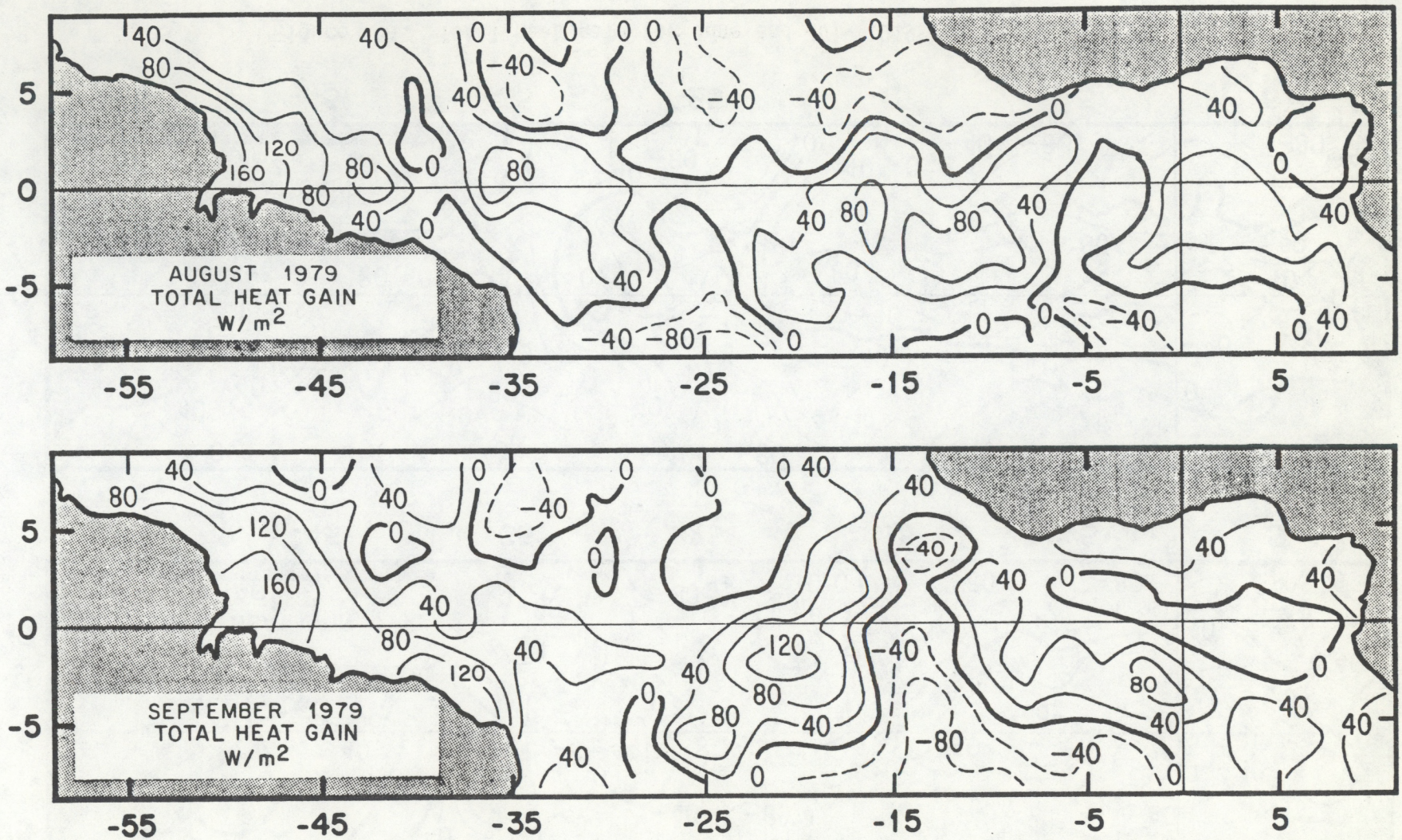

Figure 65. Total heat gain for August and September 1979 (as in Figure 61).

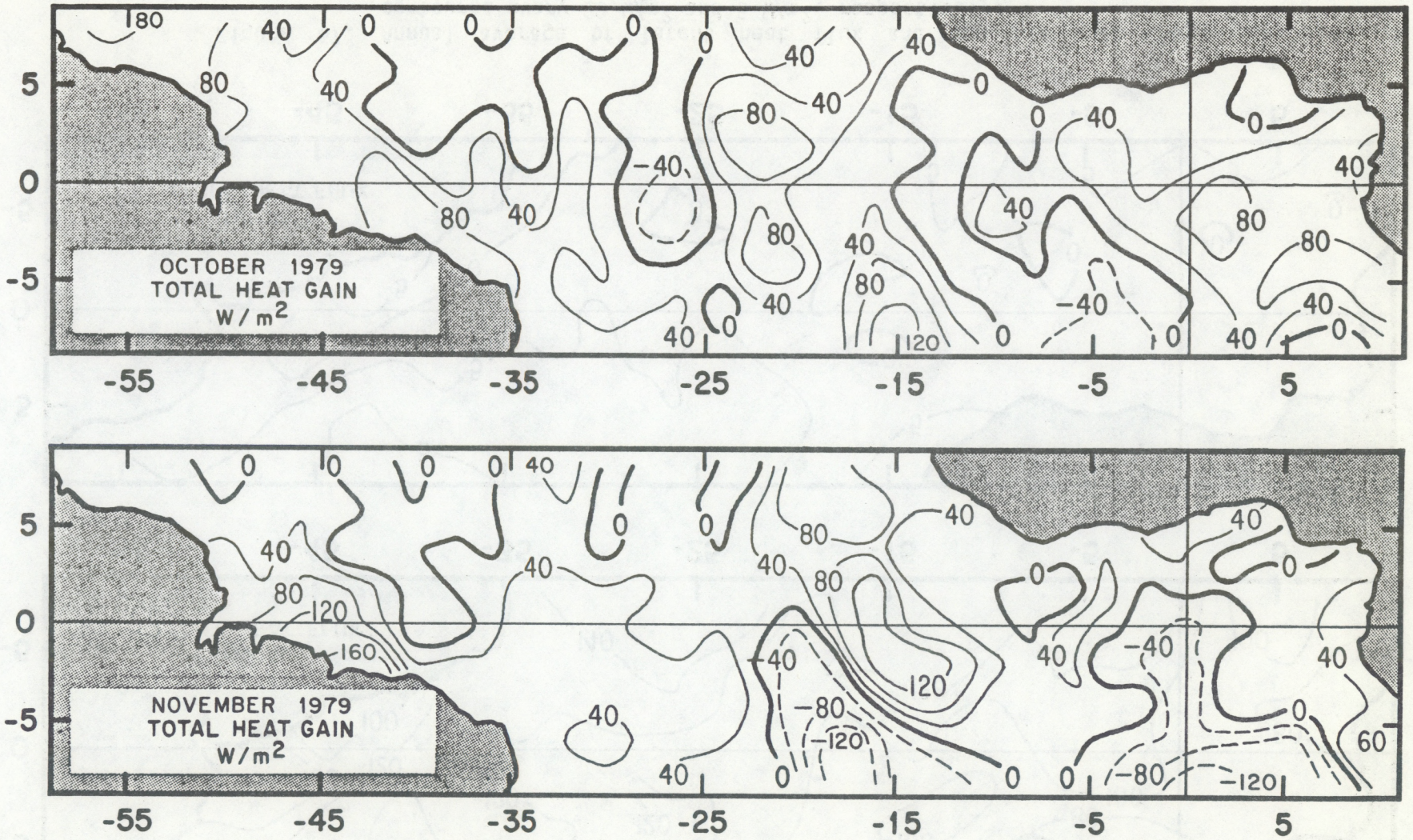

Figure 66. Total heat gain for October and November 1979 (as in Figure 61).

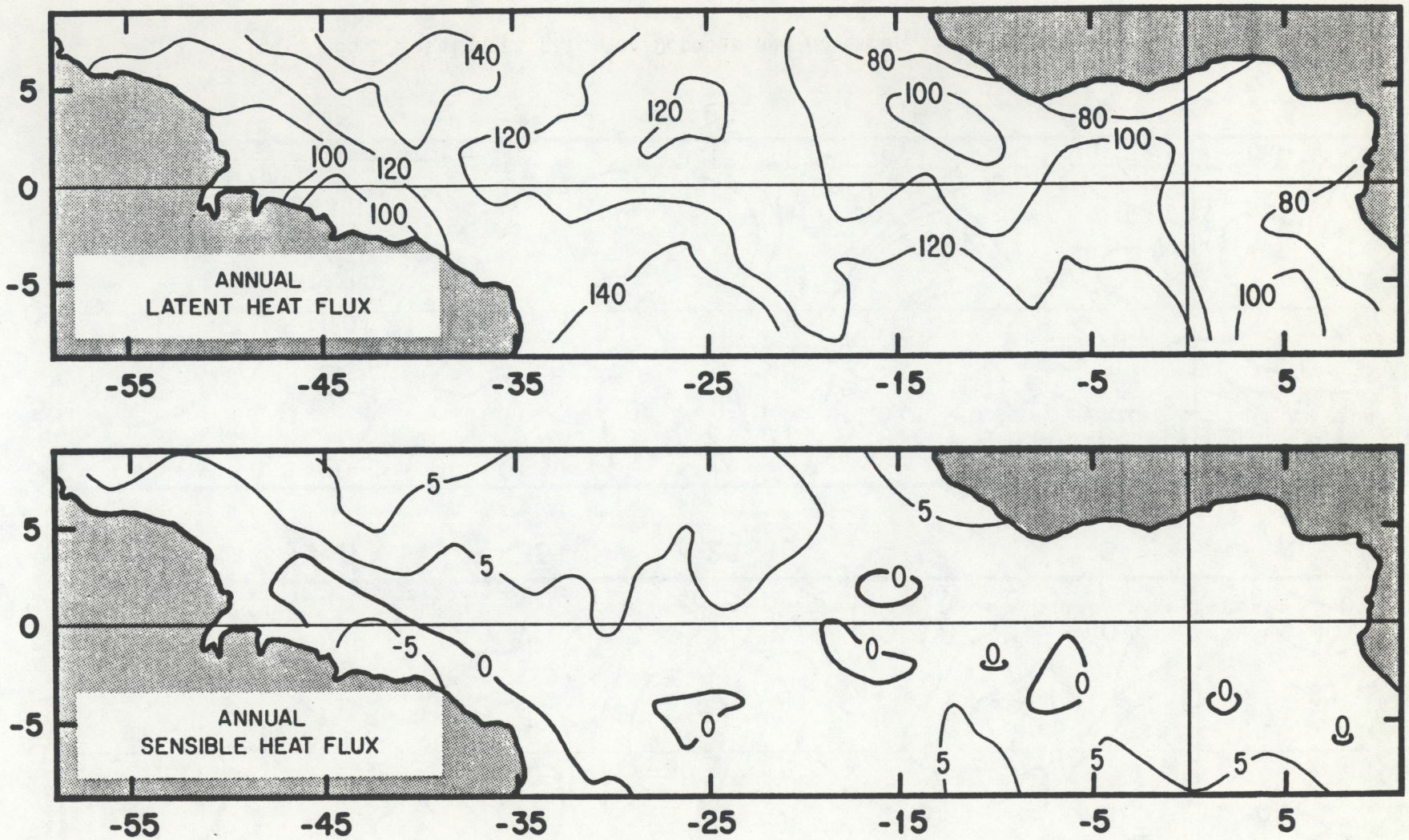

Figure 67. Annual average of latent heat flux and sensible heat flux, contoured every 20 W/m^2 and 5 W/m^2, respectively.

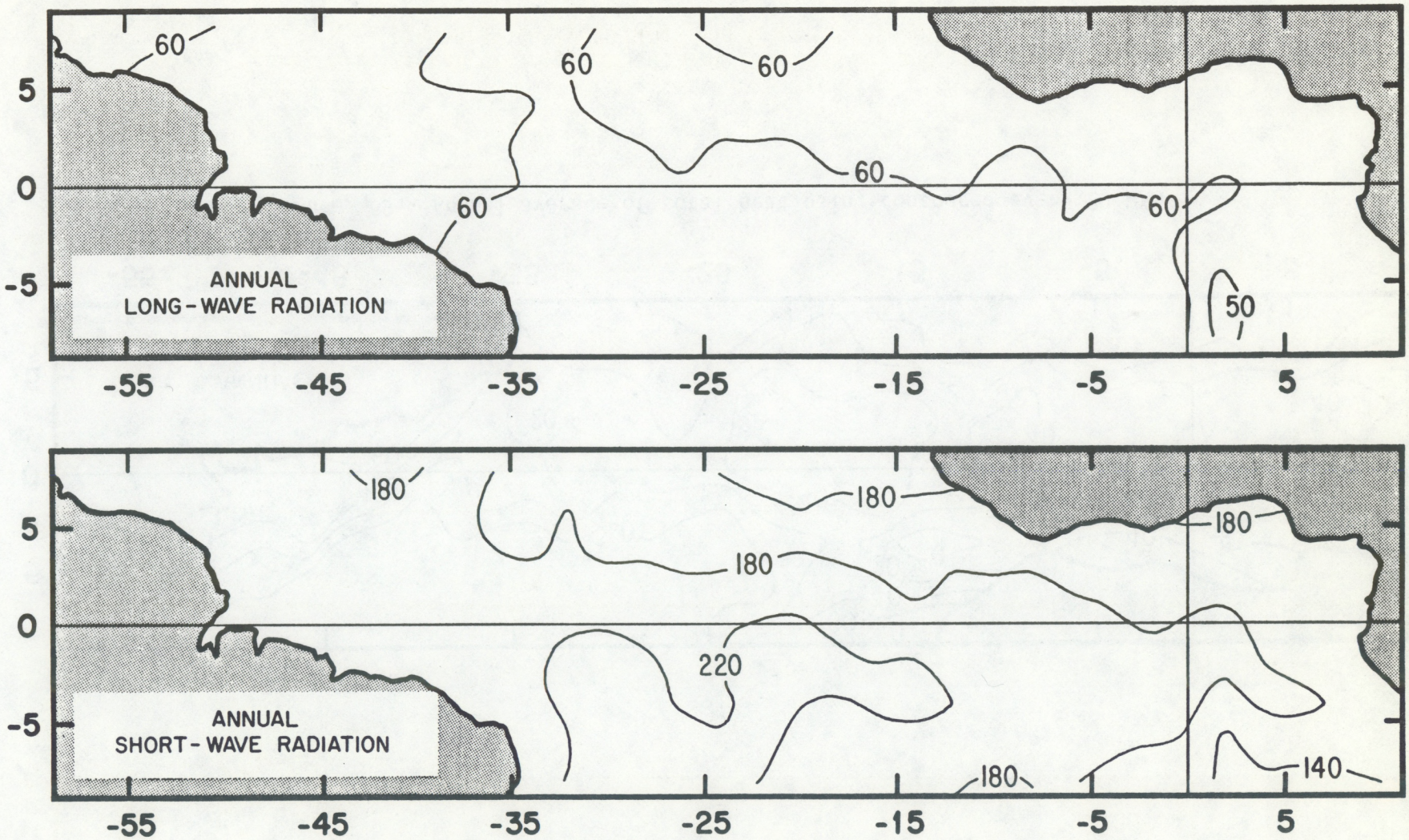

Figure 68. Annual average of long-wave radiation and short-wave radiation, contoured every 10 W/m^2 and 40 W/m^2, respectively.

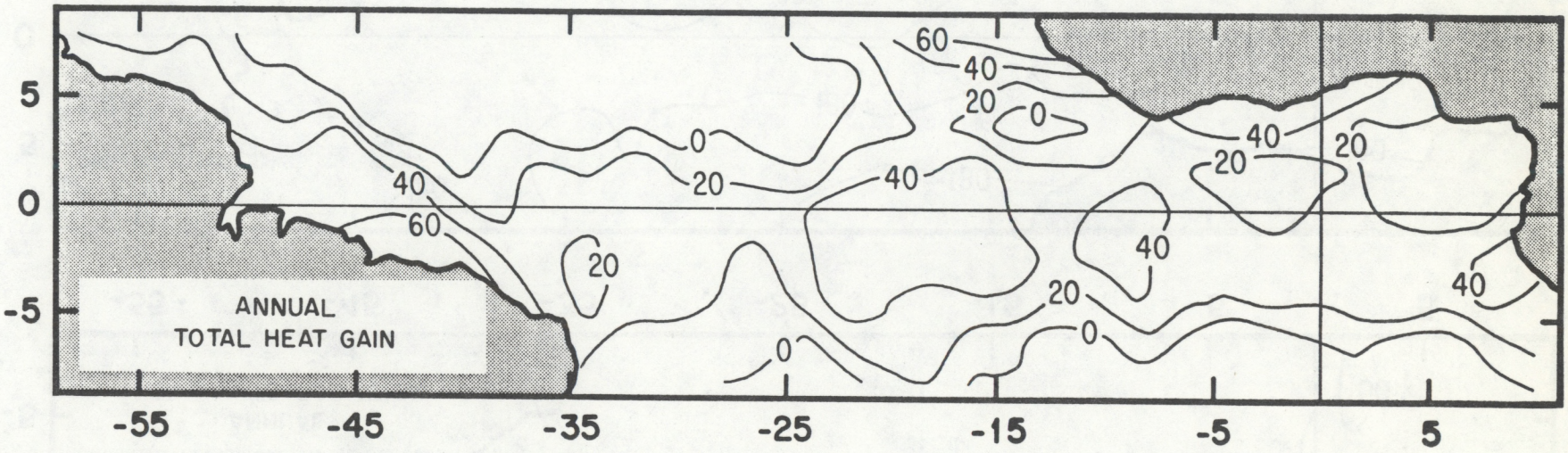

Figure 69. Annual average of total heat gain, contoured every 20 W/m^2.